UNIVERSITY OF
PATRAS

SCHOOL OF ENGINEERING
DEPARTMENT OF ENVIRONMENTAL AND NATURAL RESOURCES MANAGEMENT

Mathematical simulation of transport phenomena

Scale transition and engineering applications

PhD THESIS

By

GAVRIIL M. GAVRIIL

Submitted in Fulfillment of the Requirements for the Degree of Doctor of Philosophy (Ph.D)

Agrinion, 2018

If I have seen a little further, it is by standing

on the shoulders of Giants.

Isaak Newton

CONTENTS

LIST OF FIGURES[1]

LIST OF TABLES

---

[1] The sources of all the images presented by this Ph.D. thesis are cited in the relative captions.Images not including any references are produced by the author.

AKNOWLEDGMENTS

Even if sometimes, while studying, writing or thinking one can feel alone, doctoral studies are not a lonely journey. They are a path made of people, of guides able to inspire, of obstacles, of successes, defeats, and of knowledge and experience. In this journey there are many people that I have to thank for their help and for the inspiration that they gave to me.

First of all I would like to thank my supervisor, Associate Professor Frank A. Coutelieris for his guidance and advices throughout the Ph.D. who is not only a mentor for me but also a dear friend. The freedom, constant support and encouragement he gave me throughout the integration of my work, was the force keeping me moving and heading forward. The door to Prof. Coutelieris office was always open, while his Skype was also always online, whenever I ran into a trouble spot or had a question about my research or writing. I also would like to thank my thesis committee members, especially Dr. Kanavouras and Dr. Bountouvis for all of their guidance through this process; your discussion, ideas, and feedback have been absolutely invaluable.

It would have been impossible to arrive until this point without the love and the support of my family, my friends and of course most of all, of my wife. As I would like to answer to her question, “No, research never ends”. A new journey has just begun.

Finally, a thank you goes to all the people that in different ways have contributed to this journey.

NOMECLATURE

CFD	Computational fluid dynamics
EU	European union
FDA	Food and Drug association
HFO	Heavy fuel oil
OML	Overall migration limit

$[A..F]_m$	Migration coefficients
[Fuel]	Fuel concentration
$[N_A]$ on the surface	Component of molar flux vertical to the collector surface
[Oxidizer]	Oxidizer concentration
$[S/V]_{eff}$	Effective surface to volume ratio
A	Pre-exponential constant
A'_p	Polymer upper limit specific diffusion parameter
$a_{[1-5]}$	Heat coefficients
A_e	Surface area for face e
a_{meso}	Average pore size
a_{mw}	Additive molecular weight
a_{nb}	Link coefficients
A_p	Polymer specific diffusion parameter
B_F	Body force vector
b_{ij}	Adsorbed species stoichiometric coefficients
c	Molar concentration
$c_{[1-4]}$	Coefficients
C_e	Equilibrium concentration
C_F	Quadratic drag factor
C_i	Ith species concentration
C_{ij}	Bulk species stoichiometric coefficients
$C_{P,0}$	Initial concentration
C_{Total}	Total molar concentration
C_p	Specific heat
D	Diffusion coefficient
$D_{i,eff}$	Effective mass diffusion coefficient for species i
$D^T_{i,eff}$	Soret diffusion coefficient for species i
D_{ij}	Maxwell Stefan diffusion coefficients
d_p	Thickness of the polymer
D^*_p	Overestimated additive diffusion coefficient
D^*_p	Empirical worst case diffusion coefficient
D_p	Real additive diffusion coefficient

E_a	Activation energy
H_i	Enthalpies of gas species in the system
h_o	Total enthalpy
I	Unit tensor
i	Internal energy
$J_{Diff,i}$	Diffusion fluxes of gas species in the system
J_i	Flux of component i
k	Thermal conductivity
K	Permeability
k_c	Reaction rate constant
K_{eff}	Effective thermal conductivity
k_F	Thermal conductivity of the pores
$K_{fb/p}$	Partition coefficients between functional barrier and food
K_{fi}	Surface reaction forward rate
K_{ov}	Reaction rate constant
$K_{ov,mt}$	Overall mass transport coefficient
$K_{P,F}$	Polymer Food partition coefficient
K_{ri}	Surface reaction reverse rate
k_s	Thermal conductivity of the solid
L	Characteristic length scale
m	Total mass
M_F	Mole fraction
$M_{F,t}$	Migration value at time t
MW_i	Molecular weight of species i
MW_m	Migrant molecular weight
N	Number of components
$\underline{n}$	Vector normal to the surface
N_{as}	Number of adsorbed species
N_b	Number of bulk species
N_g	Number of gas phase species
N_{gr}	Number of grains
n_r	Number of chemical reactions
n_s	Number of involved species
$n_{x,y,z}$	Face normal unit vectors
nb	Values of neighboring cells
Pe	Peclet number
q	Heat flux
Q	Thermal energy flux
q_R	Radiative heat flux
R	Universal gas constant

R_{bed}	Radius of bed
r_i	Reaction rate for the ith species
R_i	Radius of sphere i
r_{in}	Inside radius of the coils
r_{out}	Outside radius of the coils
S	Surface area
$S_{adsorbing\_surface}$	Total adsorbing surface
S_h	Source terms
S_i	Production or destruction term rate for ith species
S_M	Rate of increase of momentum due to sources
S_Φ	Sources or Sinks of parameter Φ
Sh_o	Sherwood number
t	Time
T	Temperature
T_B	Bulk temperature
T^*	Dimensionless temperature
$\vec{u}$	Velocity vector
u	Velocity magnitude for x direction
U_{Di}	Diffusion velocity of component i
V	Volume
v	Velocity magnitude for y direction
V^n_c	Face normal component of the velocity at face e
V_F	Volume of food
V_P	Volume of Polymer
w	Velocity magnitude for z direction
X_i	Surface site fractions
X_i	Mass fraction of species i
Y_i	Mass fraction of species i
Y^w_i	Gas phase mass fraction adjacent to the wall
Y^ρ_i	Species mass fraction in the pore fluid
Z_{err}	Error function coefficient
Z_p	Polymer specific constant
Z_T	Temperature specific constant
α	Species activity
α_{ij}	Gas species stoichiometric coefficients
δ	Diffusion length scale
ε	Porosity
ε_{ce}	Characteristic energy
ζ	Chemical potential
κ	Boltzman constant

λ	Adsorption efficiency
Λ_i	Chemical Symbol of species i
μ_i	Dynamic viscosity of species i
ν'_{ij}	Forward stoichiometric coefficients for the i^{th} species in the j^{th} reaction
ν''_{ij}	Backwards stoichiometric coefficients for the i^{th} species in the j^{th} reaction
ν_{ij}	Total stoichiometric coefficients for the i^{th} species in the j^{th} reaction
ξ	Magnitude of the normal compressive stress
ρ	Density
ρ_s	Surface site density
ρ_w	Gas phase density
$\rho \not{f}_e$	Sum of external volume forces per unit volume
σ_i	Characteristic diameter of the molecules of species i
$\bar{\bar{\sigma}}$	Internal stress tensor
τ	Tortuosity of the porous media
τ_P	Polymer specific parameter
$\bar{\tau}$	Viscous shear stress tensor
Φ	Quantity
$\Phi_{i,j}$	Dimensionless quantity
$\dot{\omega}$	Volumetric production or destruction rate
ω_i	Production rates of the i^{th} species of the gas phase
Ω_μ	Collision integral

ΠΕΡΙΛΗΨΗ

Η ροή ρευστών και τα φαινόμενα μεταφοράς μάζας και ενέργειας διαδραματίζουν πολύ σημαντικό ρόλο στην ανθρώπινη ζωή και αποτελούν σημαντικό επιστημονικό πεδίο στο οποίο διεξάγεται συστηματική έρευνα. Η ανάγκη για την καλύτερη κατανόηση για την πρόβλεψη και για τον έλεγχο των φαινομένων μεταφοράς είναι απαραίτητη, κυρίως για βιομηχανικές εφαρμογές (αεροδυναμική, εξόρυξη πετρελαίου και φυσικού αερίου, εναλλάκτες θερμότητας, αντιδραστήρες, κλπ). Η δυσκολία της ανάλυσης αυτών των πολύπλοκων φαινομένων και η ανάγκη εξεύρεσης τρόπων αντιμετώπισης της αποτελεί μια πολύ ενδιαφέρουσα πτυχή τόσο για τις βιομηχανικές όσο και για τις τεχνολογικές ερευνητικές κοινότητες.

Επειδή ο πειραματισμός δεν είναι πάντοτε εύκολος, μπορεί να γίνει αναλυτική ή υπολογιστική προσομοίωση των φαινομένων χρησιμοποιώντας ως μέσο υπολογισμού ένα μαθηματικό μοντέλο. Ένα τέτοιο μοντέλο αποτελείται από πολλές διαφορικές ή / και αλγεβρικές εξισώσεις που καθιστούν δυνατή την περιγραφή των φαινομένων, αλλά και την πρόβλεψη για το πώς εξελίσσονται και αλληλοεπιδρούν (οι ποσότητες) μεταξύ τους. Αυτά τα μοντέλα βασίζονται στις θεμελιώδεις αρχές όπως η διατήρηση της μάζας, της ορμής και της ενέργειας.

Οι μαθηματικές εξισώσεις που ενσωματώνουν αυτές τις θεμελιώδεις αρχές είναι γνωστές εδώ και πολύ μεγάλο χρονικό διάστημα, αλλά στο παρελθόν είχαν περιορισμένο πεδίο εφαρμογής μέχρις ότου αναπτύχθηκαν οι πρώτες αριθμητικές μέθοδοι υπολογισμού και οι ψηφιακοί υπολογιστές. Προφανώς, η ποιότητα των αποτελεσμάτων εξαρτάται άμεσα από την επιλογή των δεδομένων που εισάγονται στο μοντέλο και από την ακρίβεια της αριθμητικής μεθόδου. Παρά τα αναπόφευκτα σφάλματα που προκύπτουν, οι κατά προσέγγιση λύσεις εξακολουθούν να παρέχουν πολλές σημαντικές πληροφορίες για το υπό εξέταση πρόβλημα.

Τα σύγχρονα περιβάλλοντα προσομοίωσης (τα οποία παρουσιάζονται λεπτομερώς στο Κεφάλαιο 2) είναι εφοδιασμένα με εργαλεία δημιουργίας και προσαρμογής πλεγμάτων, αξιόπιστους μηχανισμούς ελέγχου σφαλμάτων και αποτελεσματικούς επαναληπτικούς μηχανισμούς (μεθόδους) επίλυσης για τα αλγεβρικά συστήματα που προκύπτουν. Πλέον, είναι διαθέσιμα αρκετά εξελιγμένα μοντέλα με εκτεταμένο φάσμα εφαρμογής, ενώ ταυτόχρονα βελτιώνεται συνεχώς η διαχείριση πόρων που κάνουν, με αποτέλεσμα να είναι εφικτή η χρήση τους σε φορητό ή επιτραπέζιο υπολογιστή με μικρούς χρόνους εκτέλεσης, σε εφαρμογές όπου στο παρελθόν απαιτούνταν εβδομάδες υπολογισμών με την χρήση υπερ-υπολογιστών.

Η εργασία αυτή ασχολείται με την μαθηματική προσομοίωση φαινομένων μεταφοράς και με την εφαρμογή των προσομοιώσεων αυτών σε προβλήματα που ενδιαφέρουν τους μηχανικούς.

Η εργασία αυτή χωρίζεται σε τρία μέρη:

- Το πρώτο μέρος παρουσιάζει το απαραίτητο γνωστικό υπόβαθρο και αποτελείται από τα πρώτα δύο κεφάλαια. Αρχικά, στο πρώτο Κεφάλαιο παρουσιάζεται το υπόβαθρο που αφορά στις προσομοιώσεις καθώς και οι βασικές και απαραίτητες θεωρητικές περιγραφές των φαινομένων μεταφοράς. Στη συνέχεια, παρουσιάζεται στο Κεφάλαιο 2 μια αρκετά εκτενής βιβλιογραφία με αναφορές στις βασικές εξισώσεις των φαινομένων μεταφοράς και των εργαλείων προσομοίωσης (μοντελοποίησης).
- Το επόμενο δεύτερο μέρος περιλαμβάνει τα κεφάλαια 3 και 4, όπου παρουσιάζονται συγκεκριμένες εφαρμογές της προσομοίωσης των φαινομένων μεταφοράς. Πιο συγκεκριμένα, το κεφάλαιο 3 μελετά *το πρόβλημα της αλλαγής κλίμακας* και παρουσιάζει μια νέα εύκολη και γρήγορη μέθοδο για τον προσδιορισμό μεγεθών σε συνθήκες αλλαγής κλίμακας όταν μελετώνται φαινόμενα μεταφοράς που συμβαίνουν μέσα σε πορώδεις δομές. Το κεφάλαιο 4 περιέχει τις *εφαρμογές* των πιο πάνω σε τρία διαφορετικά συστήματα λύνοντας προβλήματα μεταφοράς μάζας και θερμότητας.
- Το τελευταίο τρίτο μέρος περιέχει τα *συμπεράσματα* αυτής της έρευνας (κεφάλαιο 5) καθώς και κάποιες *προτάσεις για μελλοντική εργασία* (κεφάλαιο 6).

Αναλυτικότερα, στο κεφάλαιο 3 παρουσιάζεται λεπτομερώς το πολύ σημαντικό πρόβλημα της εναλλαγής από μικρή κλίμακα εργαστηρίου σε μεγαλύτερη κλίμακα πεδίου και αντιστρόφως. Η λύση του προβλήματος αυτού μπορεί να χρησιμοποιηθεί σε αρκετές εφαρμογές τεχνολογικού και επιστημονικού ενδιαφέροντος και να διευκολύνει την δημιουργία μοντέλων ανάλυσης της μεταφοράς ρύπων, την αποκατάσταση μέσω απορρύπανσης των εδαφών ή/και του νερού όσο και για την εκπόνηση αναλύσεων επικινδυνότητας, αλλά και να βρει εφαρμογή σε πολλές άλλες περιοχές ενδιαφέροντος των μηχανικών.

Η αλλαγή κλίμακας είναι μια διαδικασία αντικατάστασης ενός ετερογενούς μέσου με ένα ομογενές μεγαλύτερης κλίμακας, μεταφέροντας τις παραμέτρους από την μικρή στην μεγαλύτερη ή και αντίστροφα. Ο στόχος της μεθόδου αυτής είναι η ανάκτηση των ισοδύναμων χαρακτηριστικών των μεγεθών που αφορούν σε διάφορους τρόπου υπολογισμού του μέσου όρου τους. Οι γεωμετρίες στις οποίες εφαρμόστηκε η συγκεκριμένη τεχνική είναι η γεωμετρία ενός κόκκου μέσα σε ένα όγκο ελέγχου (μικροσκοπική κλίμακα), μια συστοιχία σφαιρών σε ένα όγκο ελέγχου (μεσοσκοπική κλίμακα) και τέλος ένα πορώδες παραλληλεπίπεδο (μακροσκοπική κλίμακα). Οι γεωμετρίες αυτές επιλέχθηκαν καθώς η κάθε μια από αυτές χαρακτηρίζει την αντίστοιχη κλίμακα.

Για την αριθμητική επίλυση των εξισώσεων, επιλέχθηκε το προγραμματιστικό περιβάλλον CFD-ACE+, το οποίο χρησιμοποιεί την μέθοδο πεπερασμένων όγκων. Η αριθμητική επίλυση των εξισώσεων δίνει μια διακριτή λύση, η οποία αποτελείται από τις τιμές των μεταβλητών στα κέντρα των κελιών. Η αριθμητική μέθοδος για την επίλυση των Μερικών Διαφορικών Εξισώσεων

(ΜΔΕ) που περιγράφουν τη φυσική για κάθε ενότητα, περιλαμβάνει τη διακριτοποίηση των ΜΔΕ σε ένα υπολογιστικό πλέγμα, την παραγωγή ενός συστήματος εξισώσεων και τη λύση τους, συνήθως με μια επαναληπτική μέθοδο. Για να ξεκινήσει η διαδικασία της αριθμητικής επίλυσης, γίνεται πρώτα η διακριτοποίηση της γεωμετρίας στην οποίαν εφαρμόζονται οι διαφορικές εξισώσεις, έτσι ώστε να παραχθεί ένα σύνολο αλγεβρικών εξισώσεων. Στην προσέγγιση των πεπερασμένων όγκων που χρησιμοποιείται από το λογισμικό CFD-ACE+, οι εξισώσεις που διέπουν τα φαινόμενα γράφονται σε κάθε έναν από τους όγκους ελέγχου και μπορούν να εκφραστούν με την μορφή μιας γενικής εξίσωσης μεταφοράς,

$$\frac{\partial \rho \Phi}{\partial t} + \nabla \cdot (\rho \vec{u} \Phi) = \nabla \cdot (\Gamma \nabla \Phi) + S_{\Phi}$$

όπου, ο πρώτος όρος είναι η ρυθμός μεταφοράς, ο δεύτερος όρος είναι η μεταφορά με συναγωγή, ο τρίτος είναι η μεταφορά λόγω διάχυσης και ο τελευταίος όρος είναι οι πηγές/καταβόθρες. Μετά την αριθμητική ολοκλήρωσή τους, ο όρος της μεταφοράς, η διάχυση και οι πηγές τοποθετούνται μαζί, με αποτέλεσμα την ακόλουθη γραμμική εξίσωση,

$$\left(a_p - S_p\right)\Phi_p = \sum_{nb} a_{nb}\Phi_{nb} + S_U$$

όπου, nb οι τιμές γειτονικών κελιών και a_{nb} ο συντελεστής σύνδεσης μεταξύ τους. Αυτή η εξίσωση των Πεπερασμένων Διαφορών, είναι η διακριτή ισοδύναμη της εξίσωσης συνεχούς μεταφοράς. Είναι γενικά μη γραμμική επειδή οι συντελεστές σύνδεσης είναι συνάρτηση των p, nb, κλπ. Όταν ένα τέτοιο σύστημα είναι σχεδιασμένο για κάθε υπολογιστικό κελί και οδηγεί σε ένα σύνολο συζευγμένων μη γραμμικών αλγεβρικών εξισώσεων, οι οποίες γραμμικοποιούνται και επιλύονται επαναληπτικά.

Αρχικώς, τα μαθηματικά μοντέλα εφαρμόστηκαν με στόχο να μελετηθεί η αλλαγή κλίμακας σε προβλήματα μεταφοράς μάζας. Το ερώτημα εδώ αφορά στον προσδιορισμό των τιμών των παραμέτρων προκειμένου να μπορούν να μεταφερθούν τα αποτελέσματα της μεταφοράς μάζας από την μια κλίμακα στην άλλη. Ως μελέτη περίπτωσης, επελέγη η μεταφορά μάζας σε κοκκώδες μέσο, ενώ όλες οι προσομοιώσεις έγιναν για ίδια πορώδη και ίδιες συνθήκες ροής διατηρώντας το εύρος των αριθμών Peclet (*Pe*), ίδιο για την κάθε κλίμακα. Τα αποτελέσματα της προσομοίωσης είναι πως ο συντελεστής απόδοσης προσρόφησης, λ, που συμβολίζει το ποσοστό του προσροφημένου συστατικού, εξαρτάται από τις συνθήκες ροής και από το πορώδες της κάθε γεωμετρίας. Πιο συγκεκριμένα, όσο ο αριθμός *Pe,*που περιγράφει τον λόγο της συναγωγής προς την διάχυση, μειώνεται, (δηλαδή όσο πιο σημαντική γίνεται επίδραση της διάχυσης στο σύστημα) το λ αυξάνεται. Αυτή η συμπεριφορά παρουσιάζεται σε όλες τις προσομοιώσεις ενώ είναι συμβατή με όσα αναφέρονται στην βιβλιογραφία για άλλα συστήματα. Σε όλες τις προσομοιώσεις η επίδραση του πορώδους στο λ έχει ως αποτέλεσμα, όσο μειώνεται το ε, να αυξάνεται το λ. Αυτό όμως δεν πραγματοποιείται στην προσομοίωση της μικροσκοπικής κλίμακας. Στην μικροσκοπική κλίμακα παρατηρούμε πως για Pe>100 η συμπεριφορά είναι η αντίθετη, γεγονός που οφείλεται στις τοπικές πάρα πολύ μεγάλες τιμές της ταχύτητας που οδηγούν σε τυρβώδη ροή, αλλά και στην επίδραση της ασυνέχειας που εγγενώς έχουν τα μοντέλα αυτά.

Για να γίνει η μεταφορά των χαρακτηριστικών για την αλλαγή της κλίμακας εφαρμόστηκαν τα πιο κάτω βήματα. Αρχικά υπολογίστηκαν όλα τα γεωμετρικά χαρακτηριστικά της συστοιχίας των σφαιρών και στη συνέχεια προσαρμόσαμε την ταχύτητα εισόδου ώστε να διατηρήσουμε τον αριθμό Peclet ίδιο και για τις δύο κλίμακες. Στην συνέχεια έγινε η θεώρηση πως οι συντελεστές διάχυσης, εφ’ όσον τα συστατικά και οι περιβαλλοντικές συνθήκες είναι ίδιες, είναι ίσοι και στις δυο περιπτώσεις. Επόμενο βήμα είναι η προσαρμογή της αναλογίας επιφάνειας προς όγκο του πορώδους υλικού (S/V) με αποτέλεσμα τον κανόνα που ορίζει ότι, αν θέλουμε να αλλάξουμε την κλίμακα για “x” τάξεις μεγέθους, θα πρέπει να μειώσουμε το S/V κατά τις ανάλογες “x” τάξεις μεγέθους. Ως τελικό βήμα είναι η προσαρμογή του μέσου μεγέθους των πόρων της πορώδους δομής. Το μέγεθος αυτό για την μεσοσκοπική κλίμακα υπολογίζεται αναλυτικά ολοκληρώνοντας πάνω στη σχετική επιφάνεια έτσι ώστε να έχουμε μια αντιπροσωπευτική τιμή. Ο κανόνας αλλαγής για αυτό το μέγεθος είναι παρόμοιος με το προηγούμενο βήμα με μικρές διαφοροποιήσεις.

Μετά τη λύση του προβλήματος της μετάβασης της κλίμακας, πραγματοποιήθηκαν οι εφαρμογές των προαναφερθέντων φαινομένων σε 3 διαφορετικά προβλήματα: (α) στην περίπτωση της απορρύπανσης μιας κλειστής λίμνης που εμφανίζει ευτροφισμό, (β) στην μελέτη της θέρμανσης καυσίμου για τροφοδοσία πλοίων, και (γ) στη μελέτη της μετανάστευσης ουσιών σε τρόφιμα.

Στην πρώτη εφαρμογή διερευνήθηκε η διαδικασία προσρόφησης φωσφορικών αλάτων από ρυπασμένο νερό, τόσο πειραματικά όσο και θεωρητικά (μοντελοποίηση). Ως προσροφητική ουσία επιλέχθηκε το Phoslock^{TM}, ένα ευρέως διαδεδομένο υλικό αποκατάστασης που στοχεύει στον έλεγχο της ελαχιστοποίησης του φωσφόρου στα φυσικά υδάτινα οικοσυστήματα. Στα πλαίσια της έρευνας αυτής πραγματοποιήθηκαν πειράματα σε εργαστηριακή κλίμακα εξετάζοντας την απόδοση του Phoslock™ ως προσροφητικού υλικού και παράλληλα διεξήχθησαν λεπτομερείς προσομοιώσεις, επιτρέποντας καλύτερη κατανόηση της διαδικασίας αφαίρεσης του φωσφόρου από το νερό. Η αποτελεσματικότητα της προσρόφησης όπως εκτιμήθηκε σύμφωνα με τις προσομοιώσεις βρέθηκε να είναι περίπου 87,41%, η οποία βρίσκεται σε εξαιρετική συμφωνία με αυτή που μετρήθηκε πειραματικά (περίπου 87%). Ωστόσο, αν και η εκτίμηση συμφωνεί και με τις δύο μεθόδους για θερμοκρασία 25°C, όσο μειώνεται η θερμοκρασία διαπιστώθηκε ότι είναι όλο και πιο κακή, με διαφορά περί το 10% για τη χαμηλή θερμοκρασία των 10°C. Αυτή η ασυνέπεια μεταξύ της πειραματικής και της θεωρητικής απόδοσης μπορεί να αποδοθεί στις εσωτερικές ανεπάρκειες της προσέγγισης «unit cell», η οποία διαπιστώθηκε πως υπερεκτιμά την αποτελεσματικότητα της προσρόφησης. Όπως αναφέρθηκε και πιο πάνω η προσέγγιση του «unit cell» παρουσιάζει μια ασυνέχεια στο σημείο όπου η επιφάνεια εισόδου της ροής συναντά την επιφάνεια εξόδου της.

Τα φαινόμενα μεταφοράς θερμότητας σε βιομηχανική κλίμακα, εφαρμόστηκαν για την διερεύνηση μιας κοινής πρακτικής για τη ναυτιλία, κατά την οποία υπερθερμασμένο νερό χρησιμοποιείται σε σωληνώσεις για την θέρμανση αργού πετρελαίου. Η απόδοση της διαδικασίας μεταφοράς θερμότητας συνδέεται έντονα με τις διαστάσεις της σωλήνωσης (μήκος, πάχος και διάμετρος) καθώς και με τις λειτουργικές παραμέτρους (θερμοκρασία πετρελαίου, θερμοκρασία ατμού, πίεση ατμού). Σε αυτή την περίπτωση, μελετήθηκε η μεταφορά θερμότητας από υπερθερμασμένο νερό, σε υψηλή θερμοκρασία (424K) και σταθερή πίεση (5bar) σε δεξαμενές καυσίμου πετρελαίου ειδικών διαστάσεων και διαφόρων μηκών, διαμέτρων και πάχους, τόσο μακροσκοπικά, μέσω μιας δυναμικής προσέγγισης καθώς και μικροσκοπικών προσομοιώσεων. Σκοπός αυτής της μελέτης είναι η εκτίμηση του αναγκαίου μεγέθους και μήκους των σωλήνων υπό την προϋπόθεση πλήρως μονωμένης δεξαμενής. Στα πλαίσια της μελέτης διενεργήθηκε και μια παραμετρική ανάλυση ώστε να προσδιοριστεί η σχετική επίδραση της κάθε παραμέτρου στην απόδοση της διεργασίας. Η επίδραση των πιο κρίσιμων παραμέτρων στα αποτελέσματα είχε ως τελικό αποτέλεσμα το βέλτιστο μήκος περίπου 160m για το οποίο παρατηρήθηκε το συντομότερο χρονικό διάστημα επίτευξης του στόχου της διαδικασίας. Ειδικότερα, το μέγιστο μήκος που μπορεί να καθοριστεί λόγω των περιορισμών στα γεωμετρικά χαρακτηριστικά της δεξαμενής δεν μπορεί να υπερβεί τα 160m για ένα στρώμα σπειροειδούς χάλυβα με διάμετρο 50mm και πάχος 4mm. Το σύστημα αυτό μπορεί να αυξήσει τη θερμοκρασία κατά 30K σε περίπου 9,5 ώρες σύμφωνα με τη θερμοδυναμική ανάλυση το οποίο βρίσκεται πολύ κοντά στις 10 ώρες που υπολογίζονται σύμφωνα με τις λεπτομερείς τρισδιάστατες προσομοιώσεις. Το πιο αποτελεσματικό σενάριο διαπιστώθηκε ότι είναι η εγκατάσταση διπλής στρώσης σωλήνα άνθρακα-χάλυβα, η οποία αύξησε το συνολικό μήκος σε περίπου 300m και περιόρισε το χαρακτηριστικό χρόνο σε διάστημα 5 ωρών. Ωστόσο τα μειονεκτήματα για ένα τέτοιο σενάριο εντοπίζονται στην ομοιογένεια του προφίλ της θερμοκρασίας αλλά κυρίως στο αυξημένο αρχικό κόστος εγκατάστασης αυτής της κατασκευής. Τέλος, πρέπει να αναφερθεί ότι η θερμοκρασία του πετρελαίου εντός της δεξαμενής του βρέθηκε να είναι σχεδόν ομοιόμορφη.

Η τρίτη και τελευταία εφαρμογή των πιο πάνω φαινομένων αφορά την διαδικασία εκτίμησης των ποσοτήτων που μεταφέρονται από τα πολυμερή υλικά συσκευασίας προς τα τρόφιμα. Η έννοια της μετανάστευσης από τα υλικά συσκευασίας τροφίμων, υπό τις περιβαλλοντικές συνθήκες που αναμένονται κατά τον πλήρη κύκλο ζωής των τροφίμων, διερευνήθηκε ως η τρίτη μελέτη περίπτωσης κατά την οποία εξετάζεται η ανάγκη βελτιστοποίησης των υφιστάμενων μηχανισμών υπολογισμού των κρίσιμων ποσοτήτων. Τα κυριότερα μοντέλα που εξετάζουν το πολύπλοκο αυτό φαινόμενο, βασίζονται κυρίως στην διάχυση (νόμος του Fick), παραβλέποντας τους πιο πολύπλοκους μηχανισμούς μεταφοράς μάζας που αντικειμενικά υφίστανται καθώς επίσης και την επίδραση από το περιβάλλον. Τα μοντέλα αυτά υπερεκτιμούν τη μετανάστευση και έτσι δίνουν ικανοποιητικά αποτελέσματα όσον αφορά στην ασφάλεια χρήσης του τροφίμου, αλλά δεν μπορούν να περιγράψουν ποσοτικά την εξέλιξη της ποιότητάς του. Σκοπός της μελέτης αυτής είναι η εξέταση των μοντέλων αυτών και η συζήτηση της εφαρμογής τους. Κατά την συζήτηση της εφαρμογής τους εντοπίστηκαν οι μεγαλύτερες ανεπάρκειες τους: (α) δεν λαμβάνουν υπόψιν το περιβάλλον ως στοιχείο του συστήματος παρά μόνον ως παράγοντα που επιβάλλει συνθήκες, (β) θεωρούν πως η μεταφορά μάζας από το υλικό συσκευασίας προς το τρόφιμο και αντιστρόφως γίνεται λόγω διάχυσης και μόνον, με συνέπεια η μαθηματική της περιγραφή να περιορίζεται αποκλειστικά στην διατύπωση του Νόμου του Fick για τη συγκεκριμένη γεωμετρία, και (γ) δεν λαμβάνει υπόψη του την μεταβολή της σύστασης του προϊόντος κατά τον συνολικό χρόνο ζωής του. Όμως το περιβάλλον είναι ένα δομικό στοιχείο του συστήματος, το οποίο δύναται να προκαλέσει (και όχι μόνο να καθορίσει) σε κάποιον, ενδεχομένως σημαντικό βαθμό, τη μεταφορά μάζας στο τρόφιμο. Επίσης στην πραγματικότητα, υπάρχουν πολλές περιπτώσεις όπου τα φαινόμενα που συμβαίνουν είναι πιο πολύπλοκα από την απλή διάχυση καθώς παρατηρούνται φαινόμενα partitioning, διόγκωσης, χημικές αντιδράσεις στις διεπιφάνειες, προσρόφηση, κ.α. Τέλος, περιγράφονται και προτείνονται συγκεκριμένες και πιο ολοκληρωμένες προτάσεις για την χρήση πιο εξειδικευμένων μοντέλων που θα περιλαμβάνουν τις αλληλεπιδράσεις μεταξύ συσκευασίας τροφίμων, με πλήρη συσχέτιση με τις περιβαλλοντικές επιδράσεις. Κατανοώντας το προϊόν, την αλληλεπίδραση του με το περιβάλλον και τον προστατευτικό ρόλο της συσκευασίας, θα μπορεί να σχεδιαστεί έτσι η συσκευασία ώστε να μεγιστοποιηθεί ο χρόνος ζωής του συσκευασμένου τρόφιμου και να διατηρηθεί η ποιότητά του σε υψηλό επίπεδο. Το συμπέρασμα της εξέτασης του μηχανισμού αυτού είναι η αναγνώριση της αναγκαιότητας της υπέρβασης της μονόπλευρης διαδικασίας διάχυσης, η οποία θεωρείται ως ένας ενιαίος μηχανισμός για την περιγραφή και ποσοτικοποίηση της μεταφοράς μάζας από τη συσκευασία προς τα τρόφιμα. Για πιο ακριβή αποτελέσματα πρέπει να ενσωματωθούν στους μηχανισμούς εκτίμησης πιο περίπλοκα φαινόμενα που μέχρι τώρα δεν λαμβάνονται υπόψη (π.χ ρόφηση, επιφανειακές αντιδράσεις κλπ.), καθώς και οι συνθήκες του περιβάλλοντος (π.χ. θερμοκρασία, ακτινοβολία, κλπ.)

Συνολικά, στην παρούσα διατριβή μελετήθηκαν και αναλύθηκαν τα φαινόμενα μεταφοράς και δείχθηκε ότι η χρήση της προσομοίωσης μέσω εξελιγμένων μαθηματικών μοντέλων μπορεί να μιμηθεί αποτελεσματικότερα τη συμπεριφορά της διαδικασίας ή του συστήματος με την πάροδο του χρόνου, εφόσον τροφοδοτηθεί με τα σωστά δεδομένα. Η προσομοίωση χρησιμοποιήθηκε και κατέστη σαφές ότι μπορεί να περιγράψει, να αναλύσει και να προβλέψει τη συμπεριφορά ενός συστήματος. Η χρήση μοντέλων μπορεί να αποτελέσει σημαντική βοήθεια στο σχεδιασμό πραγματικών συστημάτων, βελτιστοποιώντας την απόδοσή τους εξαρχής και μειώνοντας το κόστος αλλά και τον χρόνο σχεδιασμού.

ABSTRACT

The main aim of the work of this PhD was to investigate the need and the applicability of a fast and easy method in order to define quantities when transport phenomena are under investigation. After the introduction and the background review presented in the first chapter, Chapter 2 investigates the fundamental transport processes, affected by advection and diffusion, for all the used scales, microscopic, mesoscopic and macroscopic. Chapter 2 includes a brief but detailed discussion regarding the most widely used CFD models and the modules utilized by the selected CFD-ACE.

A big part of this study, aims to develop a fast and easy method to match the macroscopic quantities (such as adsorption efficiency) during a scale transition process, from mesoscopic to macroscopic (scale-up), or to microscopic (scale-down) and vice versa, geometries. In order to be able to transit from one scale to another, the fundamental transport processes (laminar flow, convection, diffusion and heterogeneous reaction) were described in detail for all three scales, following the same flow conditions given by the use of the dimensionless Peclet number. Furthermore, a surface catalytic reaction on species mass fractions is analyzed. The reactants are consumed on the catalytic surface and their mass fraction as expected decreases as the exit of the porous media is reached. On the other hand, the steam and carbon dioxide are produced due to the oxidization reaction and their mass fractions increase towards the exit. It should be noted that, for the microscopic case (sphere-in-cell) and the mesoscopic scale (assemblage of spheres), which represent a more analytical view of the porous media, formed a gradient from the catalytic surface towards the pores due to the combinatory effect of the prevailing transport phenomena.

Next, a method of matching the geometrical parameters when scale transition occurs is proposed, underlying the necessary steps that should be followed. As the first step the calculation of the geometrical characteristics of the detailed geometry is a necessity as it will be the base where the transition will be relied on. Then, the inlet mixture flow needs to be adjusted in order to preserve the Peclet number for all of the scales. Since the diffusion coefficients are practically constant, this adjustment can be made only by adapting the velocity to the necessary value. Finally, the last two most important adjustments are required to be made in order to have an identical characterization of the geometry without any discrepancies. The characteristic ratio, S/V of the porous material, is a measurement value of the available surface where the reaction may occur.

After studying the scale transition problem, three case studies implementing the transport phenomena (as presented and discussed in Chapter 2) were analyzed. The three studies considered the applicability of the mathematical simulation of transport phenomena in the case of water remediation, heating of marine heavy oil and migration in packed foods.

The first study simulates the case of water remediation, investigating the adsorption process

from both experimental and theoretical (modeling) point of view. The adsorption process of phosphate onto Phoslock^{TM}, is an increasingly used worldwide restoration tool aiming the control a minimization of phosphorus in natural water ecosystems. Bench-scale batch experiments were performed examining Phoslock's^{TM} efficiency as an adsorbent and detailed simulations were carried out, allowing a better understanding of the phosphate removal process.

The second case study simulated the heat transfer case utilized in an industrial scale problem investigated a rather common marine practice. In marine industry, the use of superheated water in heating coils for heating up heavy fuel oil is essential. The goal of this study was to estimate the necessary size and length under the assumption of an insulated tank. A parametric analysis was also performed to identify the relative influence of each parameter on the process performance.

The concept of migration from polymeric packaging materials to food and food simulants, under the environmental conditions expected during the food products' complete life cycle, was investigated for the third case study. The aim of this case study was to consider these models and weight them against their extensive use. After having identified the areas of their inadequacies in validating the migration during food process applications were found to potentially affect food quality rather than safety. This study outlined and proposed specific and eventually more complete directions, for future modeling approaches regarding the food–packaging interactions, comprehensively involving the storage environment in terms of both conditions and constituents. The outcome of this work is the proposal to go beyond the consideration of the diffusion process as being the single mechanism to describe the migration from packaging to foodstuffs, but rather to incorporate more complicated phenomena (sorption, surface reactions, etc.) to overcome the above-mentioned discrepancies.

Overall, in the present thesis the transport phenomena, were analytically studied from modelling point of view and it was proved that the use of simulation with a computerized mathematical model imitates the behavior of a real-world process or system over time. Simulations are used to describe and analyze the behavior of a system when asking "what-if" questions about real-life systems. Furthermore, mathematical models could be very helpful tools for designing artificial systems, while the easy and quick description of phenomena occurring in porous media could be feasible.

1. INTRODUCTION

1.1. BACKGROUND AND MOTIVATION

Transport phenomena and fluid dynamics, such as heat and mass transfer, play a very important role in human life. Gases and liquids surrounding us, flowing inside our bodies and have a profound influence on life. Real life phenomena such as wind, rain, flood, and hurricanes are understood by the fundamental transport phenomena equations. For example, convection and diffusion are responsible for the transport of pollutants in air, water and soil.

The need for a better understanding, for a prediction ability, and even for the control on the transport phenomena is essential for numerous industrial applications, such as aerodynamics, oil recover, gas application, heat exchangers, and chemical reactors. A way to overcome the difficulty of analyzing these complex phenomena is a very intriguing aspect for both industrial and technological communities.

An analytical or computational study can be performed on the basis of a suitable mathematical model. Such a model is consisted by several differential and/or algebraic equations which make it possible to predict how the quantities of interest evolve and interact with one another. A drawback to this approach is the fact that complex physical phenomena give rise to complex mathematical equations that usually cannot be solved analytically.

These fluid flow models are based on the fundamental principles such as conservation of mass, momentum, and energy. The mathematical equations that embody these fundamental principles have been known for a very long time but found hard to use until numerical methods and digital computers were developed. The principal equations of fluid dynamics are based on the dynamical behavior of a fluid determined by conservation laws, presented below:

i. the conservation of mass,
ii. the conservation of momentum, and
iii. the conservation of energy.

The above fundamental principles have led to widely accepted mathematical descriptions, such as Navier-Stokes equations for the flow, Fick’s equations for the diffusion, etc.

During the second half of the twentieth century, a new branch of applied mathematics dealing with numerical simulation of fluid flows, known as, Computational Fluid Dynamics (CFD), was introduced. Nowadays, computer codes based on CFD models are used to predict a variety of complex flow phenomena. These events are related by taking into consideration of action and interaction of the occurring phenomena such as dissipation, diffusion, convection, slip surfaces, boundary layers, reactions, adsorptions etc. (Blazek, 2001) (Harvard et al, 1999).

Over the last four decades, the market for CFD software has expanded rapidly, and remarkably making huge progress. The rapid development of numerical algorithms with an astonishing variety of finite difference, finite element, finite volume, and spectral schemes were developed. The equations of fluid mechanics were applied almost for every flow problem of practical importance. (Malekjani and Jafari, 2018)

Before we turn to the basic theories and equations describing the transport phenomena and the behavior of a fluid, it may be appropriate to clarify what is the meaning of “fluid dynamics”. The dynamics of fluids flow through a medium is a relatively old topic. It stands for the investigation of the motion of a large number of individual particles through or around a medium. Generally, this concludes to the hypothesis that the density of the fluid is high enough, allowing it to be approximated as a continuum. By following this hypothesis, we are able to define velocity, pressure, temperature, density and other important quantities at each point of the medium (Blazek, 2001).

The use of CFD software as a tool for analyzing complex phenomena offers huge economic benefits and can contribute to the human well-being. The traditional approach to investigate and explain a physical process is based on observations, experiments, and measurements. The amount of information that can be obtained in this way is usually very limited and subject to measurement errors. Moreover, experiments are only possible when a laboratory-scale model or the actual equipment has already been built. An experimental investigation may be very time consuming, dangerous, expensive, or even impossible for many reasons.

The quality of the results depends directly on the choice of the data imported to the model and on the accuracy of the numerical method. In spite of the inevitable numerical and modeling errors, the approximate solutions still can provide a lot of important information at a fraction of the cost that a full-scale and accurate investigation would require. The basic principle of the CFD modeling method is simple. The flow regime is divided into small cells within each of which the flow either kept constant or varies smoothly. The differential equations of momentum, energy and mass balance are discretized and represented in terms of variables at the cell centers or at a predetermined position within the cells. These equations are solved until the solution reaches the desired accuracy (Chapra and Canale, 2015).

The choice of a CFD model is based on the nature of the physical process to be simulated, by the objectives of the numerical study, and of course by the available resources. As a rule, the mathematical model should be as detailed as possible without making the computations too expensive in memory and time. The use of a universally applicable model makes it difficult to develop and implement efficiently the numerical algorithm within. In many cases, the desired information can be obtained incorporating empirical correlations supported by theoretical or experimental studies. Thus, an hierarchy of fundamental, phenomenological, and empirical models is usually available for particularly difficult problems.

Modern CFD codes, which will be discussed in detail later on, are equipped with automatic mesh generation/adaptation tools, reliable error control mechanisms, and efficient iterative solvers for sparse linear systems. The rapid growth of computing power has stimulated implementation of more sophisticated models and extended the range of its applicability to very complex problems. Nowadays, 3D complex simulations of transport processes can be performed on a laptop or desktop computer, where decades ago supercomputers were required (Blazek, 2001)(Silbert et al, 2001).

Such a complex simulation may be the result of the simulation of a phenomenon in a porous medium. Modeling seems to be a grateful tool for understanding transport phenomena in the complex invisible internal structure of porous materials. CFD has been successfully used in modeling various multiphase flow systems, such as gas-solid mixtures, etc. Multiphase CFD models can help to understand the complex interactions between the different phases and provide detailed, 3D, transient information that experimental approaches may not be able to provide. These applications amongst others, demonstrate the ability to simulate complex flows, even with the presence of chemical reactions and therefore the possibility of exploiting it to investigate a wide range of processes (Bode, 1994) (Harris et al, 1996) (Anderson et al, 1984).

Before analyzing the field of modeling in depth, a brief introduction to porous materials has to be made. In general, the processes occurring within, must be defined explaining what actually is a porous medium/material. In fact, as porous, is meant to be the void space between at least two surfaces of a number of solids that air or any other fluid can flow through. Porous material is called any solid that contains cavities, channels and interstices. Porous medium is a region in space comprising of at least two homogeneous material constituents, presenting identifiable interfaces between them in a resolution level, with at least one of its constituents remaining fixed or slightly deformable (Coutelieris and Delgado, 2012).

As far as the nature of a porous material has been defined, it’s time to explain why porous materials are so interesting and the reason this PhD is partly engaged with this type of materials. Besides the wide spectrum of applications that porous materials have found during the last centuries, these structures are not transparent, thus it’s necessary to describe any processes occurring within them without local observation, and based only on macroscopic data regarding the inlet and outlet of the domain. The complexity of porous structures usually corresponds to very complex local scale phenomena, which should be integrated with simpler macroscopic ones. For instance, when the geometry of the porous material is constituted by very narrow pores (capillarity), a very low volumetric flow-rate would lead to extremely high local velocity and consequently high Reynolds number (turbulence).

Granular materials are made up of individual spherical or spheroidal particles, in nature, or even in a laboratory. These materials do not receive much kinetic energy from increases in temperature as gas particles would; and this is explained due to the large size of the particles keeping them ungoverned by temperature changes. The particles in granular materials are large enough so that their motion can be described without having to use quantum physics, which accurately describes the motion of particles approaching atomic and subatomic size.

Fluid flow within granular materials can be described using just regular, classical physics, which means that it is easy to predict the path of one particle when it is set into motion. Another property of granular materials is that they collide in elastically, meaning that when multiple particles collide, the act of collision helps to dissipate the particles kinetic energy and as a result, the particles come to rest shortly after they collide with each other. This is assuming that the particles are roughly of the same mass and size.

Finally, maybe the most important point regarding granular materials is that they are surrounded by a fluid or vacuum. The two most common media in which granular materials may be found are air and water. Transport phenomena of granular materials are studied, on many different length scales, on a wide range of dynamic situations such as shear flow and vibration experiments, studies of geological debris flows, etc. Yet for all the intense activity in this field over the years, the rheology of granular systems still remains a largely unsolved problem (Silbert et al, 2001).

The development of the particles follows Newton's equations, with repulsive forces between particles that are non-zero only when there is a contact between particles. Although these materials are very simple to describe, they exhibit a tremendous amount of complex behavior, much of which has not yet been satisfactorily explained. They behave different from solids, liquids and gases, which have led many scientists to characterize them as a new form of matter.

1.2. RESEARCH OBJECTIVES AND SCOPE

The main objective of this PhD is to establish and describe the applicability of a fast and easy method of simulating different transport phenomena occurring in systems that have never been simulated before. All three transport phenomena have been implemented in industrial scale systems confirming their applicability in different scales. To this end, the focus of this research is placed on the following aspects:

The main aim of the work of this PhD was to investigate the need and the applicability of a fast and easy method in order to define quantities when transport phenomena are under investigation

1. Description of transport phenomena,
2. Definition and solution of scale transition problem,
3. Applicability of transport phenomena in three different case studies.

2. THEORY

The study of fluid mechanics and transport phenomena involves the association of difficulties which are encountered in different disciplines such as thermodynamics, diffusion, chemical reactions, etc. This chapter is intended to cover all of the aforementioned disciplines in a detailed fashion. The main objective is to present the study of the fluids flow and the main equations in terms of the mass and heat transfer. The development of new tools which are at the same time specialized and universal was very much a characteristic of science in the 20th century. Thus, numerical methods, is an autonomous tool for engineers or researchers working in the domain of fluid mechanics and chemical engineering. In the same way, various domains in industrial design require a solid knowledge of fluid mechanics in addition to that of their specific topics. (Peube, 2010)

2.1. TRANSPORT PROCESSES

Transport phenomena are various mechanisms by which extensive thermodynamic quantities (particle number, mass, electric charge, heat) move from one place to another. These phenomena include the flow of liquids or gases, the diffusion of particles, convection, electric current, heat conduction, etc.

In spite of the obvious differences between these phenomena, there are many similarities in the description of the transport processes, and also in the general principles that underlie these processes. The principles underlying these phenomena are the conservation laws and more specifically, the conservation of mass, energy and momentum.

Before analyzing the complexities of fluid mechanics, the basic governing laws must be established. It is certainly recognized that many flow situations can be very complex, with phenomena which are globally encountered in nature and in technology. In addition, numerical analysis has led to a new approach and a new way of looking at the laws of fluid mechanics. Although these laws can be written in many different mathematical forms, they have led us to put forward a specific form, through the concept of conservation and of conservation laws. This concept will be presented to most of this subchapter.

We present here the most general form of a conservation law, without specifying the nature of the ‘conserved’ quantity. To achieve this, we have to define first what conservation is and how we recognize an equation written in that form. This is a fundamental concept for numerical methods and it is connected to the requirement that, after the equations are discretized, essential quantities such as mass or energy will be conserved at the discrete level. This is certainly the most essential law, because a numerical simulation wherein mass or energy would be lost, due to numerical artifacts, would be totally useless and not reliable.

A conservation law is strongly associated to the concept of fluxes and we will introduce in Section 2.1.2 the extremely important distinction between convective and diffusive fluxes. This distinction is crucial to the whole world of fluid mechanics. Based on the discussion presented here, now we may proceed to apply the general conservation laws to the three quantities that define the laws of fluid mechanics; mass, momentum and energy, described and developed in detail in Sections 2.1.2, 2.1.3 and 2.1.4.

2.1.1. CONTINUITY EQUATION

The conservation law is very simple and with fundamental logic, but it also can become complicated by its internal content. Conservation, means that the variation of a quantity flowing within a given volume is due to the net effect of some internal sources and of the amount of that quantity which is crossing the boundary surface. This amount is called the flux and its expression results from the properties of the fluid. The fluxes and the sources are in general dependent on the space –time coordinates, as well as on the motion of the fluid. The associated fluxes are vectors for a scalar quantity and tensors for a vector quantity like momentum (Bird et al, 1960).

The main equation that always must be satisfied is the generic transport equation,

$$\frac{\partial \rho \Phi}{\partial t} + \nabla \cdot (\rho \vec{u} \Phi) = \nabla \cdot (\mathcal{D} \nabla \Phi) + S_{\Phi} \qquad (2.1)$$

where the first term is the rate of transport of quantity Φ, the second term is transport due to convection, the third is transport due to diffusion and the last term are the sources or sinks. Given that equation (2.1) applies for the conservation of anything, it is now straightforward to consider conservation of the 3 most important quantities, mass, energy and momentum (force balance). This is represented in total five equations, as the momentum, defined as the product of density and velocity, is a vector with three components in space. Reviews by Kaviany (1991) and Calmidi (1998) are good sources for detailed derivations and discussion.

2.1.2. MASS CONSERVATION LAW

The law of mass conservation is a general statement of kinematic nature, which is independent of the nature of the fluid or of the forces acting on it. It expresses the empirical fact that in any system closed to all transfers of mass and energy, mass cannot disappear from it, nor be created. Hence, the quantity of mass is conserved over time.

We can state the mass conservation law for a quantity as (Bird et al, 1960) (Perry, 1999), (McCabe et al, 2004):

$$\frac{\partial (\rho c)}{\partial t} + \nabla \cdot (\vec{u} \rho u) - \nabla \cdot (\mathcal{D} \nabla c) = S \qquad (2.2)$$

The terms that appear in this equation admit the following physical interpretation:

the rate-of-change term $\frac{\partial(\rho c)}{\partial t}$ is the net gain/loss of mass per unit volume and time,

the convective term $\nabla \cdot (\vec{u}\rho u)$ is due to the downstream transport with velocity u,

the diffusive term $-\nabla \cdot (\mathcal{D}\rho\nabla c)$ is due to a non-uniform spatial distribution of *c,*

the source or sink term S combines all other effects that create or destroy ρ and c.

For the time being, we assume that the parameters ρ, ν, D, and *s* are known. In real-life applications, these parameters may depend on the concentration and/or other variables involved. The simplest component of this PDE system is the continuity equation and is expressed as (Bear, 1972), (Kaviany, 1991), (McCabe et al, 2004):

$$\frac{\partial \mathrm{\rho}}{\partial \mathrm{t}} + \nabla \cdot (\mathrm{\rho}\vec{\mathrm{u}}) = 0 \qquad (2.3)$$

where the first term on the left-hand side is the time rate of change of the density (mass per unit volume) and the second term is the net mass flow across the control volume’s boundary and is called the convective term.

2.1.3. MOMENTUM CONSERVATION LAW (EQUATION OF MOTION)

Momentum is a vector quantity defined as the product of mass and velocity, which becomes, when expressed per unit of volume, the product of density and velocity leading to a general form of the conservation law.

As with the mass conservation equations, it is assumed that no diffusion of momentum is possible in a fluid at rest, and hence there is no diffusive contribution to the flux tensor. In order to determine all the terms of the conservation equations, it is necessary to define the sources influencing the variation of momentum (Bird et al, 1960), (Perry, 1999), (McCabe et al, 2004), (Himmelblau and Riggs, 2012).

It is known, from Newton’s law, that the sources for the variation of momentum in a physical system are the forces acting on it. These forces are consisted by external and internal volume forces defined per unit mass. The most important is the definition of the internal force, acting on a surface element dS. In the general case, the internal force acting on this surface element depends both on its position and on its orientation, defined against the normal vector. Therefore, it should be expressed mathematically by a tensor (Bird et al, 1960), (Perry, 1999), (McCabe et al, 2004). By assuming a Newtonian fluid, the total internal stress tensor is taken to be:

$$\vec{\sigma} = -\xi\vec{I} + \vec{\tau} \tag{2.4}$$

Where ξ is the magnitude of the normal compressive stress, $\vec{I}$ is the unit tensor and $\vec{\tau}$ is the viscous shear stress tensor which equals to:

$$\tau_{ij} = \mu\left[\left(\frac{\partial u_j}{\partial x_i} + \frac{\partial u_i}{\partial x_j}\right)\right] - \frac{2}{3}(\vec{\nabla}\cdot\vec{u})\delta_{ij} \tag{2.5}$$

Where μ is the dynamic viscosity of the fluid.

The differential form of the equation of motion is expressed by the following equation:

$$\frac{d\rho\vec{u}}{dt} + \left(\vec{\nabla}\cdot\rho u\vec{u}\right) = -\vec{\nabla}\xi - \vec{\nabla}\cdot\vec{\tau} + \rho\overrightarrow{f_e} \tag{2.6}$$

where $\rho\overrightarrow{f_e}$ is the sum of the external volume forces per unit volume.

By introducing the shear stress tensor to the equation of motion we get the well-known Navier-Stokes equations of motion, where for an incompressible flow they are written as (McCabe et al, 2004), (Himmelblau and Riggs, 2012):

$$\rho\frac{d\vec{v}}{dt} + \rho\left(\vec{v}\cdot\vec{\nabla}\right)\vec{v} = -\vec{\nabla}\xi + \mu\Delta\vec{u} + \rho\overrightarrow{f_e} \tag{2.7}$$

2.1.4. ENERGY CONSERVATION EQUATION

For a single-phase material, the amount of heat per unit volume is given by the product $\rho c_P T$ where c_P is the specific heat at constant pressure and T is the temperature. The heat flux has two components due to conduction and transport. In the absence of transport, the heat flux is $-k_{eff}\nabla T$ where k is the thermal conductivity. Finally, unlike mass, heat can be created in a region due to terms like radioactive decay or viscous dissipation and shear heating. All the source terms are summed up into the term S_h. Therefore, the simplest conservation of heat equation is expressed in a differential form of the energy conservation equation:

$$\frac{\partial(\rho h_o)}{\partial t} + \nabla\cdot\left(\rho\vec{V}h_0\right) = \nabla\cdot\left(k_{eff}\nabla T\right) + \frac{\partial P}{\partial t} + \vec{\nabla}\cdot(\vec{\tau}\cdot\vec{u}) + S_h \tag{2.8}$$

where,	ρ	is the density
	h_o	is the total enthalpy
	$\vec{V}$	is the control volume
	k_{eff}	is the effective conductivity

P is the static pressure

T is the temperature

S_h are the sum of sources and sinks

2.2.CFD MODELS

The modeling approach allows for dividing complex problems into flexible and smaller sub-problems and utilizes ways of achieving the project objectives with the allocated resources. A detailed knowledge on the steps of implementation of these models is essential, for selecting the most suitable modeling approach. The steps for the implementation of a computational model on a computer are presented below.

- *Geometrical modeling of the domain under study*.

It is necessary to select the appropriate solution domain to dissociate the system under study from its environment. Special care must be taken to understand and eliminate the influence of the domain boundaries on the final model results. Once the domain is finalized, it is important to decide the essential geometrical features to be modeled in order to capture the influence on the system of the process(es) of interest (Ranade, 2002).

- *Grid generation.*

When generating the suitable grid for the problem under study, care should be taken to avoid extreme aspect ratios. It is also necessary to implement the necessary grid independency tests in order to sufficiently eliminate the influence of the grid spacing on the simulations' results. Often, it is difficult to obtain a truly grid independent solution for complex problems, especially in industrial scales (Lőhner, 1988b), (Peube, 2010), (Ranade, 2002).

- *Specification of data related to the process under consideration.*

Once the suitable grid has been generated, the necessary information concerning the physicochemical properties of the problem must be specified. If the problem to be solved involves chemical reactions, all the necessary chemical data on them like stoichiometry, reaction kinetics, heat of reaction, *etc*., must be supplied at this step, in order to be imported to the model data file. In addition to the system data, specification of boundary conditions of the domain is an essential parameter affecting the solution process (Ranade, 2002).

- *Solution of model equations for the generated grid for a specific problem.*

Once the grid and the required input data are completed, the main task of implementing a numerical method to solve the necessary equations can be initiated. The numerical solution discretizes the model equations on the generated grid and solves the consequent system of algebraic equations using iterative numerical methods, until the required convergence is reached (Ranade, 2002).

- *Analysis of simulated flow results.*

The solution process generates large amounts of data regarding the simulated flow process. With large numerical simulations it is almost impossible to navigate and/or analyze a so big volume of numbers/data. At this point the need of the necessary tools and strategies for analyzing these data must be mentioned. Some ways of identifying the key features are also useful for qualitative evaluation of simulation results. Methods and tools for error analysis and validation are also essential to derive the maximum information from the simulation results and to plan any further studies (Ranade, 2002), (Glatzel et al, 2008).

Regarding their application, the computational tools are classified in three categories: pre-processors, solvers and post-processors. The pre-processors include geometry modeling and grid generation tools. In some cases, pre-processors include specifications on the required information about the system under consideration and the numerical technique specification. Solvers implement the numerical methods to solve the relative equations produced by mathematical modeling/description. Most commercial codes provide ease of use and maintainability along with the very important capability of handling complex grids. Post-processing tools allow easy exchange of information among different levels of models. The optimal use of the post –processor is essential because a misunderstanding of the output data can alter the whole understanding of the simulated case.

A brief overview of the major, available commercially, CFD codes are presented here since it is crucial to explain why the selection of the specific solver has been made. The relevant CFD codes of some of the leading vendors are listed in the table below (Ranade, 2002), (Malekjani and Jafari, 2018), (Bhutta et al, 2012).

Table 2.1. Major commercially available CFD codes

Vendor	Products
CFDRC	Pre-processor: CFD-GEOM Main code: CFD-ACE Post-processor: CFD-VIEW
CFX	Pre-processor: CFX-Build

	Main code: CFX Post- processor: CFX-Visualize
FLUENT	Pre- and Post- Processor: GAMBIT Main code: Fluent5

The software codes mentioned in Table 2.1 were examined prior to the decision of the utilization of one of them for the solution of the case study models. All the codes presented above are based on the finite-volume method (FVM) to solve the Navier–Stokes equations (Anderson and Wendt, 1995), (Glatzel et al, 2008), (Malekjani and Jafari, 2018).

CFDRC from ESI Group provides all the necessary advanced simulation tools, which employ the state-of-the art numerical schemes and the most advanced physical models to provide solutions to a wide variety of complex industrial applications. The suite consists three main parts, an advanced pre-processing program (CFD-GEOM), a program for setting boundary and initial conditions (CFD-GUI) and a post-processing program (CFD-VIEW). CFD-GEOM supports all grid technologies such as multi-block structured, general polyhedral unstructured, arbitrary interfaces, and moving and deforming grids. After setting up the geometry in CFD-GEOM the desired solver settings can be setup in the CFD-GUI, where the solvers for different physical problems are divided into "modules", specifying the kind of problem that can be switched on and off separately. Almost all the modules can be combined with other modules, giving the opportunity to simulate different physical domains at the same time, e.g. flow problems in combination with chemical reactions, porous media, free surfaces, etc. CFD-VIEW is an interactive graphics program for post-processing numerical results from the solver. It provides an easy-to-use and interactive environment with many tools to visualize graphically the flow physics, animate transient data sets and to extract data (ESI GROUP, 2004), (Glatzel et al, 2008), (Bouteville, 2005).

In CFX, to define physical properties such as material properties and boundary conditions as well as solver settings, the preprocessor CFX-Pre is provided. Both CFX-Pre, as well as the postprocessor, CFX-Post can be either controlled by the CFX-Expression-Language (CEL) or by Perl scripting. The CFX-solver can handle multiphase flows of any number of different fluids and all material properties can either be constant or dependent on any variable in the simulation. Similar to CFD-ACE+, all problems can be modeled on structured and unstructured meshes. In contrast to the other similar tools, CFX does not use separate flow solvers for velocity and pressure, but a fully coupled solver. CFX can perform all types of simulations on multiple processors, where parallelization can be achieved using message-parsing interface MPI or PVM (parallel virtual machine) (Geist et al, 1996), (Glatzel et al, 2008), (Ramachandran et al, 2017).

The Fluent software package includes the solver with only few limitations concerning mesh-types, the pre-processor Gambit for geometry modelling and mesh generation as well as an additional pre-processor called TGrid for generating volume meshes from existing boundary meshes. (Malekjani and Jafari, 2018).

For the geometry creation Gambit provides a common set of CAD-functions as well as a built-in scripting functionality that allows for a fast geometry creation. Gambit provides, unstructured hybrid and non-conformal meshes. Structured meshes can either be created manually or by using the Cooper-scheme allowing for a fast meshing with good grid quality (Fluent, 2005), (Glatzel et al, 2008).

After an appropriate mesh is provided, Fluent is used for the simulation setup, the solving process and the post-processing of the results. During the simulation setup all GUI-commands are scripted by the program, but one has to be aware of the fact that not all possible settings are accessible by the GUI. Some special functions are only available if entered on the command line level leading sometimes to difficulties in finding the appropriate settings.

Glatzel et al (2008), compared these three models and presented some very interesting conclusions. Best qualitative consistency with their experiments was achieved with CFDACE+ while the consistency of the rest simulation environments with the experimental results was found to be considerably weaker. As they conclude, CFD-ACE+ is found to be easy to set-up but the user has to be very careful in applying the correct boundary conditions. CFD-ACE+ was found to be the fastest tool in their case studies and was five to ten times faster than the others. Fluent needed more time to simulate the same case because an iterative method had to be used, as described before, to achieve a correct solution instead of one single solver run (Glatzel et al, 2008).

For this work and by taking under consideration all of the aforementioned discussion, the CFD-ACE environment was used where several modules have been utilized. This software is able to provide the unique capacity to perform highly reliable three-dimensional simulations of heat and mass transport with complex phenomena and chemical reactions for industrial and academic applications (Glatzel et al, 2008). For the solution of the equations describing the case studies mentioned in the next chapters the following modules were used: Fluid Dynamics, Heat Transfer, Chemistry and Porous Media. Each one of these modules is tightly integrated within the CFD-ACE solver for efficient execution.

2.3. MASS TRANSPORT PHENOMENA –*Chemistry Module* by CFD-ACE$^+$

The chemistry module by CFD-ACE+ has been used to solve mixing and reacting flow problems, such as the cases investigated by this PhD. In the following part of this chapter, the simulation process theory is going to be described in detail. It is important to understand how each module treats the problems submitted to it. The Species Mass Fraction approach of the chemistry module is used and it requires the solution of a transport equation for every species in the system.

This approach is required for:

- Multi-component diffusion problems
- Surface reaction problems
- A multi-step finite rate gas-phase reaction.

For solving the mass diffusion equations, the "multi-component diffusion" option is selected. Therefore, the solver calculates the diffusion of the mixture instead of reading a specific constant value imposed by the user. However, when species diffuse at different rates, their mass fractions do not automatically add up to unity and some corrections have to be invoked to guarantee the species conservation. In order to treat this problem, the "Stefan-Maxwell" option is selected. This option enforces the species conservation by employing the Stefan-Maxwell equations. This is the most rigorous of all the approaches, even if it is more computationally expensive (ESI CFD Inc., 2008), (Bird et al, 1960), (Perry, 1999), (McCabe et al, 2004) (Himmelblau and Riggs, 2012).

The Stefan-Maxwell equations are:

$$\frac{\nabla\zeta_i}{RT} = \nabla \ln \alpha_i = \sum_{j=1\ j\neq i}^{n} \frac{{M_F}_i {M_F}_j}{\mathfrak{D}_{ij}} \left(\overrightarrow{u_j} - \overrightarrow{u_\iota}\right) = \sum_{j=1\ j\neq i}^{n} \frac{c_i c_j}{c_{total}\mathfrak{D}_{ij}} \left(\frac{\overrightarrow{J_j}}{c_j} - \frac{\overrightarrow{J_\iota}}{c_\iota}\right) \tag{2.9}$$

where,

M_F	Mole fraction
ζ	Chemical potential
a	Activity (effective concentration of a species in a mixture)
$_{i,\,j}$	Indexes for component i and j,
n	Number of components,
D_{ij}	Maxwell–Stefan-diffusion coefficient,
u_{Di}	Diffusion velocity of component i,
c_i	Molar concentration of component i,
c_{total}	Total molar concentration,
J_i	Flux of component i,

The chemical rate used by the chemistry module can be expressed in a general way, for a system of n_r chemical reactions, involving n_s species, as:

$$\sum_{i=1}^{N_s} \acute{v}_{ij}\, \Lambda_i = \sum_{i=1}^{N_s} v"_{ij}\, \Lambda_i,\ j = 1, \dots, n_r \tag{2.10}$$

where,	Λ_i	Chemical symbol for species i,
	v'_{if}, v''_{if}	Forward and backward stoichiometric coefficients for the ith species that encountered in the jth reaction.

The stoichiometric coefficients are integer numbers, normally being for elementary reactions 0, 1 or 2. The following equations can be used to write the equation (2.10) in a more compact way,

$$V_{ij}=v''_{ij}-V'_{ij} \tag{2.11}$$

$$\sum_{i=1}^{N_s} v_{ij}\, \Lambda_i = 0,\ j = 1, \dots, N_r \tag{2.12}$$

For the simulations of this work the “Surface Reaction Option” is used. The oxidization reaction is placed onto the surface of the particles when neccessary. The surface reaction provides a boundary condition for the mass fractions of species in the fluid, rather than a source term in then transport equations.

The general form of the surface reaction considered in CFD-ACE+ is:

$$\sum_{i=1}^{N_g} a'_{ij}A_i + \sum_{i=1}^{N_{as}} b'_{ij}B_{(s)} + \sum_{i=1}^{N_b} c'_{ij}C_{(b)} = \sum_{i=1}^{N_g} a''_{ij}A_i + \sum_{i=1}^{N_{as}} b''_{ij}B_{(s)} + \sum_{i=1}^{N_b} c''_{ij}C_{(b)} \tag{2.13}$$

where,	a_{ij}	Gas species stoichiometric coefficient
	b_{ij}	Adsorbed species stoichiometric coefficient
	c_{ij}	Bulk species stoichiometric coefficient
	N_g	Total number of gas-phase species
	N_{as}	Total number of adsorbed species
	N_b	Total number of bulk species

For the above reaction the surface reaction rate can be expressed as:

$$\dot{S_J} = k_{fj} \prod_{i=1}^{N_g} [A_i]_w^{a'_{ij}} \prod_{i=1}^{N_s} [B_{(s)}]^{b'_{ij}} - k_{rj} \prod_{i=1}^{N_g} [A_i]_w^{a''_{ij}} \prod_{i=1}^{N_s} [B_{(s)}]^{b''_{ij}} \tag{2.14}$$

where,	k_{fj}	Surface reaction forward rate
	k_{rj}	Surface reaction reverse rate

As seen from the above expression, the surface reaction rate is assumed to be independent of the concentration of the bulk species. The gas-phase concentrations at the surface are expressed as:

$$[A_i]_w = \frac{\rho_w Y_i^w}{m_i},\ [B_{i(s)}] = \rho_s X_i \tag{2.15}$$

where,

ρ_w Gas -phase mass density

ρ_s Surface site density

Y_i^w Gas-phase mass fractions adjacent to the wall

X_i Surface site fractions

The mass flux of reacting species to the surface or in the bulk for species produced by the reaction equals the rate at which the species are consumed or produced respectively by the reaction on the surface.

The species flux balance at the reacting surface yields,

$$j_{i,n} = M_i \sum_j \left(a"_{ij} - a'_{ij}\right)\dot{S}_j\ , \quad i = 1, \dots, N_g \tag{2.16}$$

$$\frac{d[B_i(s)]}{dt} = \sum_j \left(b"_{ij} - b'_{ij}\right)\dot{S}_j\ ,\ i = 1, \dots, N_s \tag{2.17}$$

where, the left-hand side of equation (2.16) is the diffusive flux of species *i* normal to the surface. The right-hand side of equation (2.16) is the production rate of species *i* per unit area of surface, on mass basis. Equation (2.16) and equation (2.17) are solved by coupled Newton-Raphson iterations.

The mass-reactive flux can be computed by using two different approaches, namely the sticking coefficient method and the general rate method. The sticking coefficient method evaluates the production rate based on sticking probability and precursor thermal flux, while the finite-rate chemistry uses the kinetic expression (see equation (2.14)) to evaluate the reaction rate. In this study, the finite rate has been used for the simulations since we are interested in calculating the production/consumption of species throughout porous media rather than studying in detail the surface phenomena.

The need for a macroscopic and dimensionless quantity aiming for a direct comparison of complex phenomena occurring in different scales and geometry arises. For this application, the most useful quantity found to be adsorption efficiency, λ (Coutelieris and Delgado, 2012). Adsorption efficiency is the ratio of the solute adsorption rate divided by the rate of the upstream influx:

$$\lambda = \frac{\iint_{S\,inlet}[c_A\vec{v}]\underline{n}dS - \iint_{S\,outlet}[c_A\vec{v}]\underline{n}dS}{\iint_{S\,inlet}[c_A\vec{v}]\underline{n}dS} \tag{2.18}$$

where, $\iint_{S\,inlet}[c_A\vec{u}]d\underline{n}S$ is the total mass entered the volume of interest through the inlet surface.

$\iint_{S\,outlet}[c_A\vec{u}]\underline{n}dS$ is the total mass exit the volume of interest through the outlet surface.

c_A	Concentration of passive solute
$\vec{u}$	Velocity in the medium
$\underline{n}$	Vector normal to the surface

2.4. MOMENTUM TRANSPORT PHENOMENA – Flow module by CFD-ACE$^+$

For the simulation of flow through the porous media, the “Flow Module” is used. Both, inlet and outlet flows, in and out of the porous medium, with the velocity magnitude set by the user as normal velocity, can be simulated to obtain the velocity and pressure fields. The simulated flow of the gas phase is set as laminar flow aiming low to medium Reynolds numbers. Implementing the conservation laws, CFD-ACE+ develops the governing equations used for this module as presented next.

CFD-ACE+ uses an iterative method to solve the well-known Navier-Stokes equations, from which their results show the satisfaction of the two laws mentioned above.

The equations used by the flow module are presented and described next. The x-component of the momentum equation is found by setting the rate of change of x-momentum of the fluid particle equal to the total force in the x-direction on the element due to surface stresses plus the rate of increase of x-momentum due to sources (Bird et al, 1960), (Peube, 2010), (Perry, 1999):

$$\frac{\partial(\rho u)}{\partial t} + \nabla\cdot\left(\rho\vec{V}u\right) = \frac{\partial(-P+\tau_{xx})}{\partial x} + \frac{\partial\tau_{yx}}{\partial y} + \frac{\partial\tau_{zx}}{\partial z} + S_{Mx} \tag{2.19.1}$$

Similar equations can be written for the y- and z- components of the momentum equation:

$$\frac{\partial(\rho u)}{\partial t} + \nabla\cdot\left(\rho\vec{V}v\right) = \frac{\partial(-P+\tau_{xy})}{\partial x} + \frac{\partial\tau_{yy}}{\partial y} + \frac{\partial\tau_{zy}}{\partial z} + S_{My} \tag{2.19.2}$$

$$\frac{\partial(\rho u)}{\partial t} + \nabla\cdot\left(\rho\vec{V}w\right) = \frac{\partial(-P+\tau_{xz})}{\partial x} + \frac{\partial\tau_{yz}}{\partial y} + \frac{\partial\tau_{zz}}{\partial z} + S_{Mz} \tag{2.19.3}$$

where, p Static pressure

τ_{in} Viscous stress tensor

S_{Mxyz} Rate of increase of x_y_z -momentum due to sources

The momentum equations, given above, contain as unknowns the viscous stress components τ_{ij}, therefore a model must be provided to define the viscous stresses.

In Newtonian flows, the viscous stresses are proportional to the deformation rates of the fluid element. The nine viscous stress components (of which six are independent for isotropic fluids) can be related to velocity gradients to produce the following shear stress terms:

$$\tau_{xx} = 2\mu\frac{\partial u}{\partial x} - \frac{2}{3}\mu(\nabla \cdot \vec{V}) \tag{2.20.1}$$

$$\tau_{yy} = 2\mu\frac{\partial v}{\partial y} - \frac{2}{3}\mu(\nabla \cdot \vec{V}) \tag{2.20.2}$$

$$\tau_{zz} = 2\mu\frac{\partial w}{\partial z} - \frac{2}{3}\mu(\nabla \cdot \vec{V}) \tag{2.20.3}$$

$$\tau_{xy} = \tau_{yx} = \mu(\frac{\partial u}{\partial y} + \frac{\partial v}{\partial x}) \tag{2.20.4}$$

$$\tau_{xz} = \tau_{zx} = \mu\left(\frac{\partial u}{\partial z} + \frac{\partial w}{\partial x}\right) \tag{2.20.5}$$

$$\tau_{zy} = \tau_{yz} = \mu(\frac{\partial v}{\partial z} + \frac{\partial w}{\partial y}) \tag{2.20.6}$$

The substitution of the above shear stress terms (see equations (2.20.1) – (2.20.6)) into the equations of momentum (see equations (2.19.1) - (2.19.3)) yields the Navier-Stokes equations:

$$\frac{\partial(\rho u)}{\partial t} + \nabla \cdot (\rho\vec{V}u) = \frac{\partial P}{\partial t} + \nabla \cdot (\mu \nabla u) + S_{Mx} \tag{2.21.1}$$

$$\frac{\partial(\rho v)}{\partial t} + \nabla \cdot (\rho\vec{V}v) = \frac{\partial P}{\partial t} + \nabla \cdot (\mu \nabla v) + S_{My} \tag{2.21.2}$$

$$\frac{\partial(\rho w)}{\partial t} + \nabla \cdot (\rho\vec{V}w) = \frac{\partial P}{\partial t} + \nabla \cdot (\mu \nabla w) + S_{Mz} \tag{2.21.3}$$

The “Mix Kinetic Theory” option that uses the kinetic theory of gases for the calculation of viscosity of the whole mixture has been used. For monatomic gas the viscosity is defined (Chapman and Cowling, 1990), (Kauzmann, 1966), (Verberg and Ladd, 1999) as:

$$\mu_i = 2.6693 * 10^{-5}\frac{\sqrt{MW_i T}}{{\sigma_i}^2 \Omega_\mu} \tag{2.22}$$

where,	μ_i	Dynamic viscosity of species i,
	MW_i	Molecular weight of species i
	T	Temperature,
	σ_i	Characteristic diameter of the molecule,
	Ω_μ	Collision integral.

The collision theory is given by:

$$\Omega_\mu = \frac{1.16145}{T^{*0.14874}} + \frac{0.52487}{\exp(0.77320T^*)} + \frac{2.16178}{\exp(2.43787T^*)} \tag{2.23}$$

where T^* is the dimensionless temperature given by:

$$T^* = \frac{\kappa T}{\varepsilon_{ce}} \tag{2.24}$$

where,	ε_{ce}	Characteristic energy
	κ	Boltzmann constant

These equations are used for calculating the viscosity of each gas in the mixture. To calculate the mixtures viscosity using the previous equations, the following equation is also applied:

$$\mu_{mix} = \sum_{i=1}^{N} \frac{x_i \mu_i}{\sum_j x_j \Phi_{ij}} \tag{2.25}$$

Where x_i, x_j are mass fraction of species i and species j, μ_i is viscosity of species i and $\Phi_{i,j}$ is a dimensionless quantity given by:

$$\Phi_{i,j} = \frac{1}{\sqrt{8}}\left(1 + \frac{\mathrm{MWi}}{\mathrm{MWj}}\right)^{-1/2}\left[16 + \left(\frac{\mu_i}{\mu_j}\right)^{1/2}\left(\frac{\mathrm{MWi}}{\mathrm{MWj}}\right)^{1/4}\right] \tag{2.26}$$

2.5. ENERGY TRANSPORT PHENOMENA – Heat transfer module by CFD-ACE$^+$

The heat transfer analysis has been performed with the use of the Heat Transfer Module, which is an internal part of the CFD-ACE-SOLVER. The use of the Heat Transfer Module implies the solution of the total enthalpy form of the energy equation. Many types of heat transfer analysis can be performed with this module, from basic conduction/convection to complex radiation.

Heat transfer analysis can be performed in stand-alone mode (pure heat transfer analysis) or coupled with other modules (such as the Flow, Mixing, etc.) for a multi-physics simulation.

Heat transfer processes are computed by solving the equation for the conservation of energy. This equation can take several forms and CFD-ACE+ numerically solves the energy equation in the form known as the total enthalpy equation. This form is fully conservative and is given as:

$$\frac{\partial(\rho h_o)}{\partial x} + \nabla\cdot\left(\rho\vec{V}h_0\right) = \nabla\cdot\left(k_{eff}\nabla T\right) + \frac{\partial p}{\partial t} + \left[\frac{\partial(u\tau_{xx})}{\partial x} + \frac{\partial\left(u\tau_{xy}\right)}{\partial y} + \frac{\partial(u\tau_{xz})}{\partial z}\right]$$

$$+\left[\frac{\partial(v\tau_{xy})}{\partial x} + \frac{\partial(v\tau_{yy})}{\partial y} + \frac{\partial(v\tau_{zy})}{\partial z}\right] + \left[\frac{\partial(w\tau_{xz})}{\partial x} + \frac{\partial\left(w\tau_{yz}\right)}{\partial y} + \frac{\partial(u\tau_{zz})}{\partial z}\right] + S_h \qquad (2.27)$$

Where h_0 is the total enthalpy and is defined as:

$$h_0 = i + \frac{P}{\rho} + \frac{1}{2}\left(u^2 + v^2 + w^2\right) \qquad (2.28)$$

where, i = Internal energy as a function of the state variables ρ and T,

k_{eff} = Effective thermal conductivity of the material.

Under laminar flow conditions, the effective thermal conductivity is the thermal conductivity of the fluid, k. Static pressure is defined as p and as τ_{ij} is referred to the viscous stress tensor. S_h contains terms for additional sources due to reactions, body forces, etc. The method used to evaluate the specific heat and conductivity properties for the use in the simulation is the "MIX_JANNAF" method (ESI CFD Inc., 2008), which uses the input data to create fitting curves of the following form,

$$\frac{C_p}{R} = a_1 + a_2T + a_3T^2 + a_4T^3 + a_5T^4 \qquad (2.29)$$

$$\frac{H}{RT} = a_1 + \frac{a_2T}{2} + \frac{a_3T^2}{3} + \frac{a_4T^3}{4} + \frac{a_5T^4}{5} + \frac{a_6}{T} \qquad (2.30)$$

The coefficients used for the simulation can be found in (Goos, 2011).

2.6. POROUS MEDIA MODULE by CFD-ACE$^+$

For the simulation of the macroscopic case the "Porous media module" has been used. The Porous Media feature allows (among many other applications) to model fluid flow in a volume representing a material consisting of a rigid solid matrix with interconnected void. The interconnectedness of the void (the pores) allows the flow of one or more fluids through the material. In the simplest situation (single-phase flow) the void is saturated by a single fluid (In two-phase flow, a liquid and a gas can share the void space).

In most porous media, the distribution of pores with respect to shape and size is irregular. On the pore scale (the microscopic scale) the flow quantities (velocity, pressure, etc.) will clearly be irregular. But for most applications, the quantities of interest are space-averaged (macroscopic) in nature (measured over areas that cross many pores). Experiments have shown that such macroscopic quantities change in a regular manner with respect to space and time and are therefore amenable to numerical modeling. Flow through porous media plays an increasingly important role in a multitude of engineering applications and the porous media module in CFD-ACE+ can be applied to many such problems (ESI CFD Inc., 2008).

In the next section the treatment of the conservation equations by porous media module will be described. The mass conservation equation is as follows:

$$\frac{\partial(\varepsilon\rho)}{\partial t} + \nabla \cdot (\varepsilon\rho u) = 0 \qquad (2.31)$$

where, ε is the porosity of the medium.

Equation (2.31) is actually the same equation as equation (2.3) with the addition of the parameter ε. The porosity of the medium represents the volume occupied by the pores to the total volume of the porous solid.

The equation for momentum conservation within the porous media is written as:

$$\frac{\partial(\varepsilon\rho u)}{\partial t} + \nabla \cdot (\varepsilon\rho \overrightarrow{u}\overrightarrow{u}) = -\varepsilon\nabla P + \nabla \cdot (\varepsilon\vec{\tau}) + \varepsilon B_F - \frac{\varepsilon^2\mu}{K}u - \frac{\varepsilon^2 c_f \rho}{\sqrt{K}}|u|u \qquad (2.32)$$

where,

C_F	Quadratic drag factor
τ	Shear stress tensor
B_F	Body force vector
u	Fluid velocity
K	Permeability of the porous matrix

while permeability is a measure of the ability of a porous material to allow fluids to pass through it, the last two terms in the equation represent an additional drag force imposed by the pore walls on the fluid within the pores, and usually results in a significant pressure drop across the porous solid. In a purely fluid region, the standard Navier-Stokes equation is recovered.

In terms of boundary conditions, no special treatment to the momentum and pressure correction equations is required at fluid-porous solid interfaces (ESI CFD Inc., 2008), (Das, 2018).

The energy conservation equation within the porous regions is written as:

$$\frac{\partial(\varepsilon\rho \mathrm{h}_o)}{\partial \mathrm{t}} + \nabla(\varepsilon\rho\vec{\mathrm{u}}\mathrm{h}_o) = \nabla \cdot \mathrm{q} + \varepsilon\vec{\tau} : \nabla \mathrm{u} + \varepsilon\frac{\mathrm{dP}}{\mathrm{dt}} \tag{2.33}$$

where, h_o Total enthalpy of the fluid

q Heat flux which is comprised of contributions due to thermal conduction, thermal radiation and species diffusion, and is written as (ESI CFD Inc., 2008) (Wang and Cheng, 1997):

$$\mathrm{q} = k\nabla \mathrm{T} + \mathrm{q}_\mathrm{R} + \sum_{\mathrm{i}=1}^{\mathrm{N_g}} \mathrm{J}_{\mathrm{Diff,i}}\,\mathrm{h}_\mathrm{i} \tag{2.34}$$

where, N_g Total number of gas phase species in the system

h_i Enthalpies of gas species in the system

$J_{Diff,i}$ Diffusion fluxes of gas species in the system

T_B Bulk temperature

q_R Radiative heat flux.

The thermal conductivity of the porous medium, k, is an effective thermal conductivity of the pores and solid regions in combination and may be written as (Wang and Cheng, 1997).

$$k = -2k_s + \frac{1}{\frac{\varepsilon}{2k_S+\mathrm{k}_\rho}+\frac{1-\varepsilon}{3\mathrm{k}_S}} \tag{2.35}$$

where k_S and k_F are the thermal conductivities of the solid and pores, respectively.

The mass conservation equation for individual gas phase species (i.e., for i= 1,…,N_g) is written as,

$$\frac{\partial(\varepsilon\rho \mathrm{Y_i})}{\partial \mathrm{t}} + \nabla \cdot (\varepsilon\rho \mathrm{u} \mathrm{Y_i}) = \nabla \cdot \mathrm{J_i} + \omega_\mathrm{i} \tag{2.36}$$

where, Y_i Mass-fractions of the *i*-th species

ω_i Production rates of the *i*-th species in the gas phase.

When heterogeneous surface reactions are treated within the porous solid, this production rate term (ω_i) will be modified so that the species are produced in a volumetric sense, having the basic physics governing their production (ESI CFD Inc., 2008).

The species diffusion flux may be written as:

$$\mathrm{J_{Diff,i}} = \rho \mathrm{D_{i,eff}} \nabla \mathrm{Y_i} + \rho \mathrm{D^T_{i,eff}} \frac{\nabla \mathrm{T}}{\mathrm{T}} + \frac{\rho \mathrm{Y_i}}{\mathrm{MW}_{mix}} \mathrm{D_{i,eff}} \nabla \mathrm{MW}_{mix} - \mathrm{MW}_{mix} \sum_\mathrm{j} \mathrm{D_{j,eff}} \nabla \mathrm{Y_j} - \nabla \mathrm{MW}_{mix} \sum_\mathrm{j} \mathrm{D_{j,eff}} \mathrm{Y_j} - \rho \mathrm{Yi} \sum_\mathrm{j} \mathrm{D}_{\mathrm{j}_{\mathrm{j,eff}}}^{\mathrm{T}} \frac{\nabla \mathrm{T}}{\mathrm{T}} \quad (2.37)$$

where, MW_{mix} Mixture molecular weight.

The first term represents Fickian diffusion due to concentration gradients, and the second term represents Soret (or thermo) diffusion. The last four terms are correction terms necessary to satisfy the "Stefan-Maxwell" equations for multi-component species systems.

In this case, $D_{i,eff}$ and $D^T_{i,eff}$ are the effective mass diffusion and Soret diffusion coefficients of specie *i*, within the porous medium, respectively, and depend on the porosity of the medium.

The following expression of Dagan model (ESI CFD Inc., 2008) has been provided for the effective diffusion coefficient through porous media:

$$\mathrm{D_{j,eff}} = \mathrm{MAX}(0, \frac{3\varepsilon - 1}{2\varepsilon}) \mathrm{D_i} \quad (2.38)$$

An alternate correction is the Bruggeman type:

$$\mathrm{D_{eff}} = \varepsilon^{\tau} \mathrm{D} \quad (2.39.1)$$

where, τ Tortuosity of the porous media.

Tortuosity is the degree of interconnection resulting in paths through the solid, which are some percentage longer than a direct path. The value of tortuosity is obtained by using a method proposed in (Shen, 2007). The real tortuosity can be obtained by averaging over all possible flow paths in porous media. For simplicity though, they made a review of the available formulations for the scaled diffusion coefficient with tortuosity containing all the available relations for tortuosity with porosity.

Such relations are presented next, for monosized spheres (Bruggemann, 1935):

$$\tau^2 = \varepsilon^{-1/2} \quad (2.39.2)$$

while for overlapping spheres (Akanni et al, 1987) it is:

$$\tau^2 = 1 - \frac{\ln(\varepsilon)}{2} \quad (2.39.3)$$

and for heterogeneous catalyst (Beekman, 1990) it is:

$$\tau^2 = \frac{\varepsilon}{(1-(1-\varepsilon)^{1/3})} \tag{2.39.4}$$

The preferred relation for the case studied is the relation of Beekman (Beekman, 1990) (equation (2.39.4) because as it is mentioned above the surface where the reaction occurs is platinum catalyzing the reaction.

The cell sizes used in performing CFD analysis are typically much larger than the characteristic pore dimensions in a porous media. This makes it impossible to grid individual surfaces adjoining the pores. Therefore, modeling the heterogeneous chemical reactions occurring within catalyst-lined pores requires a volume-averaged implementation of the net effect of heterogeneous reactions occurring on the catalyst surfaces (ESI CFD Inc., 2008).

Surface reaction within porous media is treated by performing a reaction-diffusion balance at the surfaces of the catalysts. The balance equation is given by:

$$\rho D_i \nabla Y_i = S \tag{2.40.1}$$

where S_i is the production-destruction rate per unit area of the *i*-th specie due to chemical reactions.

In discrete form, equation (2.40.1) may be re-written as:

$$\rho D_i \frac{Y_i - Y_{\rho,i}}{\delta} = S_i \tag{2.40.2}$$

where, $Y_{\rho,i}$ Species mass-fraction in the pore fluid

Y_i Mass-fraction at the pore-fluid/catalyst interface

δ Diffusion length scale

When considering surface reactions on a well-defined flat substrate, such as in chemical vapor deposition applications, this length scale is extracted from the computational grid. For the case of porous media, this length scale cannot be obtained from the grid since the region under consideration is already much smaller than the size of a typical control volume. This length scale can be computed using various correlations available in the literature. The simplest approach is to assume that this length scale is equal to the volume to surface ratio of the porous media in question (ESI CFD Inc., 2008).

The volumetric production/destruction rate, (in kmol.$m^{-3}\cdot s^{-1}$) of species, *i*, due to heterogeneous surface reaction, can be obtained from the surface flux in equation:

$$\dot{\omega} = S_i \left[\frac{S}{V}\right]_{eff} = \rho D_i \frac{Y_i - Y_{\rho,i}}{\delta} \left[\frac{S}{V}\right]_{eff} \tag{2.41}$$

where, $[\frac{S}{V}]_{eff}$ is the effective surface to volume ratio of the catalyst.

2.7.NUMERICAL METHODS

For the numerical solution of the mathematical formulations describing the phenomena under study, the finite volume method is used. The “Numerical Methods” feature yields a discrete solution of the field, which is comprised of the values of the variables at the cell centers. The Partial Differential Equations (PDEs) describing the physics for each module are presented in the chapter above. A numerical method to solve these PDEs consists of the discretization of the PDEs on a computational grid, the derivation of a set of algebraic equations, and their solution, usually by an iterative method (Kuzmin, 2010).

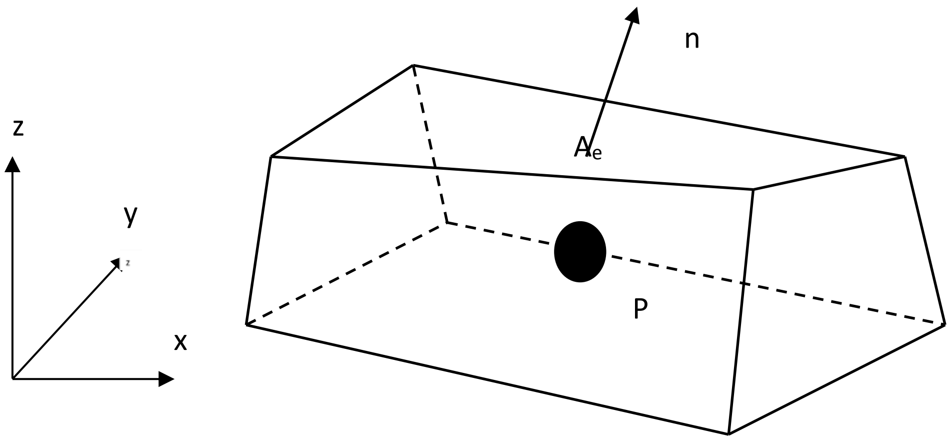

Figure 2.1 Computational cell (Control Volume)

To start the numerical solution process, discretization of the domain where the differential equations are app lied, is introduced to produce a set of algebraic equations. In CFD-ACE+, the finite-volume approach is adopted due to its capability of conserving solution quantities. The solution domain is divided into a number of cells known as control volumes. In the finite volume approach of CFD-ACE+, the governing equations are numerically integrated over each of these computational cells or control volumes. An example of such a control volume is shown in Figure 2.1.

The geometric center of the control volume, which is denoted by P, is often referred to as the cell center. CFD-ACE+ employs a co-located cell-centered variable arrangement, i.e. all dependent variables and material properties are stored at the cell center *P*. In other words, the average value of any quantity within a control volume is given by its value at the cell center. For a detailed explanation on the numerical methods Roache (1972), LeVeque (1990), Anderson et al, (1984) have excellent in-depth descriptions.

After numerically integrated, the transient, convection, diffusion and source terms presented in the generic transport equation (see equation 2.1) are assembled together, resulting the following linear equation:

$$\left(a_p - S_p\right)\Phi_p = \sum_{nb} a_{nb}\Phi_{nb} + S_U \tag{2.42}$$

where,	nb	Values at neighboring cells,
	a_{nb}	Link coefficients.

This Finite Difference Equation (FDE) is the discrete equivalent of the continuous flow transport equation we started with. It is in general nonlinear because the link coefficients themselves are functions of P, nb, etc. When such a system is formulated for each computational cell, it results in a set of coupled nonlinear algebraic equations (Burden, 2010). No direct matrix inversion method is available to solve a set of nonlinear algebraic equations. Therefore, an iterative procedure is employed in CFD-ACE+ at every time step. A linear FDE is formed by evaluating the link coefficients with the values of available at the end of the previous iteration (Anderson, 1984).

Integrating the mass conservation equation (see equation 2.3) over the cell, we have:

$$\frac{\rho\vartheta^{\circ} - \rho\vartheta^{\circ}}{\Delta t} + \sum_e \rho_e V_e^n A_e = \dot{\omega}\vartheta \tag{2.43}$$

Where A_e is the surface area of the face e, while V^n_e is the face-normal component of the velocity at face *e,* which is obtained by the inner product of the velocity vector (u,v,w) and the face-normal unit vector $(\overrightarrow{n_x}, \overrightarrow{n_y}, \overrightarrow{n_z})$,

$$V_e^n = u_e\overrightarrow{n_x} + v_e\overrightarrow{n_y} + w_e\overrightarrow{n_z} \tag{2.44}$$

Because the fluid density and velocities are available only at cell centers, their face values need to be interpolated from cell-center values. Linear interpolation de-couples the velocity and pressure fields giving rise to the well-known checkerboard instability, in particular, for incompressible flows.

In CFD-ACE+, the checkerboard problem is avoided by following the method proposed in (Rhie and Chow, 1983) and later refined in (Peric et al, 1988). In accordance to this method, the cell-face mass flux is evaluated by averaging the momentum equation to the cell faces and relating the cell face velocity directly to the local pressure gradient Without going into the details of the derivations, the three Cartesian components at the center of face *e* are obtained as follows,

$$u_e = Y_e u_p + (1 - Y_e)u_E + D_{ue}\big(P_e - P_p\big) - D_{ue}(\nabla P)_e \cdot (\overrightarrow{r_e} - \overrightarrow{r_p}) \tag{2.45.1}$$

$$v_e = Y_e v_p + (1 - Y_e)v_E + D_{ve}\big(P_e - P_p\big) - D_{ve}(\nabla P)_e \cdot (\overrightarrow{r_e} - \overrightarrow{r_p}) \tag{2.45.2}$$

$$w_e = Y_e w_p + (1 - Y_e)w_E + D_{we}\big(P_e - P_p\big) - D_{we}(\nabla P)_e \cdot (\overrightarrow{r_e} - \overrightarrow{r_p}) \tag{2.45.3}$$

where,

Y_e	Geometrical weighting function at face *e*
D_s	Evaluated from link coefficients of momentum equations.

The density at the face may be estimated with any one of the differencing schemes described in online help. With the face values of both velocity and density obtained, the mass flux evaluation is completed.

Using the three momentum equations (2.45.1) - (2.45.3), the three Cartesian components of velocity are calculated. Pressure based methods use the continuity equation to formulate an equation about pressure. In CFD-ACE+, the SIMPLEC (Semi-Implicit Method for Pressure-Linked Equations Consistent) scheme has been adopted.

The basic framework of this method is presented in the next 8 steps (ESI CFD Inc., 2008) (Versteeg and Malalasekera, 1995), (Patankar, 1980):

1. Guess a pressure field
2. Obtain the three Cartesian components of velocity by solving discretized momentum equation
3. Evaluate the mass flux from density and velocity
4. Evaluate mass source
5. Obtain the pressure correction value and correct the pressure and velocity fields
6. Solve the discretized equations for other flow variables such as enthalpy, turbulent quantities, scalars etc.
7. Go to step 2 and repeat the procedure until convergence is obtained.

The general treatment of boundary conditions by CFD-ACE+ finite volume equations is discussed in the next paragraphs. A control cell is adjacent to the west boundary (node labeled B) of the calculation domain is shown in Figure 2.2.

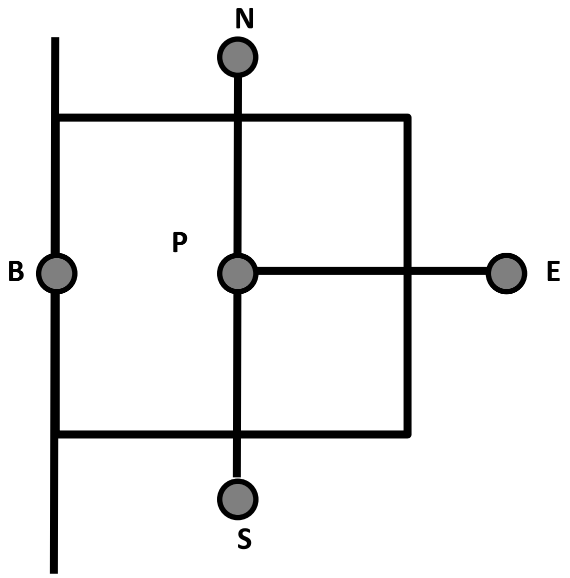

Figure 2.2 Computational boundary cells

A fictitious boundary node labeled *B* is shown. The finite-volume equation on for node *P* will be constructed as:

$$a_p \Phi_p = a_E \Phi_E + a_N \Phi_N + a_S \Phi_S + S \qquad (2.46)$$

Coefficient a_w is set to zero after the links to the boundary node are incorporated into the source term S in its linearized form:

$$S = S_U + S_p \Phi_p \qquad (2.47.1)$$

It's important to note that all boundary conditions in CFD-ACE+ are implemented in this way.

For fixed value (Φ_B) boundary conditions (i.e. Fixed Velocity) the source term is modified as:

$$S_U = S_U + a_w \Phi_B \qquad (2.47.2)$$

$$S_P = S_P - a_w \qquad (2.47.3)$$

For zero flux boundary conditions, the boundary link coefficients are simply set to zero (ESI CFD Inc., 2008).

2.8.QUALITY CONTROL

In order to allow direct comparisons between the results, it is necessary to transform the adsorption efficiency to a dimensionless number. The most frequently used dimensionless number for this case is the overall Sherwood number, which represents the overall mass transfer from bulk to solid phase (Yadav, 2011), (Kløv et al, 2003). The overall Sherwood number, Sh_0, is defined as:

$$\mathbf{Sh_o} = \frac{\mathbf{Lk_{0v\_mt}}}{\mathbf{D}} \tag{2.48}$$

where k_{ov_mt} is the overall mass transport coefficient, defined by the relation:

$$k_{ov\_mt} \Delta c S_{adsorbing\_surface} = \iint_{S_{adsorbing\_surface}} [-N_A]_{on\_the\_surface} dS_{adsorbing\_surface} \tag{2.49}$$

where $[N_A]_{on\_the\_surface}$ is the component of the molar flux which is vertical to the collector surface, $S_{adsorbing\_surface}$ is the total adsorbing surface, Δc is the concentration difference between the characteristic concentration far from the adsorbing surfaces (that is usually C_{inlet}) and the average concentration on the adsorbing surface. By using simple mathematical manipulations, equation (2.48) becomes:

$$\lambda = \frac{\varphi\omega}{Pe} Sh_o \tag{2.50}$$

where

$$0 \leq \varphi = \frac{\Delta c}{C_{inlet}} \leq 1 \tag{2.51}$$

and

$$0 \leq \omega = \frac{S_{adsorbing\_surface}}{S_{inlet}} \tag{2.52}$$

3. SCALE TRANSITION

The main objective of this part of the research is to enhance our understanding of and obtain quantitative relation between the parameters and quantities under investigation, using three-dimensional porous media models. This helps to achieve a better scale up from a simplified but reasonable representation of microscopic physics to the scale of interest in practical applications. The upscaling is performed in two stages: (i) from micro -unit cell- scale to the meso -pore- scale and (ii) from the meso -pore- scale to the macro scale.

A good understanding of the dependence of parameters and quantities on pore-scale processes would require measurements of concentrations at various scales. Such measurements are, often, very difficult and quite expensive. Therefore, alternative ways to understand and transfer pore-scale information to larger scales, and to establish relationships among them, must be found.

Using mathematical simulations, one can simulate the transport phenomena under study in detail by explicitly model the interfaces and mass exchange at surfaces. Then, comparing the results of the different scale simulations, one can study the relation between these scales.

3.1. PROBLEM DEFINITION

The major reason why scale transition is investigated is the need to obtain a scale dependence of the results occurring by a transport process (Rizzi et al, 2009). It is well established that small-scale heterogeneities can have a significant impact on macroscopic results; therefore, the average effects of small-scale heterogeneities in large-scale numerical grids must be accounted for. Actually, the “how-to” upscale the reactive transport parameters from a small lab-scale to a large field-scale for modeling, is one of the most important issues in applications of the reactive transport modeling to contaminant remediation and related risk assessments (Cushman et al, 2002), (Zhou, 2007).

Upscaling is the process of replacing a heterogeneous domain by a homogeneous one, which reproduces the equivalent response with the same boundary conditions imposed (Cushman et al, 2002), (Rubin, 2003). This process inevitably has to maintain parameters known in a small scale, by spatial averaging to obtain values for larger scales when the same processes are considered. There are various upscaling methods (see the review article by Cushman et al., (2002) and the references therein), including volume averaging (Whitaker, 1967), (Slattery, 1967), homogenization (Horung, 1997), renormalization (King, 1989), (Noetinger, 1994), fractals (Neuman, 1990), (Molz et al, 2004), ensemble averaging (DyKaar and Kitanidis, 1992), Eulerian perturbation (Dagan, 1989), spectral integral approach (Gelhar and Axness, 1983), (Rajaram, 1997), Lagrangian perturbation schemes (Rajaram, 1997), central limit approach (Bhattacharya and Gupta, 1990), fast Fourier transform and Green's function method (Huang et al, 2001), continuous time random walk (Noetinger and Estebenet, 2001), (Berkowitz et al, 2003), effective medium theory (Fokker, 2001) and indicator geostatistics-based approach (Dai et al, 2004). A brief description of the major upscaling methods is given below.

The volume averaging method is in many aspects similar to the asymptotic homogenization, although it employs different mathematical formulation. A comparison of the two approaches can be found in the paper by Bourgeat et al (1988). This method is used by numerous authors for modeling transport phenomena in porous media (see for instance (Bear, 1972), (Bachmat and Bear, 1991). In recent years the formalism of the volume averaging method has been substantially developed (Whitaker 1999) and applied to various problems including multiphase phenomena (Quintard and Whitaker, 1988). The derivation of the equations, describing the process at a larger scale, is performed by taking the volume average of the governing equations from a smaller scale. Various levels of averaging are possible. The local volume averaging is used for passing from the pore scale to the local (Darcy) scale (Whitaker 1986). The resulting equations can be successively up-scaled using the large-scale averaging technique (Quintard and Whitaker, 1988). The large-scale equations are written in terms of averaged (macroscopic) variables. The local variables are represented as a sum of the averaged value and the spatial deviation. The averaged large-scale equations should be completed by the relations between the averaged values and their local scale deviations. These relations are given by differential equations, which constitute the closure problems. The solution of the closure problem allows, obtaining the large-scale effective parameters of the system from the smaller scale to use for the large one.

Homogenization is an asymptotic method for upscaling parameters of periodic media (Ene, 1990). The basic idea for homogenization is as follows. Consider a porous medium with microscopic structure characterized by period ℓ and a macroscopic structure with the characteristic length of L. A spatial scale parameter can be defined as $\varepsilon = \ell/L$. Instead of working on one function (i.e. velocity field) u, a family of functions u^{ε} is considered to find the limit of u^{ε} as $\varepsilon \rightarrow 0$. The limit is considered as the result of upscaling procedure for homogenization, which consists of finding differential equations whose solutions can satisfy the above limit. The asymptotic process $\varepsilon \rightarrow 0$ stands for the transition from microscopic to macroscopic scale. Hence, the upscaling process of homogenization is completed by making the microscopic scale approximate to zero (Horung, 1997).

Renormalization approach has been initially developed by Whilson, (1971), in order to study critical phenomena in phase transition. In example this method is used to upscale permeability in fractured porous media (King, 1989). In renormalization, an overall behavior for a certain small part (a unit cell) of a fractured porous medium is considered to be controlled by heterogeneity at a particular scale. This scale is treated as the scale of the initial stage (step 0) of the renormalization procedure. Then step-by-step transformation gives the effective properties at step, n+1, resulting from the renormalization of a set of calculated properties at step n according to a probability distribution function of ƒ(n) for the property (for example, permeability). This method retrieves the effective parameters, by recurrent applications of renormalization group transformation from the basic cell to the entire domain of interest.

According to Noetinger (2000), continuous time random walk (CTRW) begins with a finite volume discretization of a fractured porous medium for small-scale diffusion equation. A particle is then released jumping from one grid block to adjacent one with transition probability proportional to the transmissivity. When the particle starts its random walk in the domain, its movement path can be defined by its coordinates on the computational grid and by a random function of time τ, whose value is 1 if the particle moves in fracture at time t, and 0 otherwise. The correlation function of τ is closely related to fluid pressures in fracture and in matrix and can be calculated by Monte Carlo simulations. Finally, the upscaled mass transfer coefficient is computed using a suitable integration of the correlation function with respect to t (Montroll and Scher, 1973), (Berkowitz and Scher, 1998), (Salamon et al, 2006).

Over the last decades a number of powerful approaches have been developed to intelligently upscale transport phenomena in porous materials. Most of the work on upscaling methods has been done by Whitaker who is probably the pioneer in the field of transport phenomena in different scales in a porous medium. Quintard and Whitaker (1993) (1994), examined the problems arising when the upscaling of transport phenomena occurring in a specific scale and in a porous material is needed. The analysis presented by them can easily be extended to include more than two regions and have shown how the method of large-scale averaging can be applied to systems in which the Darcy-scale properties vary continuously. By Darcy-scale is meant the length scale corresponding to the first averaging process. In a two-region model of a heterogeneous porous medium, the point equations are joined with boundary conditions to form local volume-averaged transport equations. In their study of incompressible flow (Quintard and Whitaker, 1994) it has been showed that discrete and continuously varying Darcy-scale properties led to the same form of the large-scale transport equations. Under these circumstances, the choice between continuous models and discrete models is largely a matter of personal preference.

The main objective of Chapter 3 is to provide a deep understanding of the phenomena occuring in a multi-scale problem solving and to develop a methodology for estimating the appropriate value for one parameter at some scale when its value at another specific scale is known. When this is assured for every parameter at any scale, a sufficient scale-up and/or scale-down procedure for the fundamental processes occurring in a porous medium, applied to many systems. The aim is to match all geometrical, flow and transport parameters in order to move from a small-scale model to a full-scale setup and vice versa. The results obtained by different scale approaches must be compared and analyzed to obtain a strategy (scale transition rule) towards a globally-valid description to cope with the physicochemical and geometrical characteristics of a porous medium in scale-transition.

3.2.PROBLEM MODELING

The main objective of a big part of this Phd Thesis is the development of a new method for matching parameters of a process occurring in a porous medium. For the sake of application, we consider a porous medium consisting of a solid phase, distributed within a defined volume of interest and of given specific geometrical characteristics, such as porosity, average pore size, surface over volume ratio, tortuosity, etc. The void space (porous) is occupied by a Newtonian liquid or gas mixture that flows under laminar flow conditions and contains a solute, which reacts heterogeneously on the solid/liquid or solid/gas interfaces. A simple, fast hydrocarbon reaction takes place on the catalytic gas/solid interfaces at relatively low temperature. This reaction process can adequately represent a sorption mechanism under the pressure and temperature conditions specified by the phenomena that take place.

The general overall reaction representing the oxidation of a conventional hydrocarbon fuel is:

$$\mathrm{n_1Fuel} + n_2 O_2 \rightarrow \mathrm{n_3C}O_2 + \mathrm{n_4}H_2\mathrm{O} \tag{3.1}$$

where n_1, n_2, n_3, and n_4 are coefficients determined by the choice of fuel. This global reaction is often a convenient way of approximating the effects of many elementary reactions, which actually occur. Its rate must therefore represent an appropriate average of all of the individual reaction rates involved. The reaction rate for the above reaction is usually expressed as:

$$k_{ov} = AT"e^{\left(\frac{-E_a}{RT}\right)}[Fuel]^{n_1}\,[Oxidizer]^{n_2} \tag{3.2}$$

where k_{ov} is the Reaction rate constant, A is the Pre-exponential constant, T is the Temperature, E_a is the Activation energy, R is the Gas constant, [Fuel] is the Concentration of the fuel, and [Oxidizer] is the concentration of the oxidizer.

In this study, the mixture is assumed to be decane rich, therefore the decane oxidization reaction is assumed to occur whenever decane ($C_{10}H_{22}$) and molecular oxygen (O_2) reach the gas/solid interface through advection and/or diffusion.

The overall reaction is as follows:

$$C_{10}H_{22} + 15.5O_2 \rightarrow 11H_2O + 10CO_2 \tag{3.3}$$

It should be noted here that the use of Decane as well as of its oxidization reaction are options taken just for presentation purposes, not affecting the mathematics and the transport itself, as next presented. Obviously, any other species and reaction could be used instead.

The oxidation mechanism generally involves many reaction steps, making it difficult to find the exact expression of the reaction rate in widely various operating conditions, especially various temperatures. According to specific kinetic studies for the oxidation of other hydrocarbons (Se and Cavendish, 1981) (Voltz et al, 1973), the reaction rate is expected to depend on both the reactants and the eventual presence of inhibiting species that influence the reaction by their competitive adsorption on the catalytic reactive sites. The functionality of such dependence is usually quite complex and might depend strictly on the rate-determining steps of the overall reaction mechanism. Thus, the reaction rate is given as:

$$r_{C_{10}H_{22}=} - k_c T C_{C_{10}H_{22}=} - A e^{-\frac{E_\alpha}{RT}} C_{C_{10}H_{22}} \qquad (3.4)$$

where k_c is the reaction rate constant, T is the temperature, $C_{C_{10}H_{22}}$ is the decane concentration, E_α is the activation energy, and R is the universal gas constant. For the current simulations, the heterogeneous reaction characteristics were as follows (Brenner, 2009): E_a=226.783 kJ/mole with a pre-exponential factor, A=1.66 X 10^{24} m^3/s kg. Further in this analysis, the reaction is set to temperatures from 473 K up to 479, with the oxygen concentration of the mixture being much higher than that of decane. Under these circumstances, it is reasonable to consider this reaction, of first order (equation 2.43), as the oxygen concentration is a constant in the Arrhenius pre-exponential factor

$$r_{C10H22} = -k_c(T)[C_{10}H_{22}] = -A\exp\left(-\frac{E_\alpha}{RT}\right)[C_{10}H_{22}] \qquad (3.5)$$

The values of the composition for the inlet mixture used as boundary conditions set for the simulations are presented in Table 3.1.

Table 3.1 Inlet fuel mixture composition

Species	$C_{10}H_{22}$	CO_2	O_2	H_2O	NO	N_2	Total
Mass Fraction	0.000222	-	0.05	0.1	0.0002	0.8496	1.0

The scale of the transport problem could be crucial in obtaining accurate results of macroscopic interest, such as adsorption efficiency. When microscopic geometry is used to model the processes described above, all the local heterogeneities have been taken into account, and thus significantly affect the results. As the final results are of macroscopic interest, it is crucial to develop an accurate, general mechanism for scale transition. The present study focuses on the exact matching of geometrical, flow and transport characteristics when scale transition is required. For this reason, a typical porous model of meso-scale is presented, and the results obtained were subsequently scaled-up (macro-scale) and scaled-down (micro-scale).

To define the 3D domain and solve the set of partial differential equations analyzed above the CFD-GEOM was used. For the microscopic scale the geometry used is a unit cell, consisting of two concentric spheres (Figure 3.1), while for the mesoscopic scale, an assemblage of space filling unit cells has been chosen (Figure 3.2). For the macroscopic scale a structured domain was created (Figure 3.3). For each scale, a different set of geometry files with different geometrical characteristics was made.

3.2.1. MICROSCOPIC MODEL

For the microscopic scale the geometry used is a unit cell or also known as sphere-in-cell. It is consists of two concentric spheres with their diameters set to result in a specific ratio describing the solid volume fraction of the represented solid. The idea behind the unit cell approach is that it represents the whole porous medium in a much smaller scale. Therefore, all the processes occurring in the unit cell represent the processes found in the real scale of the porous medium.
In the present study this model is studied to provide a comparative scale for the outcomes. A representation of the unit cell can be seen in Figure 3.1, where a typical geometry is presented for porosity 0.7. The inner sphere (smaller one) represents the surface (interface) where the catalytic reaction occurs. The outer sphere represents the control volume where the fuel is found. The hidden surface on the left is the inlet surface from which the fuel mixture enters the unit cell, and the surface on the right is the outlet surface of the medium.

All of the transport equations described above was solved by the simulator for the unit cell taking into account numerous assumptions such as steady state flow, no gravitational forces, axial symmetry (2D) etc. Regarding the boundary conditions, the inlet velocity of the mixture varied from 0.0001 to 7 m/s in order to keep the flow laminar. This was accomplished by setting up the relevant fixed pressures to the inlet and outlet surfaces in order to have the required pressure gradient and hence flow.

The inner sphere is the catalytic surface where the oxidization reaction happens and it is assumed to have zero mass flux on it. Furthermore, the fuel mixture composition is the same as for all of the cases and it is presented in (Table 3.1). The inlet temperature is set to 473 K, while zero heat flux is set to the outlet.

The porosity of the microscopic geometry is computed using (equation (3.6)) preserving the radius of the external sphere as constant and modifying the radius of the internal sphere, while tortuosity is given by (equation (2.39.4)). The permeability and diffusivity considering multi-component diffusion is calculated as described previously. The velocity for every simulation is adjusted accordingly to maintain the Peclet number the same as in the mesoscopic model. Peclet number, *Pe*, is a dimensionless quantity representing the ratio of the contributions to mass transport by convection to those by diffusion:

$$Pe = \frac{LU}{D} \tag{3.5}$$

where L is a characteristic length scale, U is the velocity magnitude, and D is a characteristic diffusion coefficient. When the Péclet number is greater than one, the effects of convection exceed those of diffusion in determining the overall mass flux.

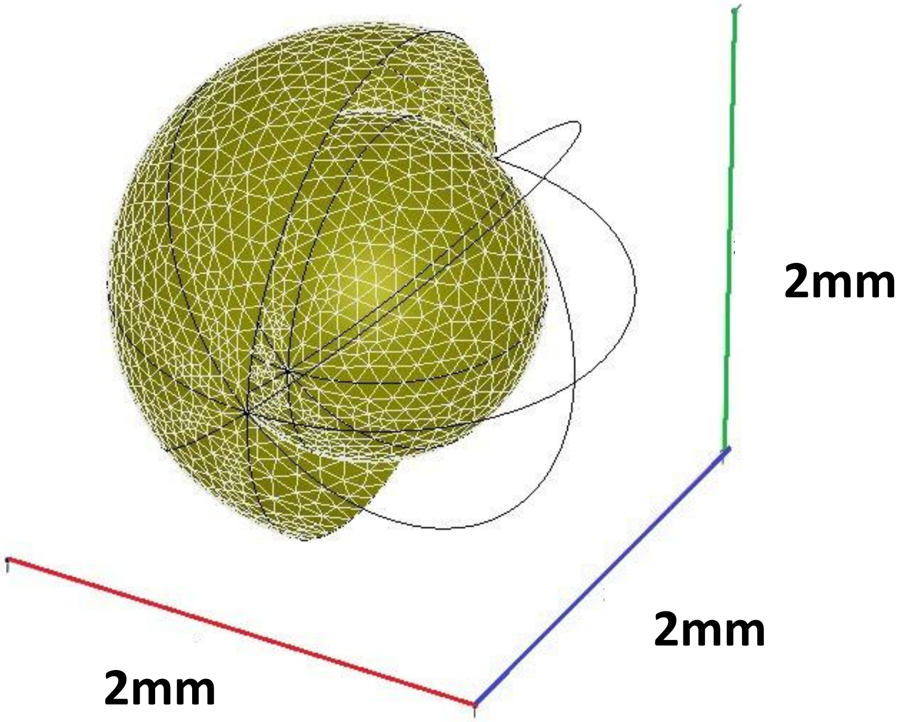

Figure 3.1 Microscopic geometry for porosity 0.7.

3.2.2. MESOSCOPIC MODEL

For the representation of the mesoscopic model an assemblage of sphere is created. The assemblage of spheres is placed in a typical orthogonal box representing the control volume of the porous medium. The spheres represent the solid part of the porous medium while the void space in between is the fluid or bulk phase. The mixture enters the control volume through an inlet surface, reaches the assemblage of the spheres and reacts on the catalytic layer on the surface of the spheres. Finally, the excess of the mixture with the products of the reaction exit the control volume through an outlet surface (Figure 3.2).

The geometrical setup and calculation of the fundamental parameters are found below. Several parameters must be defined in order to be able to proceed with the simulations. Given that each sphere radii and their total population are known, the porosity, ε, of the mesoscopic geometry can be calculated by:

$$\varepsilon = \frac{V_{void}}{V_{total}} = \frac{V_{total-}V_{sph}}{V_{total}} = 1 - \frac{V_{sph}}{V_{total}} \tag{3.6}$$

where V_{void} represents the void volume of the porous media, V_{total} is the total volume of the medium, and V_{sph} is the volume occupied by the spheres.

The geometry of the 3mm x 2mm x 3mm meso-scale porous medium with a typical porosity of 0.7 and normal distribution of sphere is depicted in Figure 3.2. The exterior walls of the control volume are hidden so the assemblage of spheres can be viewed. In order to eliminate the end effects error two extra domains have been added. The domains located attached to the inlet and outlet surfaces allow the flow to deploy before entering and exiting the porous medium volume where the Peclet number will be as required by the model.

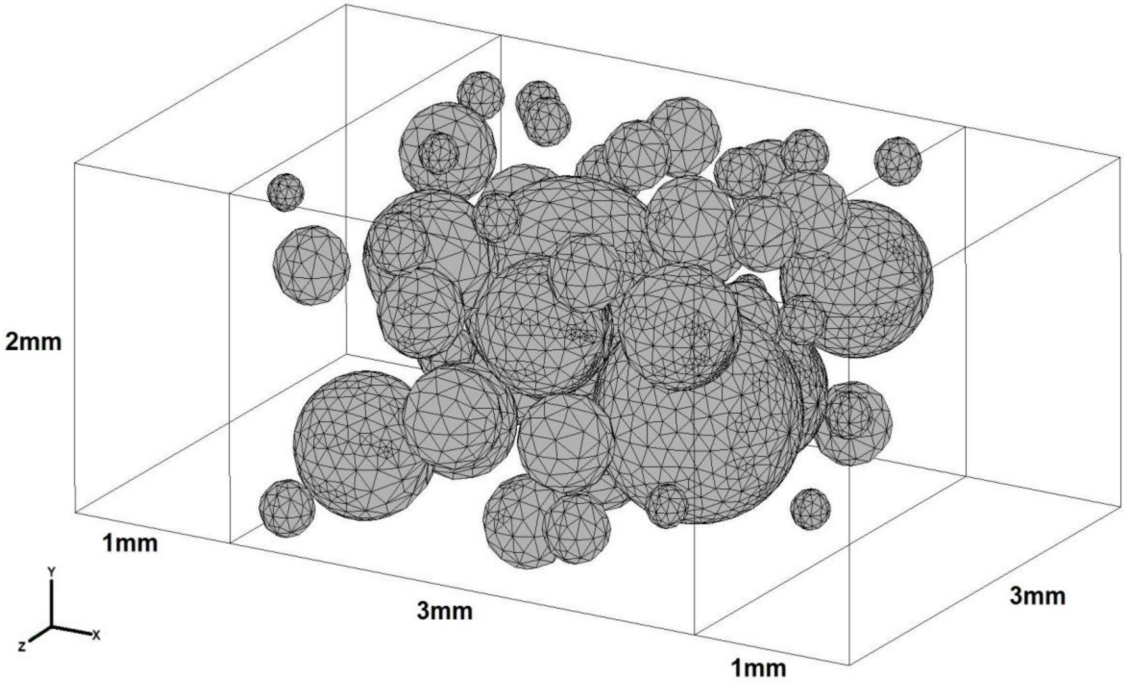

Figure 3.2 Mesoscopic geometry (porosity=0.7, normal distribution).

Sphere radii and sphere coordinates in the control volume are calculated by an algorithm implemented in Fortran 90/95 whose steps are described below:

Step (1)	Incorporating a random number generator, the position of the sphere's center is generated, always set in a box with specific dimensions (3x2x3 mm).
Step (2)	Using a random number generator along with the appropriate routine, a radius is generated, forced to follow a certain distribution (i.e. normal, random or uniform).
Step (3)	The void space surrounding each sphere is checked for availability. If it is free (not occupied by another sphere), the radius value is accepted; otherwise step 2 is repeated until an acceptable value is produced.
Step (4)	The sphere is posed.
Step (5)	Steps 1-4 are repeated until the volume of the positioned spheres satisfies the pre-defined porosity value.

Table 3.2 Geometrical characteristics for mesoscopic porous medium (normal distribution)

Porosity [-]	Permeability [m^2]	Tortuosity [-]	Average pore size [m]	S/V [m^{-1}]
0.6	8.91E-10	1.50	0.00027	8874.31
0.7	8.23E-10	1.45	0.00038	8594.38
0.8	7.40E-10	1.38	0.00036	8244.43

0.9	1.32E-09	1.30	0.0011	9098.30

The geometrical characteristics of the mesoscopic geometries (assemblage of spheres) used in the simulations are presented in Table 3.2. It is necessary to mention that the average pore size and the surface to volume ratio, S/V, are manually calculated for the mesoscopic geometries and are also used for the macro-scale model described in the following section.

A real porous medium has an unlimited combination of the structures of its porous. Hence it is necessary to examine whether the sphere radii and their locations in the porous medium have a significant effect on the mass transport occurring within. In order to examine this problem, all the necessary placing distribution tests were performed for quantifying the error levels due to the different placements of the spheres. As the sphere radii are variable, three different types of radius distribution have been used. The radii distributions examined are, the normal distribution, a random distribution and a uniform radii distribution were all spheres has the same radius. The effect of the three different distributions, on the mass transfer phenomenon for various Peclet numbers in a porous medium, with porosity 0.7, is presented in Figure 3.3a.

As it is presented on the chart below, the different type of radius distribution does not affect the overall mass transfer for the area of low and moderated Peclet numbers. However, for Peclet numbers over 100 a discrepancy is observed between the plotted values. By definition, higher Peclet numbers equal to higher convection. Hence, high velocities correlate to higher probabilities for the soluble to escape from the porous medium. Under these conditions, the radii distribution can affect the solution significantly as it defines the pore size.

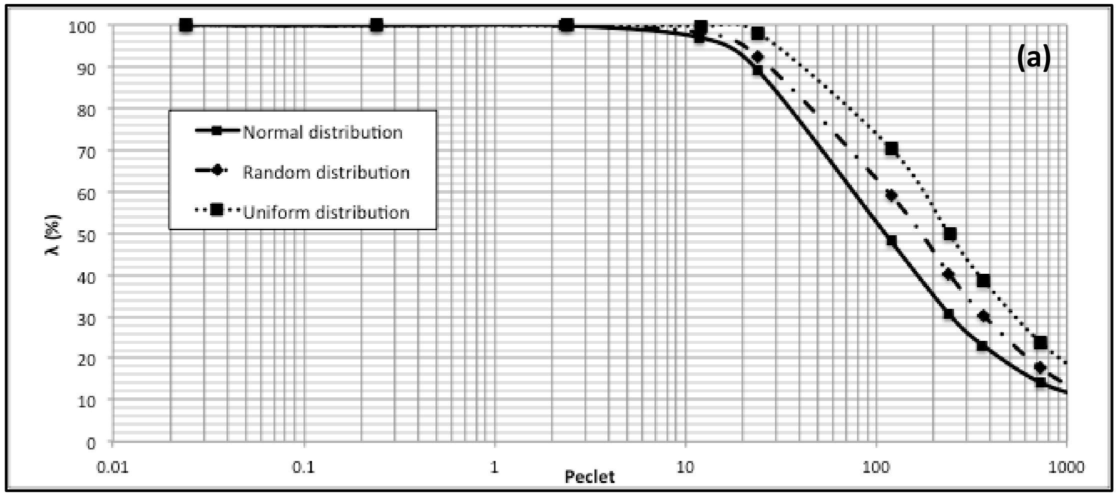

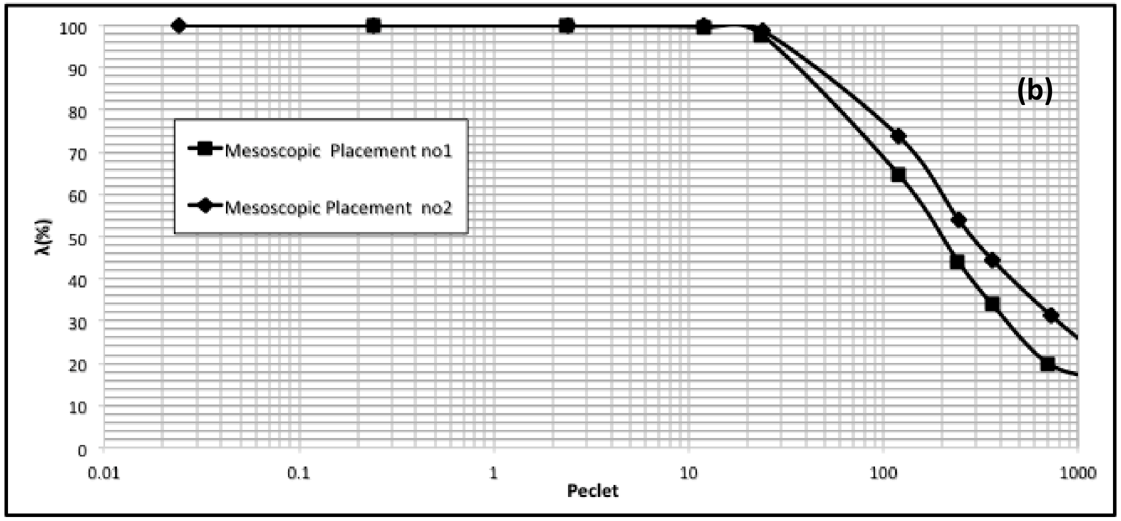

Figure 3.3 Geometry dependence tests: (a) distribution, (b) placement (ε=0.7).

Moreover, as in a real porous medium, porous can be placed with an unlimited combination of placements in space. Hence, even if the spheres follow a certain distribution it is important to study the effect of the different pore placement in the porous medium. The effect of different sphere placement in the porous volume on mass transfer occurring in a porous medium is presented in Figure 3.3b for constant porosity (0.7) and for various Peclet numbers. The behavior is very similar to the one seen in Figure 3.3a. It can be seen that for low Peclet numbers no deviation appears, while a small deviation can be seen for the higher number. As a result, since neither the distribution tests nor the placement tests, critically affect the transport processes when the regime is not strongly convectional, only the normal distribution has been considered for the detailed simulations.

3.2.3. MACROSCOPIC MODEL

In order to scale up the mesoscopic model presented in the above section, a bigger scale geometry was build representing the scale of the macroscopic model. The mesoscopic scale was built in the scale of centimeters. A representation of the macroscopic geometry is presented in Figure 6. Similarly, to the mesoscopic case, an extra volume has been added attached to the inlet and outlet surfaces respectively in order to allow to the flow to fully develop. At this scale, a porous medium is represented by a box where the pores in the solid cannot be defined in detail but only by assumptions and mathematical equations describing the porous media virtually (porosity, surface to volume ratio, tortuosity etc.). Specifically, it is assumed that both pores and voids exist in the whole control volume, while all quantities are calculated by spatial averaging. Therefore, the transport equations used to solve the model should and are modified accordingly.

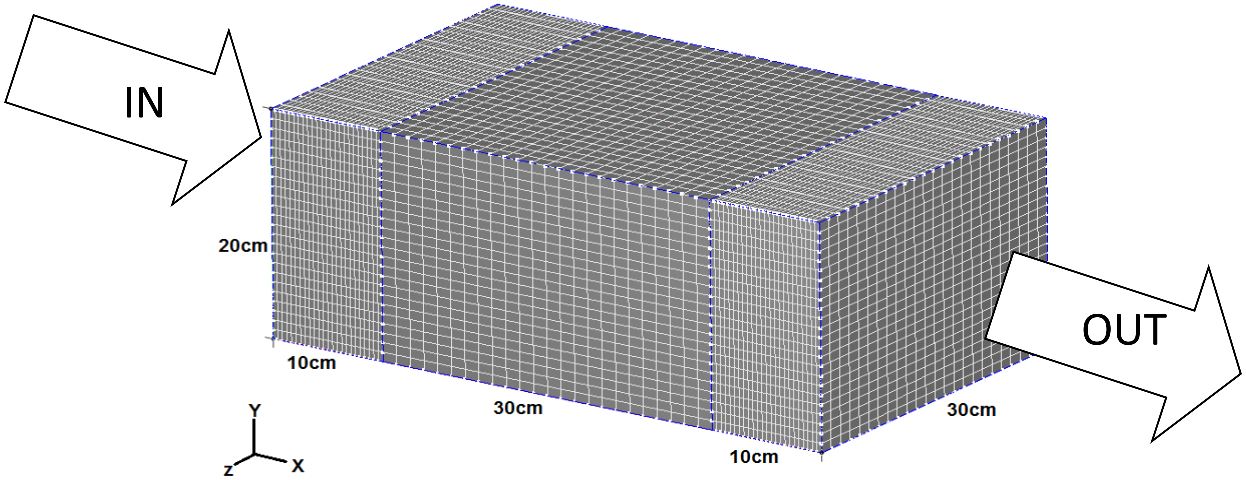

Figure 3.4 Macroscopic geometry (ε= 0.7).

The boundary conditions applied regarding the macroscopic model are presented below:

- Flow: Normal velocity varying between 10^{-6} to 7 m/s at inlet, fixed pressure of 1 atm to outlet surface, non-slip condition to walls, Darcy's law for porous region.
- Heat transfer: 473K at inlet, zero heat flux everywhere else.
- Mass transport: Constant fuel mixture at inlet (Table 3.2), zero mass flux to walls and outlet, decane oxidization on catalytic solid surfaces assuming zero accumulation.

3.2.4. MESOSCOPIC MODEL

While the micro- and meso-scopic geometries are discretized in space by an unstructured grid, the simpler macroscopic porous medium, is discretized by a non-homogeneously structured grid. In order to solve the nonlinear-coupled conservation equations described previously, the finite-volume method was adopted allowing the SIMPLEC (Semi-Implicit Method for Pressure-Linked Equations Consistent) algorithm to calculate the pressure. An HP Compaq 6000 Pro MT PC with the following characteristics was used: Intel® Core ™2 Duo CPU E7500 at 2.93GHz and 2GB RAM memory. Given the required accuracy of at least 10^{-4} for all the involved quantities, the convergence time and the maximum iterations differ for each scale.

For the mesoscopic geometry, the convergence time is significantly higher than that of the macroscopic simulations due to its complex geometry. The convergence time varies between 160 to 300 minutes, while for the macroscopic and microscopic simulations it ranges from 5 to 60 and 10 to 30 minutes, respectively. Additionally, the required iterations for convergence are 300, 2000 and 4000 for the meso-, macro- and macro-scopic simulations, respectively. To ensure that the simulation outcomes are not affected by the discretization used, grid independency tests were performed for each scale and the number of cells used was 217 000 for the meso-, 35000 for the macro-, and 110000 for the micro-scale geometry.

3.3.SCALE TRANSITION RULE

In order to upscale (or downscale) the characteristics of a mesoscopic or even a microscopic porous media volume to a larger scale the following steps are followed. First of all, the geometrical characteristics of the mesoscopic geometry (assemblage of spheres) are calculated. To change the geometry scale, i.e for this case, from the millimeters of the mesoscopic geometry to the centimeters of the macroscopic porous media, the velocity of the inlet mixture was adjusted preserving equal Peclet values for both scales. For this to be achieved, the following equations are applied:

$$Pe_M = Pe_A \frac{1}{\varepsilon} \tag{3.7}$$

$$\frac{u_M L_M}{D_M} = \frac{u_A L_A}{D_A} \frac{1}{\varepsilon} \tag{3.8}$$

As it was mentioned in Chapter III, the diffusion coefficients for all simulations, were calculated with the use of the “Mix Kinetic” theory and were practically constant. As a result, equation (3.8) becomes:

$$u_M = \frac{u_A L_A}{L_M} \frac{1}{\varepsilon} \tag{3.9}$$

where,	u_M	Inlet velocity of the macroscopic scale
	u_A	Inlet velocity of the mesoscopic scale
	L_M	Characteristic length of the macroscopic scale
	L_A	Characteristic length of the mesoscopic scale

The next step is the adjustment of a characteristic ratio of the porous materials, which defines the surface area of the pore walls per unit volume (S/V) and can be thought of as a measure of the catalyst loading. With this value CFD-ACE+ can calculate the total surface area, on which the reaction takes place in each cell by multiplying S/V by the volume of the cell.

To adjust the surface to volume ratio the following equation is used:

$$\frac{S_M}{V_M} = \frac{S_A}{V_A} \frac{L_A}{L_M} \tag{3.10}$$

where,	S_M	Surface area of the macroscopic scale

V_M	Volume of the macroscopic scale
S_A	Surface area of the mesoscopic scale
V_A	Volume of the mesoscopic scale

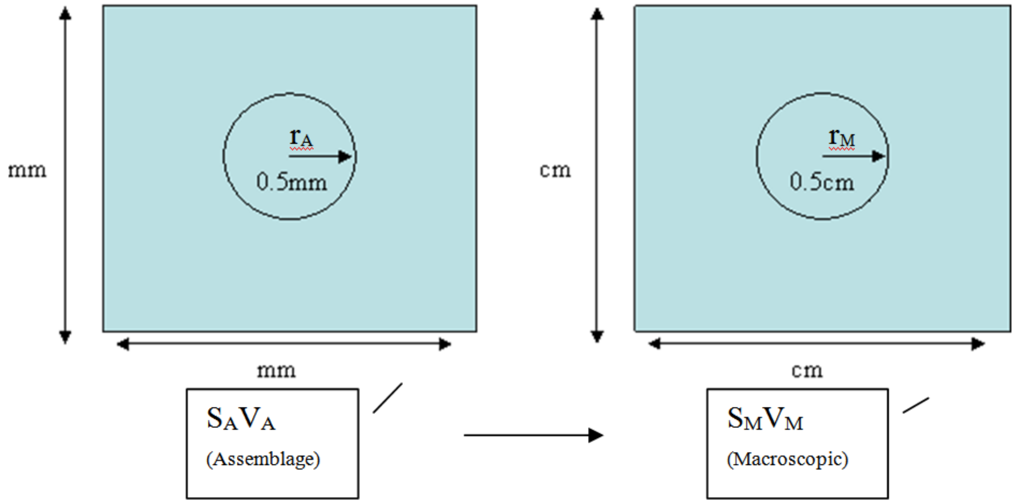

Figure 3.5 Representation of upscaling from mm to cm

The value of S/V for each simulation must be set in SI units (1/m), and since the value is not dimensionless it is affected by the geometry upscaling. This is explained briefly in the following paragraph. For the left graph in Figure 3.5, where the scale is of order or millimeters, we have:

$$S_A = 4 * \pi * r^2 = 4 * 3.14 * r_{(A)}^2 = 3.14 \text{ mm}^2 \quad (3.11)$$

$$V_A = (4 / 3) * 3.14 * r_{(A)}^3 \text{ mm}^3 \quad (3.12)$$

$$(S/V)_A = 3 / r_{(A)} = 6 \text{ mm}^{-1} = 6 * 10^3 \text{ m}^{-1} \quad (3.13)$$

If we increase the size of the pore 10 times we get:

$$S_M = 4 * \pi * r^2 = 4*3.14* r_{(M)}^2 = 3.14 \text{ cm}^2 \quad (3.14)$$

$$V_M = (4 / 3) * 3.14 * r_{(M)}^3 \text{ cm}^3 \quad (3.15)$$

$$(S/V)_M = 3 / r_{(M)} = 6 \text{ cm}^{-1} = 6 * 10^2 \text{ m}^{-1} \quad (3.16)$$

Now if we divide the two ratios, we get:

$$\frac{(S/V)_M}{(S/V)_A} = \frac{6 \cdot 10^2}{6 \cdot 10^3} = \frac{1}{10}$$

or

$$(\mathrm{S/V})_{\mathrm{M}} = (S/V)_A \frac{1}{10}$$

As a result, if we change the scale x orders of magnitude we have to decrease the surface to volume ratio of the lower scale to x order of magnitudes, or as it was shown from equation (3.10):

$$\frac{\frac{S_M}{V_M}}{\frac{S_A}{V_A}} = \frac{L_A}{L_M} \tag{3.17}$$

The final step is the adjustment of the average pore size of the porous medium. The average pore size calculation for the mesoscopic geometries was calculated manually in CFD-GEOM in order to gain a higher accuracy. The upscaling rule for this characteristic length is similar to what was presented above with only minor changes:

$$\frac{\alpha_M}{\alpha_A} = \frac{L_A}{L_M} \tag{3.18}$$

where α_M is the average pore size value of the macroscopic scale and α_A is the average pore size value of the mesoscopic scale.

If the average pore size value is not modified proportionally to the rate of the upscaling of the hypothetical sphere diameters in the porous media, the solver will assume that the hypothetical spheres are squeezed in a way of preserving the much lower void space (pores) between them.

3.4.VALIDATION

Figures 3.6-3.9 present the validation of the for all three models with results found in the relative literature. Specifically, the comparison of the trend of the results for of the microscale model with those published in Kløv et al (2003) is presented in Figure 3.6, while the comparison for the sphere assemblage scale (mesoscale) is depicted in Figure 3.7, against the trend presented by Delgado (2006). Finally, the results for the macroscopic scale are compared with the results by Abriola et al (2004) in Figure 3.8. In each case, it can be observed that the trend of the adsorption efficiency is in good accordance with the existing literature data. In all three cases the Sh_o is found to be increasing as Peclet number increases too. The fairly high discrepancy in terms of quantitative comparison, as well as the difference of the rate of increase, observed, can be attributed to the somehow arbitrary values of the parameters used and as well as to the different surface reactions and/or sorption mechanisms considered in these works.

In order to validate the results of this work, a direct comparison of experimental or theoretical results of the reaction of decane oxidation in porous materials would be necessary. However, neither experimental or theoretical results have been found as a reaction like this is not frequently used when studying mass transfer in a porous medium. Therefore and to further ensure the validity of the model, the effect of porosity on the dimensionless number known as overall Sherwood number is presented in Figure 3.9, where the results of the model of the mesoscopic scale are compared to those published by (Gunn, 1978). As expected, the results comparison shows that Sh_o number decreases as the porosity value increases validating the trend presented in this work.

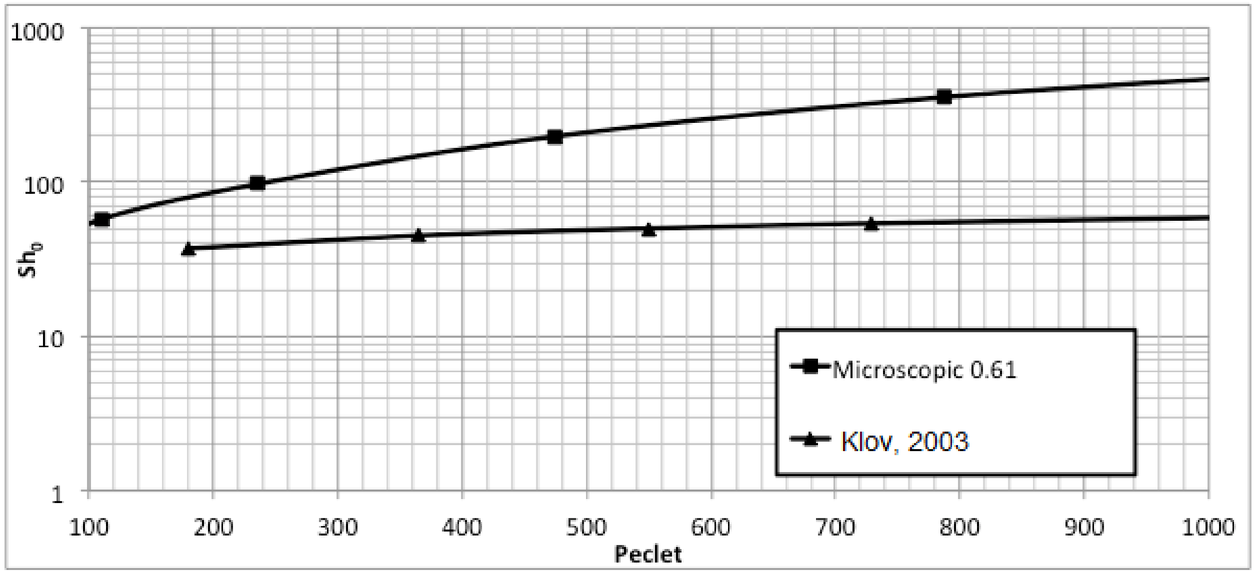

Figure 3.6 Validation of microscopic scale results for low Peclet numbers with results presented in (Klov, 2003).

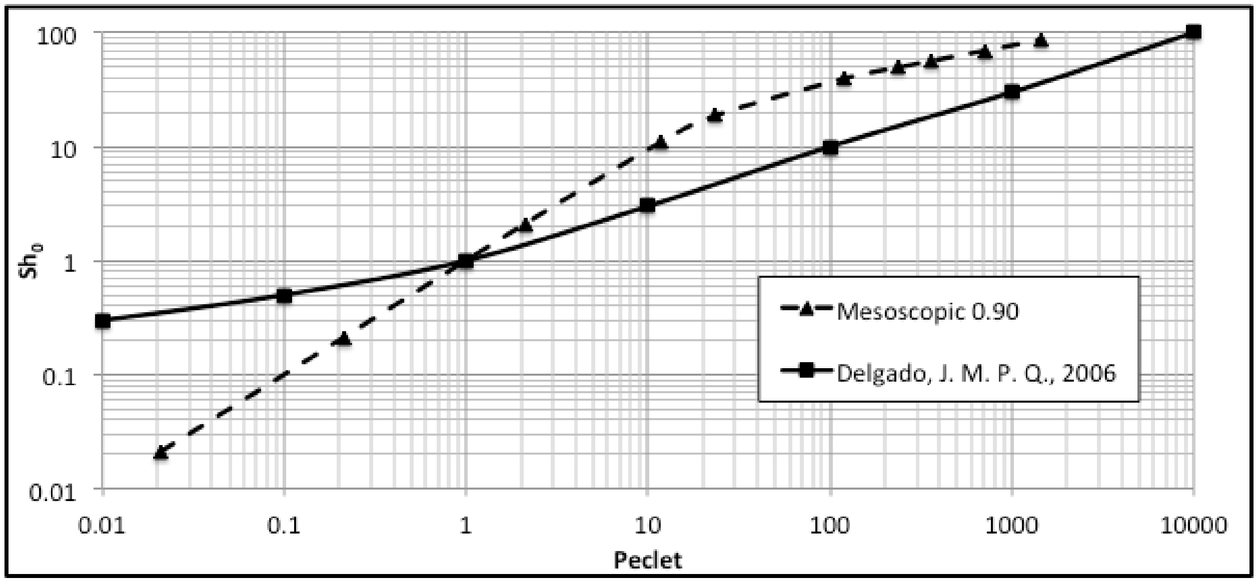

Figure 3.7 Validation of mesoscopic scale results with those presented in (Delgado J.M.P.Q., 2006).

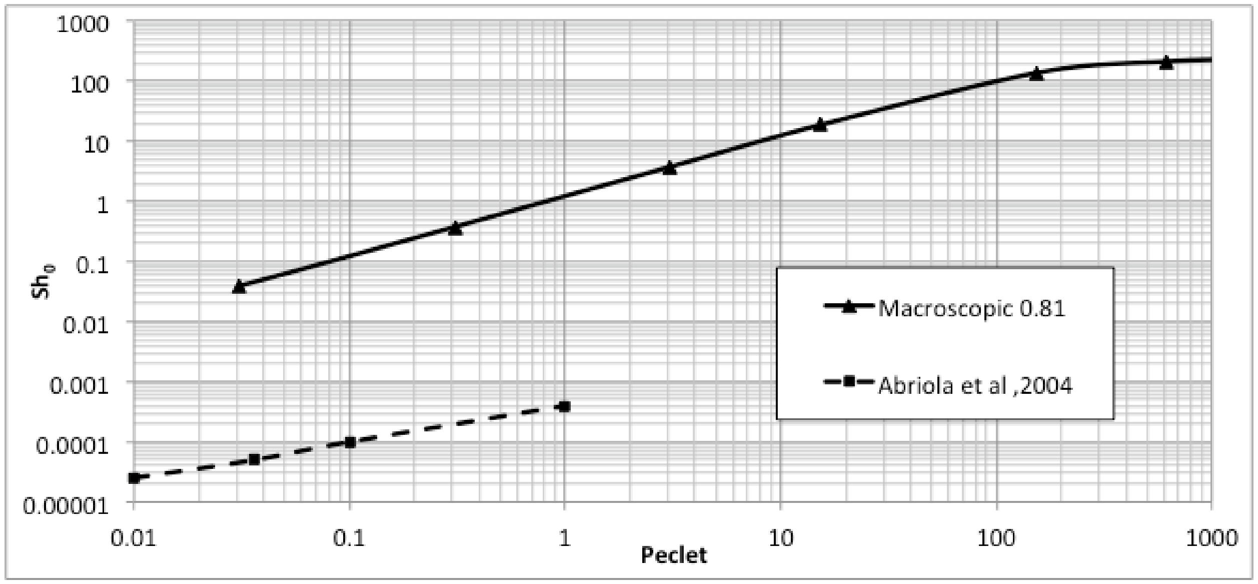

Figure 3.8 Validation of macroscopic scale results with results presented in (Abriola et al, 2004).

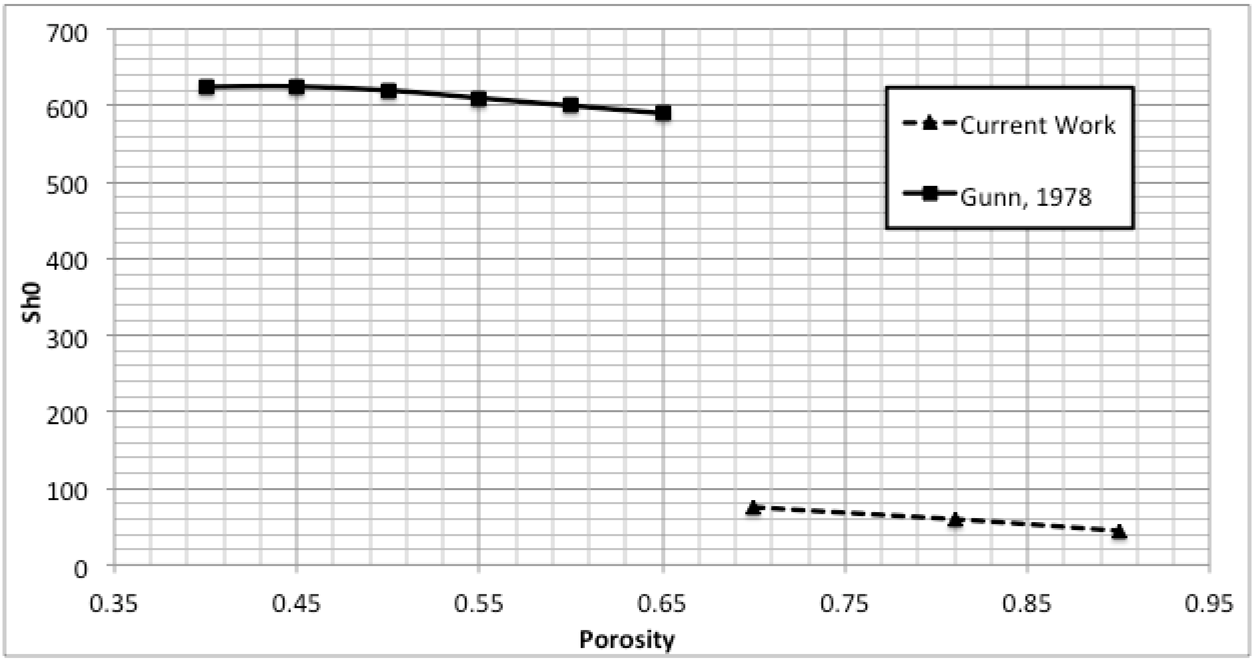

Figure 3.9 Validation of porosity effect with the behavior presented in (Gunn, 1978)

3.5.MODELING RESULTS AND DISCUSSION

Figure 3.10 presents the mass fraction of decane oxidization for all the scales taken under consideration. In order to be able to compare these results with each other, the post processing of the numerical simulations were carried out keeping both porosity and Peclet number constant (Porosity = 0.7 and Pe=50) for all scales. In Figure 3.10 it is clearly observed that the mass fraction gradient is towards the solid mass, wherever it has been explicitly defined, i.e. mesoscopic (Figure 3.10a) and microscopic (Figure 3.10b) scale, and it is proportional to the flow for the macroscopic case (Figure 3.10c) where the exact location of the solid phase is uncertain. Furthermore, decane consumption increases slightly with scale since the available adsorbing mass also increases with it. By conserving constant porosity, it ensures that the solid volume fraction is the same in all cases. However, the adsorbing surface (i.e. the adsorbing mass itself) is not the same and follows the S/V trend (see discussion).

In Figures 3.11-3.13 the adsorption efficiency, λ, is depicted for various porosity values as a function of the dimensionless Peclet number. Figure 3.11 represents the mesoscopic geometry while Figure 3.12 the macroscopic geometry, and Figure 3.13 the microscopic geometry. It can be observed that as the Peclet number increases the adsorption efficiency value decreases, for all porosities and all geometrical scales, since the flow becomes more convective and as a result the species are forced to exit the porous media before participating in the oxidization reaction. By definition low Peclet number, equals to a more dominant the diffusion regime than a convective one. This phenomenon allows the reactant species to approach the catalytic surface where the reaction happens to equalize the concentration gradient of the reacted species (Fick's law). It is important to mention that for a high reaction rate constant such as the one used in the present simulations, λ reaches the maximum value of 100%. The effect of porosity on λ values is also presented in the following figures. As porosity increases, the empty space (void volume) increases and consequently, the solid volume, which represents the catalytic surface for the heterogeneous reaction of Decane oxidation, decreases, leading to lower λ values.

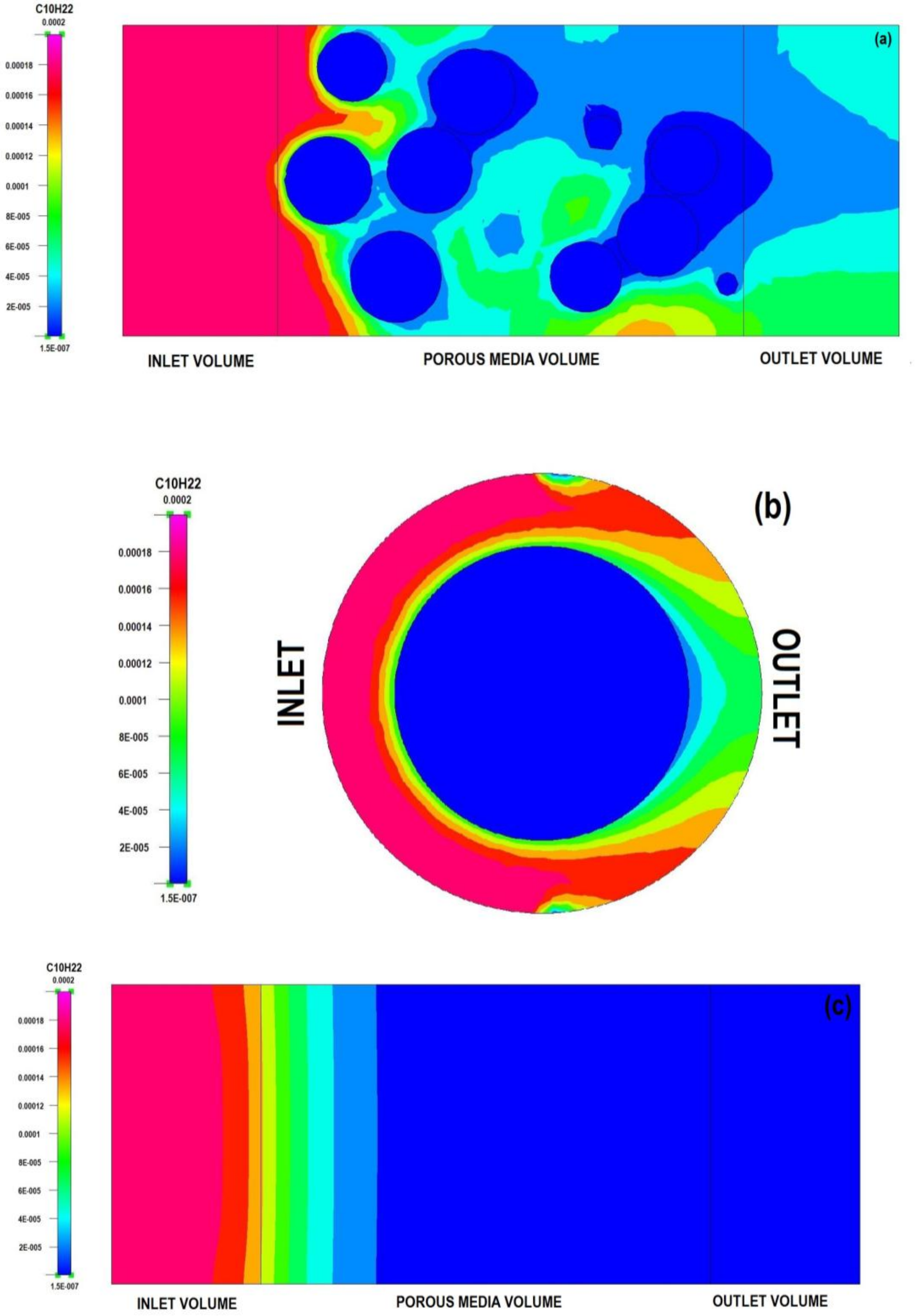

Figure 3.10. Mass fraction (a)mesoscopic, (b)microscopic, and (c)macroscopic scale (porosity=0.7, Pe=50).

Regarding the macroscopic case, Figure 9 shows an overlap of the ε=0.7 and ε=0.8 curves. This trend can be attributed to the empirical relation given by (equation (2.39.4)), which is used to calculate tortuosity, as well as to the calculation of the geometry's characteristics. (Coutelieris and Delgado, 2012)

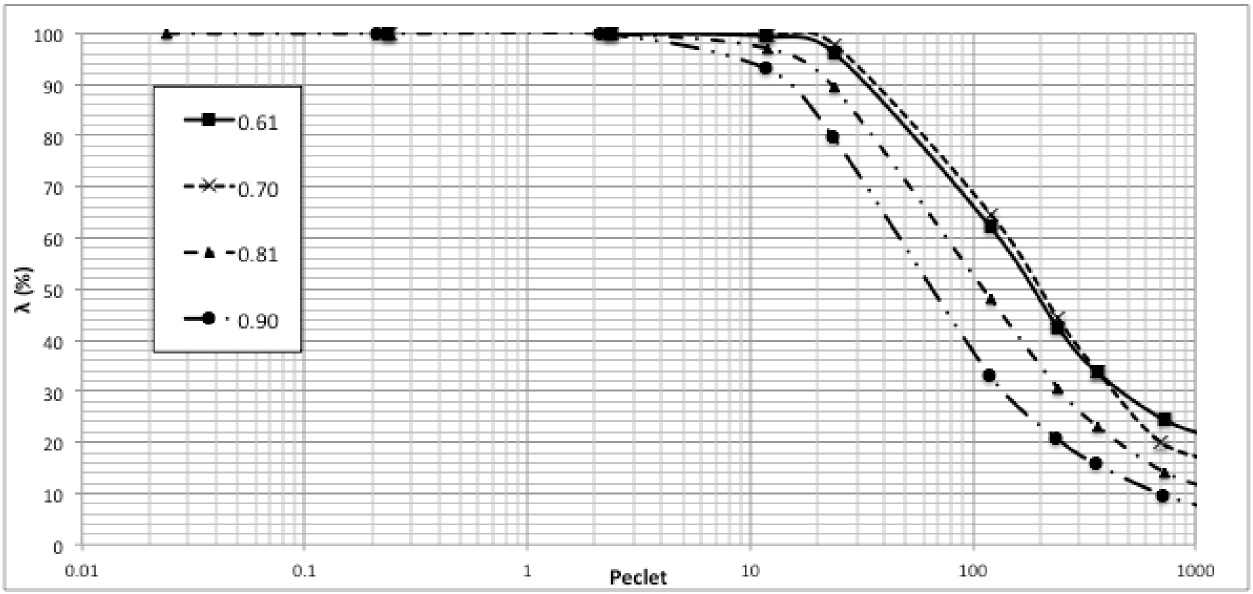

Figure 3.11 Adsorption efficiency of the mesoscopic geometry as a function of Pe for various ε.

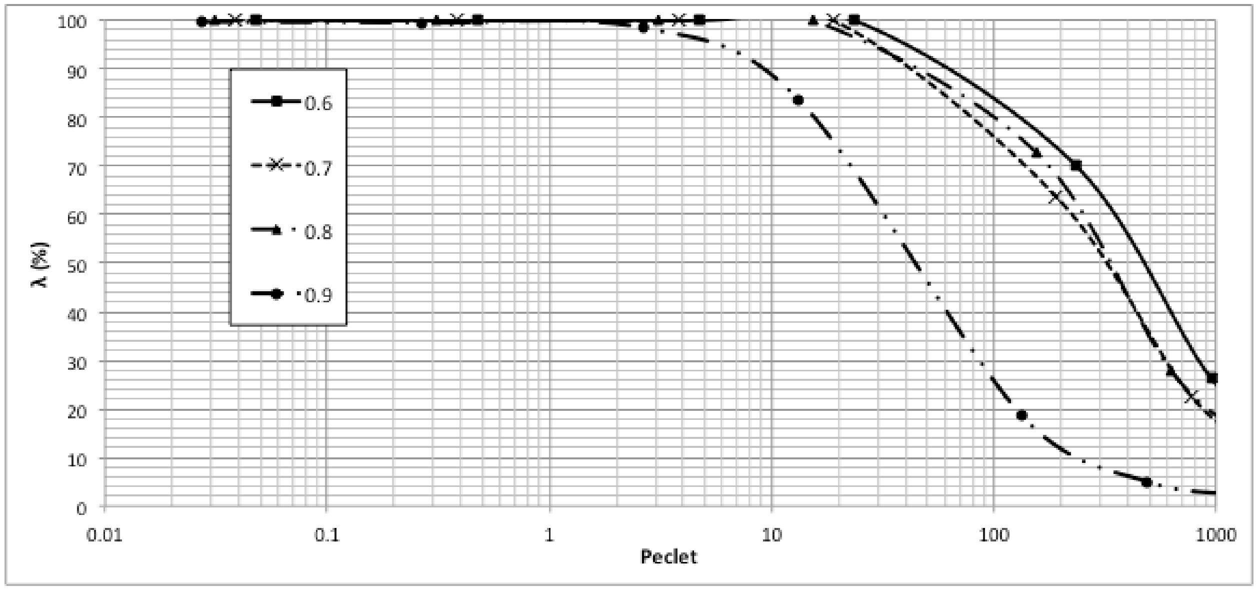

Figure 3.12 Adsorption efficiency of the macroscopic geometry as a function of Pe for various ε.

Finally, the effect of Peclet and porosity on the adsorption efficiency for the microscopic (sphere-in-cell) geometry is shown in Figure 3.13. It is noteworthy that for *Pe*>50 the sphere-in-cell is insufficient to adequately describe such physicochemical problems, since the adsorption efficiency is found to increase with porosity, although the opposite phenomenon is expected to happen. This behavior can be attributed to the presence of high local velocities at the contact area of the inlet boundary condition with the outlet boundary condition (i.e., at the area of the two - inlet and outlet - adjacent boundary cells). Conceptually, unit cell approach suffers by intrinsic disadvantages in the adequate representation of a porous structure since it is neither space filling, nor energy conservative and does not take into account the interference of other grains, etc (Kuwabara, 1959). All these limitations lead to high local advection causing gradient to the species mass fraction (Figure 3.14). As a result of these limitations, the sphere-in-cell geometry will no longer be used in the present study because the other two geometries are more efficient and accurate. Nor any future proposals will be made for the correction of the microscopic geometry, since present technology allows for the detailed numerical solution of similar models providing accurate results.

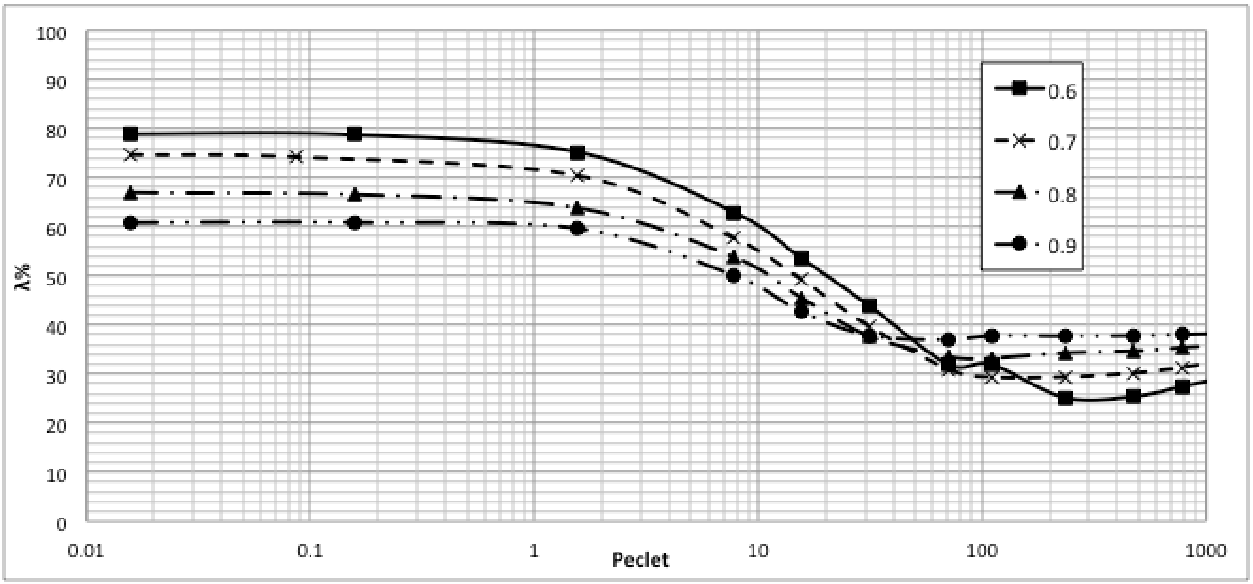

Figure 3.13. Adsorption efficiency of the microscopic geometry as a function of Pe for various ε.

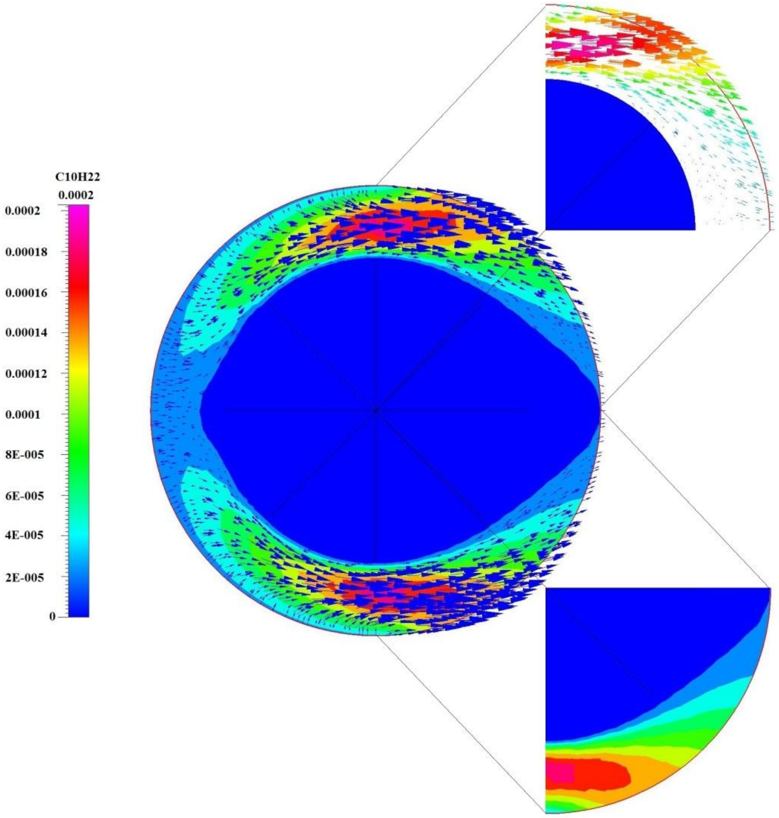

Figure 3.14 Discontinuities in the flow field for the microscopic geometry.

Applying the scale transition rule presented previously, Figure 3.15 presents a direct comparison between the mesoscopic and the macroscopic geometry for different Peclet numbers and porosities, varying between 0.60-0.90. It is found that all porosity values follow the same general trend. For the simulations with low Peclet numbers (diffusive regimes), the mesoscopic and macroscopic models predict the same λ. The difference found between the two geometries for intermediate and high Peclet values ($50<Pe<1000$) can be explained by the more detailed consideration and solution of the mesoscopic models. Furthermore, it can be observed that the decane consumption increases slightly with the scale, since the available adsorbing mass and reactive surface also increases with the scale. While constant porosity ensures that the solid volume is the same in all cases, the adsorbing surface (i.e. the adsorbing mass itself) is not the same and follows the S/V trend.

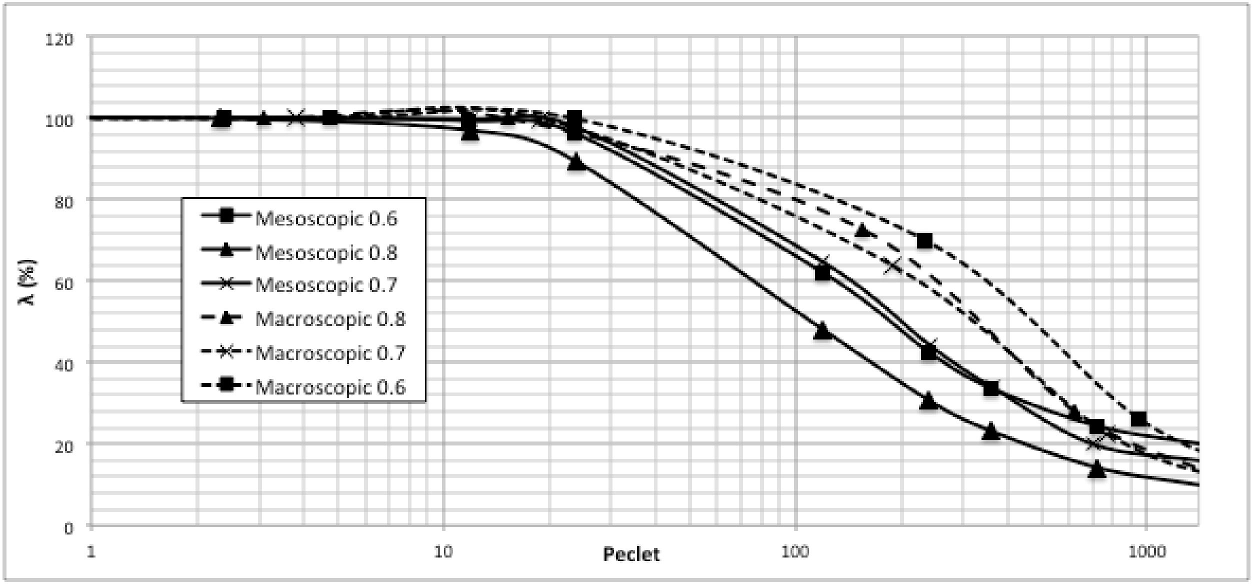

Figure 3.15 Comparison between mesoscopic and macroscopic geometry for various Peclet numbers and porosities.

The parameters used in the simulation of the macroscopic model cannot be measured manually since the pores and geometrical characteristics do not physically exist. These crucial parameters such as porosity, tortuosity and permeability can be defined from the same porosity meso-scale solution (Table 3.2). Prior to analyzing the adjustment of the parameters it is necessary to mention that similar flow characteristics such as Peclet number, should be preserved in order to allow a direct comparison of the model results between the three scales (meso-, macro- and micro-). For the mesoscopic scale, the Peclet number (Pe_{meso}) is given as:

$$Pe_{meso} = \frac{u_{meso}L_{meso}}{D} \tag{3.19}$$

where u_{meso}, and L_{meso}, are the inlet velocity and characteristic length for the mesoscopic scale, respectively, and D is the diffusion coefficient, calculated by Stefan-Maxwell equations and considered practically constant. Similarly, the Peclet number for the macroscopic scale (Pe_{macro}) can be computed as:

$$Pe_{macro} = \frac{u_{macro}L_{macro}}{D} \tag{3.20}$$

As it has been previously mentioned in order to maintain the same flow characteristics, the above dimensionless number should be equal to:

$$u_{macro} = \frac{u_{meso}L_{meso}}{L_{macro}}\frac{1}{\varepsilon} \tag{3.21}$$

Given that u_{meso}, L_{meso} and L_{macro} are already known, u_{macro} is easily computed. Additionally, the average pore size of the macroscopic geometry (α_{macro}) is given by:

$$\alpha_{macro} = \frac{L_{macro}}{L_{meso}} a_{meso} \qquad (3.22)$$

where α_{meso} is the average pore size of the mesoscopic geometry, calculated manually for each different mesoscopic geometry. Specifically, a pore size is considered to be, the distance between each two neighboring spheres. The distance is measured by subtracting the summation of the two radii from the center-to-center distance. Accordingly, the average value of these distances, for all the combinations of neighboring spheres, constituting the porous structure, is the average pore size for each case.

To maintain the constant porosity and the sphere number during scale-up, the average pore size should be modified proportionally to the rate of the scale transition (L_{macro}/L_{meso}), since otherwise it is assumed that the hypothetical spheres representing the solid in the macroscopic model are squeezed, reducing the pore spaces between them.

The surface to volume ratio, $\left(\frac{S}{V}\right)_{macro}$, can be computed for the macroscopic simulations as:

$$\left(\frac{S}{V}\right)_{macro} = \frac{L_{meso}}{L_{macro}} \left(\frac{S}{V}\right)_{meso} \qquad (3.23)$$

where $\left(\frac{S}{V}\right)_{meso}$ is the surface to volume ratio of the mesoscopic scale considering normal distribution of sphere radii. It is calculated by the summation of the spheres' surface area divided by their volume:

$$\left(\frac{S}{V}\right)_{meso} = \frac{\sum_{i=1}^{n_s} S_{meso,i}}{\sum_{i=1}^{n_s} V_{meso,i}} \qquad (3.24)$$

where n_s is the number of spheres.

4. APPLICATION OF TRANSPORT PHENOMENA

4.1. CASE STUDY 1: PHOSLOCK

4.1.1. PROBLEM STATEMENT

Due to the high bioavailability of Phosphorous it is accepted to be the most important nutrient is found in water bodies. High concentrations of phosphorous are responsible for the presence of eutrophication at several water bodies, resulting in increased aquatic plant and algal growth. Phosphorous can be released from the sediment into the water persistently preventing any improvement of the water quality for a period after the loading reduction (Søndergaard, et al., 2003) (Zamparas et al, 2014).

This case study investigates the performance of Lanthanum in the effort of reducing phosphates in water remediation techniques. As it is revealed by Douglas (2004) Lanthanum can be toxic to aquatic organizations depending on the concentration and the rate of its application. This issue is overcome by embedding the potentially toxic La into the structure of bentonite, by taking advantage of their Cation Exchange Capacity. This gave birth to Phoslock^{TM}, an increasingly used worldwide restoration tool to control phosphorus from eutrophic water bodies, developed by Common wealth Scientific and Industrial Research Organization (CSIRO) (Robb et al, 2003).

Phoslock^{TM} has demonstrated that it can reduce the Soluble Reactive Phosphorous (SRP) concentration in the water column more than 97% in less than 36 hours' time period. Phoslock^{TM} in the presence of Phosphorus reacts forming a highly stable mineral known as Rhabdophane ($LaPO_4$). Phoslock^{TM} is applied in the treated water using two main application techniques. Spreading it in a granular form or as a thick suspension and as solid/water slurry through spray manifolds. As it settles through the water column it binds the orthophosphates permanently and rests on the sediment, acting as a capping material to prevent Phosphorous being released from the sediment (Robb et al, 2003) (Lürling and Tolman, 2010) (Akhurst et al, 2004) (Ross, 2006).

The main objective of this case study is to investigate the adsorption process modeling point of view of phosphate onto Phoslock^{TM}, validating the results with experimental process. This case study utilized the mathematical simulation in order to clearly understand physics and chemistry in phosphates reducing processes along with the use of Phoslock^{TM}. Computational fluid dynamics (CFD is used to analyze the complex systems occurring in the remediation process using Phoslock^{TM} involving fluid flow, heat transfer and mass transport processes. (Rizzi et al, 2009) (Brenner, 2009).

Detailed simulations were carried out, allowing for a deep insight of the removal process. Phosphate uptake was evaluated vs pH and adsorption kinetics. The effects of temperature and salinity (fresh, brackish and marine waters) on phosphate-uptake capacity were also investigated. Bench-scale batch experiments were performed to examine its efficiency as an adsorbent for phosphate removal from natural waters and were directly compared with the numerical simulations.

4.1.2. PROBLEM MODELING

In order to adequately simulate the bed adsorption, a mathematical model, similar to the unit-cell approach (Kuwabara S. , 1959) (Uchida S. , 1949) was developed. By considering that all the grains fall towards bed's bottom under uniform velocity conditions, the active material acts like a "curtain" that falls with uniform velocity. Consequently, it's able to estimate the porosity of the model by using a 2D approach, as follows

$$\varepsilon = \frac{S_{void}}{S_{bed}} = \frac{S_{bed} - S_{grains}}{S_{bed}} = 1 - \frac{S_{grains}}{S_{bed}} = 1 - \frac{\sum_{i=1}^{N_{gr}} \pi R_i^2}{\pi R_{bed}^2} \qquad (4.1)$$

where, R_i is the radius of sphere i,

R_{bed} is the radius of bed and

N_{gr} is the number of the grains.

By assuming that the grains' radii satisfy the uniform distribution ($R_i = R = cons.$), N_{gr} can be calculated as follows:

$$N_{gr} = \frac{m}{\frac{4}{3}\pi R^3} = 7{,}156{,}592 \qquad (4.2)$$

By assuming that the grains are homogeneously distributed on the surface without touching each other, it is easy to divide the whole surface in Ngr cubic unit cells, each one containing one solid sphere located at its center. The conceptual idea behind the unit cell approach is that the unit cell is an adequate representative of the whole medium; therefore, processes occurring through the whole structure are sufficiently described by those occurring in the unit cell. The dimensions of the outer cube must be adjusted so as the ratio of the solid volume to the volume of the liquid cubic envelope to represent exactly the solid volume fraction of the porous medium. The following Figure 4.1 schematically depicts this modeling approach.

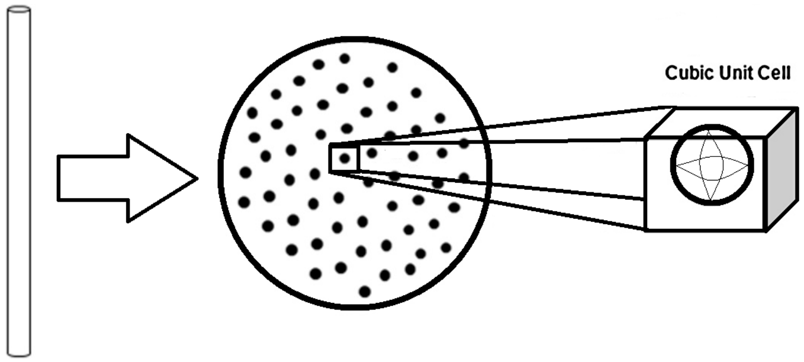

Figure 4.1 Unit cell approach

The void space (porous), is considered to be occupied by a Newtonian liquid mixture that flows under laminar flow conditions and contains a solute, which takes part in a heterogeneous reaction on the solid/liquid interface. It must be noticed that the inner sphere represents the surface (interface) where the heterogeneous catalytic reaction occurs while the outer cube represents the control volume of the eutrophicated water body. This reaction process represents a sorption mechanism under the environmental conditions specified by the phenomena that take place. The simulation assumes that the Phosphate (PO_3^{-4}) flows through the liquid phase (void space) and approaches the liquid/solid interfaces of the lanthanum-modified bentonite, Phoslock^{TM}, through advection and/or diffusion. More precisely, the solid surface is assumed to be Lanthanium (La^{3+}), which reacts with Phosphate to produce $LaPO_4$.

The overall reaction is as follows:

$$La^{3+} + PO_4^{3-} \rightarrow LaPO_4 \tag{4.3}$$

Since the temperature is fairly low and there is only one liquid reactant, it is reasonable to assume that the reaction rate depends only on the PO_4^{3-}, concentration and is of first order, given as (Atkins and De paula, 2010):

$$r_{PO_4^{3-}} = -k_c(T)C_{PO_4^{3-}} = -k_{c,0}e^{-Ea/RT}C_{PO_4^{3-}} \tag{4.4}$$

where	k_c	Reaction rate constant,
	T	Temperature,
	$C_{PO_4^{3-}}$	Phosphate concentration,
	E_a	Activation energy,
	R	Universal gas constant.

The transport processes solved in this case study were described in detail in Chapter 2. However, a brief presentation of the main equations solved is given below (steady state conditions are applied) (Bird et al, 1960). Firstly, the continuity equation is written as:

$$\nabla \cdot (\rho \vec{u}) = 0 \tag{4.5}$$

where U is the velocity vector, and ρ is the fluid density. Due to the low Reynold's numbers, flow is considered to be laminar and can be described by the following momentum equation:

$$\nabla \cdot (\rho \vec{u} \vec{u}) = -\nabla P + \nabla \cdot \tau \tag{4.6}$$

where P is the pressure and τ is the shear stress tensor. Additionally, heat transport phenomena described by the energy conservation equation are expressed as:

$$\nabla \cdot (\rho \vec{u} h_i) = -\nabla \cdot \vec{q} \tag{4.7}$$

where h_i is the enthalpy of i^{th} species (enthalpy of formation and sensible heat), and q is the heat flux given by:

$$\vec{q} = -k\nabla \mathrm{T} + \sum_{i-1}^{N_s} \overrightarrow{J_{Diff,i}} h_i \tag{4.8}$$

where k is the thermal conductivity (calculated by the kinetic theory of gaseous mixtures (Bird et al, 1960), N_s the total number of gas species, and $J_{Diff,i}$ is the mass diffusion flux of the i^{th} species, expressed as:

$$J_i = \rho \vec{u} Y_i - \rho D_i \nabla Y_i \tag{4.9}$$

where Y_i is the i^{th} species mass fraction, and Di is the diffusivity of the i^{th} species in the mixture. Lastly, the species mass fractions are calculated using the mass conservation equation:

$$\nabla \cdot (\rho \vec{u} Y_i) = \nabla \cdot (\rho D_i \nabla Y_i) + \dot{\omega} \tag{4.10}$$

where $\dot{\omega}$ is the production/consumption rate of species i, due to reaction. To investigate the performance of the grains, the macroscopic adsorption efficiency, λ, is used and as it has been mentioned begore, its defined by the ratio of the solute adsorption rate divided by the rate of the upstream flux given by equation (2.18):

The flow conditions are considered laminar. The fuel mixture at the entrance is assumed to be homogeneous, considering no mass accumulation either at the entrance or exit. In order to perform the simulations, the heterogeneous reaction characteristics were as follows (Haghseresht et al, 2009) E_a=2044.75 kJ/mole, pH=7, $k_{c,0}$=6000 m^3/s kg while the inlet composition mixture is 20 mg/water L. Regarding the boundary conditions, fixed pressure of 1atm has been applied to the outlet surface, while normal velocity of 1.6×10^{-4} m/s to the inlet one, as it was experimentally measured.

Furthermore, zero mass fluxes have been set to the walls and outlet, assuming zero accumulation. Finally, the inlet mixture is set to 273 K and zero heat fluxes have been also set to the walls and outlet. For the solution of the nonlinear, strongly coupled conservation equations described previously, the finite-volume method was adopted allowing the SIMPLEC (Semi-Implicit Method for Pressure-Linked Equations Consistent) algorithm for the calculation of pressure. The parameters applied in the simulations are presented in the following Table 4.1. An HP Compaq 6000 Pro MTPC was used having the following characteristics: Intel® Core^{TM} Duo CPU E7500 at 2.93 GHz and 2 GB RAM memory. Given the required accuracy of at least 10^{-4} all the involved quantities, the convergence time was approx. 10 min, corresponding to a maximum number of 150 iterations.

Table 4.1 Simulation parameters and equations.

Quantity	Expression	Reference
Viscosity	$\mu_i = 2.6693 \times 10^{-5}$	(Bird et al, 1960)
Collision integral	$\Omega = \frac{1{,}16145}{(T^*)^{0{,}14874}} + \frac{0{,}52487}{e^{0.77320(T^*)}} + \frac{2.16178}{e^{2.43787(T^*)}}$	(Bird et al, 1960)
Dimensionless temperature	$T^* = \frac{\kappa T}{\varepsilon}$	
Diffusion coefficient of the mixture (Bruggeman approach)	$D_{i,eff} = e^{\tau} D_i$	(Coutelieris and Delgado, 2012)
Tortuosity	$\tau^2 = \frac{1}{1-(1-\varepsilon)^{1/3}}$	(Coutelieris and Delgado, 2012)

The experimental analysis as is described in detail in the work of Zambaras et al (2015) shows the equilibrium adsorption capacity of phosphate as a function of initial concentrations. The experimental isotherm data as denoted in Figure 4.2, is described by the typical Langmuir-curve isotherm.

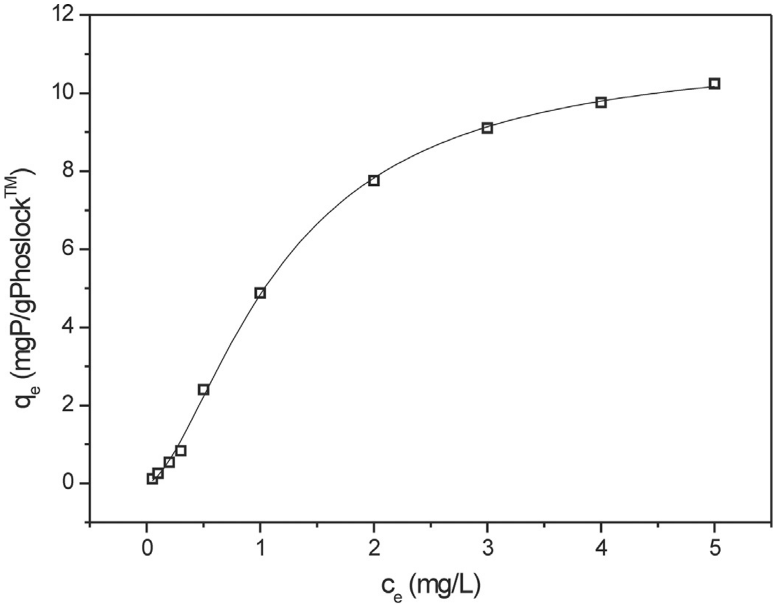

Figure 4.2 Experimental isotherm data (Zamparas et al, 2015)

In general, the isotherm shows a rise in the adsorption capacity with an increase in the equilibrium solution concentration, followed by a plateau at equilibrium. In this type of isotherm, (Langmuir type the phosphate uptake increases rapidly with the equilibrium concentration within the range of C_e from 0 to 2 mg/L, while during the further increase of the equilibrium concentration, the increase of phosphate uptake becomes less significant. The mass of the adsorbed phosphorus at an initial concentration 0.1mg P/L (which generally corresponding respectively to eutrophic waters) was 0.26 mg P/g Phoslock^{TM}.

Adsorption kinetic data of phosphate on Phoslock^{TM} for 7-time intervals ranging between 15 and 240 min are presented in Figure 4.3. The plot represents the adsorbed amount of phosphorus, which has been bonded within Phoslock^{TM} as a function of time. As is concluded, most phosphate is captured during the first 50 min of the “remediation” process. As contact time increases, the removal rate decreases considerably and is almost negligible at 100min. At approximately 120 min of duration, the sorption equilibrium begins to establish itself. The high adsorption rates observed at the beginning of the experiment are attributed to the very low saturation of adsorbed phosphate on the active while the gradual decrease observed for longer time periods relates to intra-particle diffusion processes.

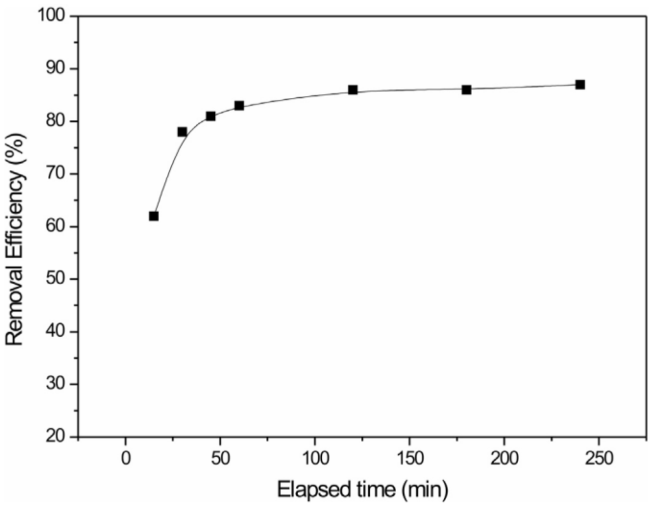

Figure 4.3 Adsorption kinetics of phosphate-uptake by Phoslock. (Zamparas et al, 2015)

Typical simulation results are depicted in Figures 4.4 (a) and (b), where the concentration of the reactant and the product within the unit cell are presented, respectively. It is clearly shown that the concentration gradient lowers towards the solid mass. As expected, areas where the reactant has the lower concentration is characterized analogously by higher concentration of product and vice versa. Furthermore, the higher product concentration is observed in the stagnant point, where the convection mechanism is found to be negligible, eliminating the possibility for the material to escape easily from the volume of interest.

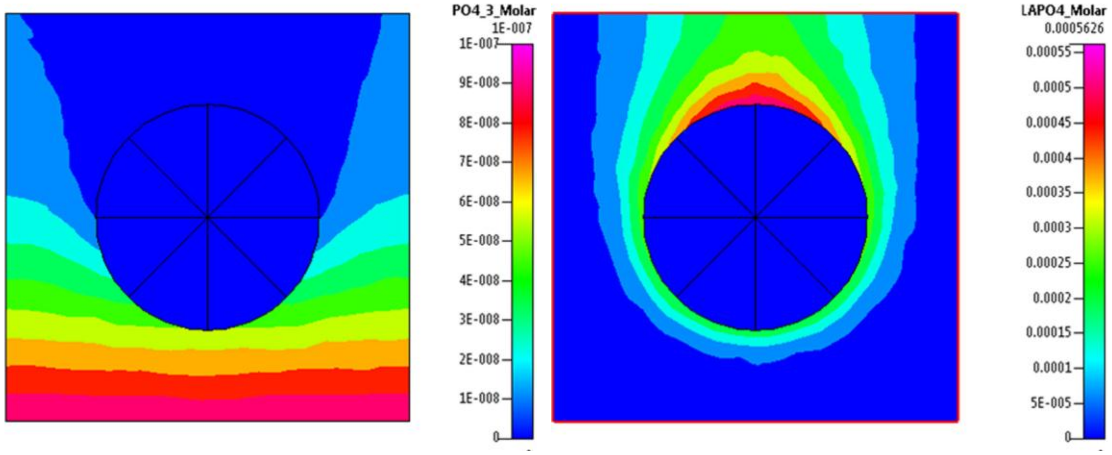

Figure 4.4 Concentration within the unit cell.

It is important to underline that the adsorption efficiency calculated by the simulations is calculated to be 87.41%, being in excellent agreement with that experimentally measured (approx. 87%). The latter was expected as far as a “reverse engineering” process has been incorporated in the simulation procedure. The first step was recognizing that the reaction rate

(Equation (3.16)) is one expression dependent on two-parameters (E_a and $k_{c,0}$) and setting the value of the first one in a widely accepted value (namely Ea= 2044.75 kJ/mol, see (Haghseresht et al, 2009). Then the other one was estimated through the constraint of the agreement between experimental and theoretical values for λ in a tolerance $< 10^{-2}$.

As a second part of the study, the influence of temperature on phosphate adsorption was determined, for temperatures ranging from 5 to 35°C. As it is shown in Figure 4.5, the high temperature is found to be advantageous for the process of phosphate adsorption. It is shown that the increase in the adsorption capacity is analogous to the increase in temperature. This phenomenon indicates that the adsorption reaction is endothermic and the ion-exchange mechanism is favored at higher temperatures. Moreover, the increases in adsorption capacity of Phoslock^{TM} at higher temperatures is strongly coupled to the stronger diffusion and higher reaction rate.

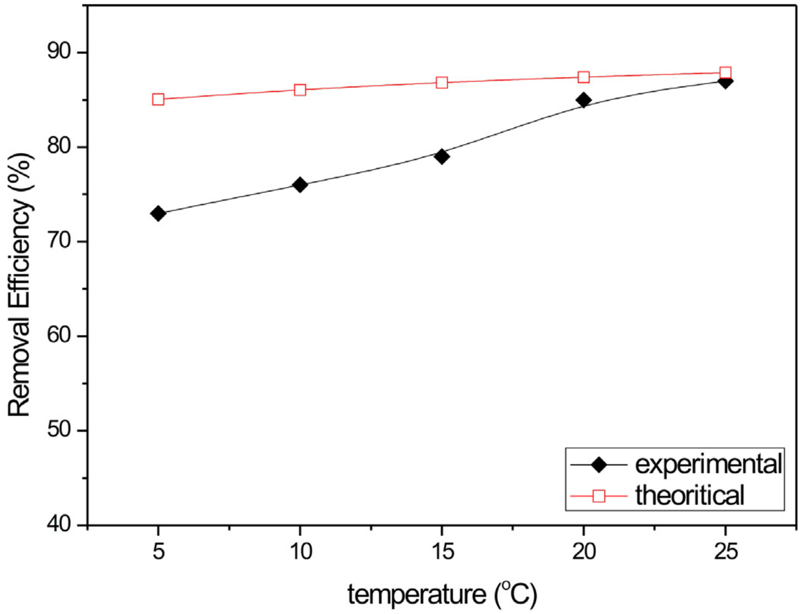

Figure 4.5 Effect of temperature on phosphate-uptake by Phoslock.

However, it is important to notice the discrepancy between experimental measures and simulation numerical estimations. Although the agreement is found to be perfect for T = 25◦C (as expected), the agreement becomes more and more poor as the temperature decreases. The deviation is approaching a 10% difference, approximately, for the low temperatures of 5-10◦C.

This inconsistency between the experimental and the numerical data can be attributed to the internal inefficiencies of the unit cell approach, which overestimates the adsorption efficiency, as discussed in detail in Chapter 3. On the contrary, the modeling approach allows a deep understanding and characterization of the processes occurring. By calculating the dimensionless

Peclet and Damköhler numbers, it is clear that, the major driving force for mass transport is the influential reaction, while convection is significantly dominant over diffusion.

Table 4.2 Dimensionless numbers controlling the process (Zamparas et al, 2015)

T (^{o}C)	Peclet [Convection / Diffusion]	Damköhler [Reaction rate / diffusive mass transfer rate]
5	10.90	210.60
10	9.54	220.49
15	8.48	230.48
20	7.63	240.55
25	6.94	250.71

This correlation demonstrates a complex behavior found through the competitive character between the transport processes:

a) the majority of phosphate molecules that approach the active surface are adsorbed (high Damköhler), and,
b) the number of phosphate molecules that escape from the volume are significantly higher than those approaching the surface (high Peclet).

Both of the above behaviors result in a slight effect on the adsorption efficiency under temperature variation.

4.1.3. MODELING RESULTS AND DISCUSSION

The current work was carried out to create a tool for the support of the pre-restoration study of a degraded lake and reservoir systems. For this reason, the investigation of the adsorption process from both experimental and modeling point of view of phosphate onto Phoslock^{TM} is of great importance. The findings can be summarized as follows:

1. The phosphate adsorption efficiency of Phoslock^{TM} calculated by the simulations was 87.41% at 25°C, being in excellent agreement with the experimental results (~87%).

2. However, a discrepancy between experimental measurements and simulation estimates was observed. Although the agreement is perfect for T = 25°C (as expected by the “reverse engineering” process), it becomes more and more poor as temperature decreases, approaching approx. 10% difference for the low temperature of 10°C. This inconsistency between experiment and model can be attributed to the internal inefficiencies of unit cell approach, which in particular overestimates the adsorption efficiency. Accordingly, to the cell approach, the medium is considered as an assemblage of unit cells gathered in a regular manner, thus one unit cell is the

adequate representative of the whole medium, and therefore processes occurring through the porous structure are described sufficiently by those occurring in the unit cell.

More precisely, sphere-in-cell models are based on the representation of the overall solid mass by a spherical or cylindrical solid body, which is embedded in a spherical or cylindrical liquid envelope, respectively. The boundary conditions imposed on the outer surface of the envelope are supposed to adequately represent the interactions with the other grains of the swarm. Obviously, the thickness of the surrounding fluid layer is adjusted so the ratio of the solid volume to the volume of the liquid envelope to represents exactly the solid volume fraction of the porous medium. The main advantage of these models is that an analytical expression for the stream function can be obtained demanding significantly less effort than that needed for numerical investigations. The spherical shape corresponds to a formulation which leads to axially symmetric flow that has a simple analytical solution of closed form and can thus be used readily for heat and mass transport calculations.

Although this analytical solution is an approximation of the real flow field in a complex porous structure, it was sufficient for the engineering applications raised until the early 1980’s. On the other hand, the model has one disadvantage in that the outer envelope is not space filling, a difficulty which must be dealt with when a scale-up from the single unit cell to an assemblage of particles is necessary. On top of this, a significant problem of unit-cell approach is that they are valid for high porosity values, a consideration which corresponds to an outer sphere of radius significantly higher than the inner one, i.e. porosity takes quite high values. In general, the lower the porosity the higher the erratic behavior is observed for this model. This behavior is due to the fact that high porosities, where analytical models are in principle applicable, correspond to a very low number of spheres for the numerical representation of the porous medium. It should be noted that at porosities lower than 0.8, the available analytical approaches become gradually less accurate and therefore less dependable (Coutelieris and Delgado, 2012).

4.2.CASE STUDY 2: HEAT TRANSFER

4.2.1. PROBLEM STATEMENT

It is rather common practice for marine industry to use water heating coils for heating up heavy fuel oil. Obviously, the efficiency of heat transfer process is strongly dependent on the dimensions of the coil (length, thickness, and diameter) as well as on the operational parameters (oil temperature, steam temperature, steam pressure). In the present work, the heat transfer from superheated water considered at high temperature (~424K) and fixed pressure (5bar) to fuel oil tanks of specific dimensions was theoretically investigated, by both macroscopic thermo-dynamical approach and microscopic simulations (by using CFD-ACE+).

Numerous merchant ships use till nowadays low-round diesel engines that are fueled by the relatively inexpensive Heavy Fuel Oil (HFO). The efficiency of these marine diesel engines approaches 48-51 % while a huge amount of heat is wasted, mainly through the flue gases (Dzida and Mucharski, 2009). In order to prepare HFO for propulsion, an increment of its temperature is necessary in order to lower its viscosity and, hence, to obtain smooth and continuous flow. In order to achieve that, a large amount of heat is necessary to increase the tanks temperature, frequently provided by superheated water (MAN). This concept of heat transfer between a heated liquid flux and a colder volume of stationary HFO is mainly encountered in applications other than ships’ supply, such as oil drainage (Butler et al, 1981) recovery in wellbores (Songyan et al, 2010), etc. The amount of the necessary heat is found to be quite huge, and an efficient energy waste management is often absolutely crucial.

Computational fluid dynamics (CFD) could be a very powerful tool towards this aim as the heat transfer process can be sufficiently described through normal thermodynamic analysis, at least from a macroscopic point of view.

The main scope of this work is to identify the appropriate geometrical characteristics and the length of the carbon-steel tube (a.k.a coil) through which the superheated water flows and exchanges heat with the HFO. This application has been studied from both thermodynamical and process-simulation points of view. Therefore, a thermodynamic analysis for heat exchange has been performed, based on heat balances throughout control volumes. On the other hand, detailed simulations were carried out, allowing for a deep understanding of the heat transfer process. The results of both approaches have been evaluated against geometrical characteristics (coil length, diameter) and operational parameters (tank insulation, steam pressure).

4.2.1.1. THE SYSTEM

Consider a tank, with dimensions 3.2m x 7.6m x 12.56m and volume 306m^3, filled up to 85% with heavy fuel oil. This settling tank receives the HFO from ashore sources at an average temperature of 303K and has to heat it up to the average temperature of 333K.

Towards this aim, heating coils are used, where the provided superheated water is at temperature 424K degrees at a constant pressure of 5bar. The coils are manufactured by boiler tube carbon-steel of 50mm external diameter with thickness 4mm, having a "serpentine" shape, as Figure 4.6 depicts.

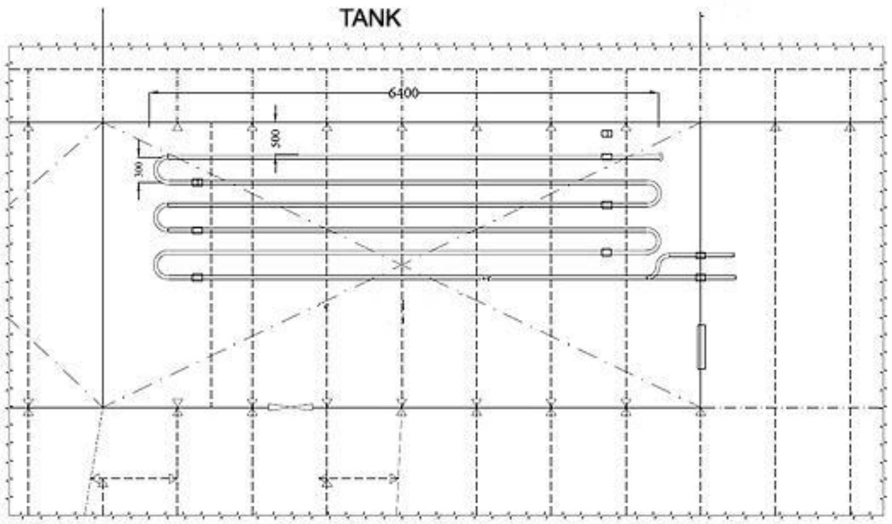

Figure 4.6 Heating coils

4.2.2. THEORY

The thermodynamics of such a system are usually based on the energy (heat) balance between the heating fluid and the heated one, namely between superheated water and HFO. As far as the only heat source is the heated steam and by considering the total insulation of the apparatus, the above balance is as follows:

$$Q_{sup\,/\,ted\ water} = Q_{oil} \tag{4.11}$$

where by Q is denoted the thermal energy transferred from the coil to the HFO. The total amount of necessary thermal energy which is appropriate to be supplied to the HFO, Q_{oil}, can be written as (Sato, 2004):

$$Q_{oil} = m[C_p(T_{fin})T_{fin} - C_p(T_{init})T_{init} \tag{4.12}$$

where Cp is the specific heat capacity which can be calculated through NASA Polynomials with the appropriate specific coefficients for each chemical element (McBride, 1993) and m is the total mass of the HFO (kg) calculated for a given tank volume through the temperature dependent density, ρ , of the HFO, which is given as (Perry, 1999).

$$\rho = \frac{C_1}{C_2^{\left\{1+\left[1-\frac{T}{C_3}\right]^{C_4}\right\}}} \tag{4.13}$$

where C_1=0.5373, C_2=0.2612, C_3=568.7, C_4=0.2803 are coefficients, T is the temperature (K) and ρ is the density (kmol m^{-3}). Given the volume of the tank as well as the filling level, the initial total mass of HFO is 1.81E+05kg at temperature equal to 303K.

In the above Eq. (4.13), $C_p(T_{init})$ and $C_p\left(T_{fin}\right)$ is the specific heat capacity (J mol^{-1} K^{-1}), T_{init} and T_{fin} the temperature (i.e. 303K and 333K), at the initial and the final stage of the heating process, respectively. The specific heat capacity for each chemical substance can be expressed through NASA polynomial as (McBride, 1993):

$$\frac{C_p(T)}{R} = a_1 + a_2T^1 + a_3T^2 + a_4T^3 + a_5T^4 \tag{4.14}$$

where R is the gas constant value 8.3144 (J mol^{-1} K^{-1}), $C_p(T)$ is the calculated specific heat capacity (J mol-1 K-1) and A_1 up to A_5 are coefficients, specific for each chemical substance. For the HFO, these coefficients are (Perry, 1999): A_1=1.25E+01, A_2=-1.01E-02, A_3=2.22E -04, A_4=-2.85E - 07, A_5 =1.12E -10.

The heat transfer takes place between the carbon-steel coil and HFO and can be described through the integral form of the Fourier's law (Holman, 1990):

$$\frac{dQ}{dt} = -k\int_A \overline{\nabla}T\,dA \tag{4.15}$$

Where dQ / dt is the amount of heat transferred per unit time (J sec^{-1}), k is the thermal conductivity of the carbon steel (W m^{-1} K^{-1}), $\overline{\nabla}T$ is the temperature gradient over the radial dimension of the system and the integral is closed over the specific surface A of the cylindrical hot coil through which the heat transfer occurs.

By considering the above geometry, equation (4.16) can be written as (Bejan, 1993):

$$\frac{dQ}{dt} = -\frac{2\pi\,L\,k\,(T_{out}-T_{in})}{ln\left(\frac{r_{out}}{r_{in}}\right)} \tag{4.16}$$

where L is the necessary length of the coil, T_{out} and T_{in} is the temperature on the outer and inner cylindrical surfaces, respectively. Finally, r_{out} and r_{in} is the outer and inner radius of the coil (thickness), where the necessary length is given as:

$$L = -\frac{Q_{oil}}{\frac{dQ}{dt}t} \tag{4.17}$$

where t is the time when the heat transfer process occurs.

4.2.3. THERMODYNAMIC RESULTS

Figure 4.7 clarifies the influence of the time on the coil's length. As it is expected, the shorter the time when heat transfer occurs, the longer coil is needed in order to assure the appropriate transfer surface. This behavior is found to be nonlinear and it is explained due to the nonlinear amounts of heat to be transferred to the oil with time. In particular, the heat transfer occurs in two dimensions (cylindrical coordinates: r, θ) where the radial component is the only important, developing on several imaginary coaxial isothermal cylindrical surfaces through the total mass of HFO in the banker tank. For long time periods, the temperature of the oil increases in such a level that gradient is low enough for considerable heat fluxes. Furthermore, given a constant thickness of the steel tube (d=4mm), the diameter is favorable parameter for the heat transfer, i.e. larger diameters assure higher available surfaces for heat transfer. It is important to underline the restrictions on the coil's length, imposed by tank's dimensions: the area covered by the coil's serpentine would not exceed 95.46m^2, which correspond to a maximum length of approx. 154m, depended on frame space.

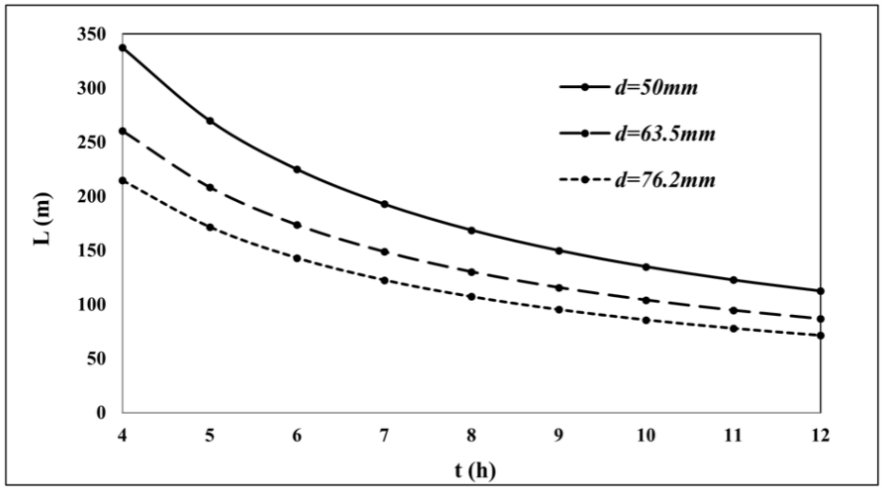

Figure 4.7 Coil's length as function of time

The importance of the geometrical characteristics of the coil is further depicted in Figure 4.8, where the same behavior of necessary length with the time is also observed. The important behavior shown here is that the length increases with the thickness, because of the consequent increment of the heat capacity of the steam coil: by increasing the thickness, the steel mass is also increased and so does the amount of energy that is wasted to heat the solid steel.

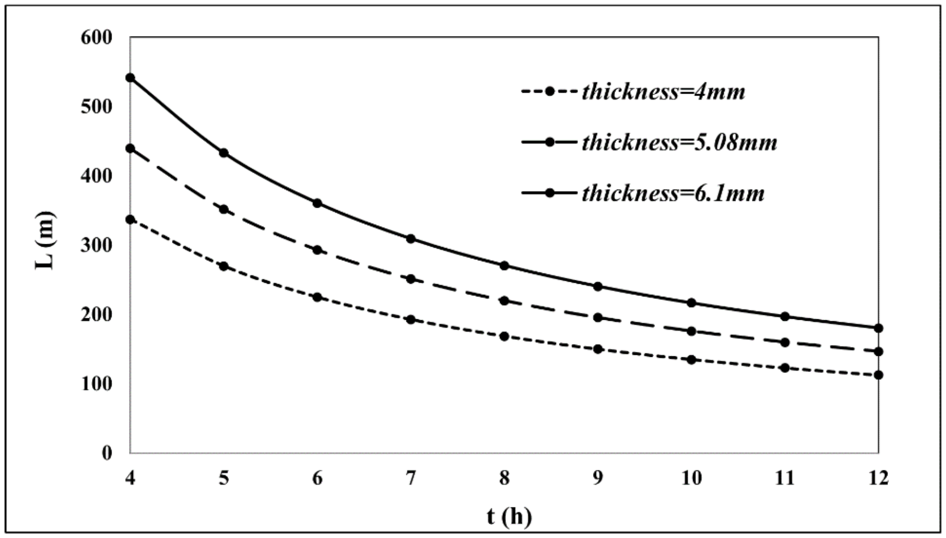

Figure 4.8 Effect of coil’s thickness on its length

The results, as depicted through the above Figures, arisen by considering constant temperature difference between the inner and the outer surface of the steam coil (in contact with HFO) equals to~2K.

The following Figure 4.9 investigates the effect of the temperature’s difference between the flowing superheated water inside the carbon-steel tube and its outer surface on the heat transfer for various periods of time, where it has been considered that the inlet temperature is 424K (superheated water). It is found that the necessary length is lower for higher temperature differences, because the latter corresponds to higher amounts of heat that are actually transferred to the HFO in the tank.

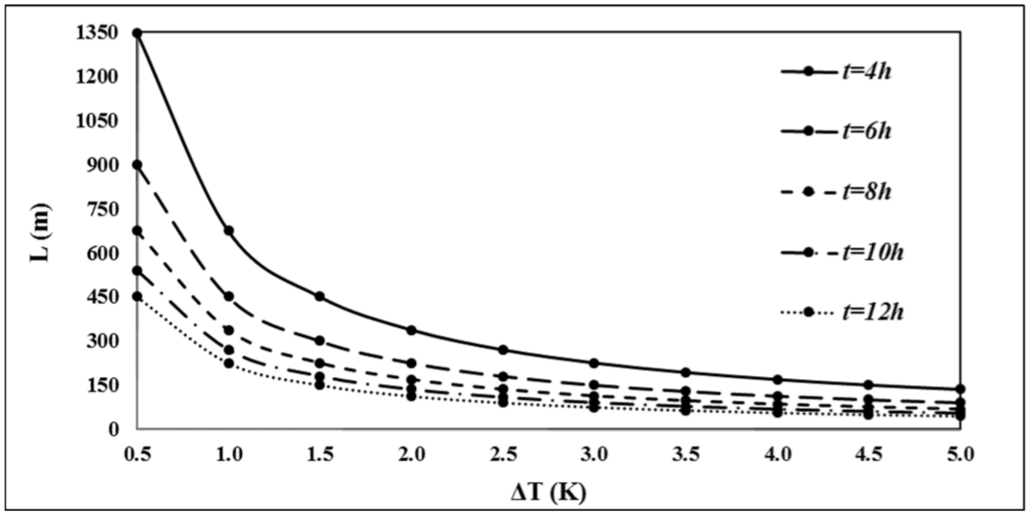

Figure 4.9 Length as a function of ΔT

As all the above figures indicate, the dependence of length on time is not linear, due to character of the heat transfer process occurring. Precisely, there is only one heat source (coils) which has to offer heat for (a) initially increasing the temperature of the coil itself and then for keeping this temperature constant, and (b) increasing HFO's temperature up to the desirable level.

Since the relationship of these two heat consumptions is not linear, the length of the coil has to follow a non-linear time evolution, in order to satisfy this requirement.

4.2.4. PROBLEM MODELING

The fundamental transport phenomena occurring in the system under consideration is the superheated water flow and the heat transfer from the coil to the HFO. Since laminar conditions are considered, the flow can be well described by the well-known Navier-Stokes.

Regarding the boundary conditions, the flow rate in the steam coil were assumed to be equal to 0.024 (m s^{-1}), while the pressure was set accordingly at the inlet and the outlet in order to assure that the fluid is liquid phase in the coil tube. Fixed heat flux and adiabatic conditions were set for the coil and tanks boundaries, respectively, for each time step. Finally, non-slip condition was assumed for the steam flow on inner tube surfaces (Verberg and Ladd, 1999).

The equations are considered to be strongly coupled, thus numerical solutions were obtained by the commercial CFD-ACE+ package, based on the finite volume method, in order to achieve residual values less than 10^{-4}, for all calculated quantities. The three-dimensional tank with the coil was discretized in space by unstructured grid consisting of approx. 2E+05 up to 5.2E+05 cells where its amount depends on the coil length. The values of the parameters used as well as the properties of the materials are listed in Table 4.3.

Typical temperature spatial distribution is presented in Figure 4.10 for a perpendicular 2-D cut and the footprint of the banker tank respectively. The coil length is 140m and the time passed is 12.5h, being the maximum sufficient time for successful integration of the heating process for this specific layout. The black line in Figure 4.10(a) indicates the level of the HFO. It is shown that the majority of the volume occupied by HFO is indeed heated to 333K.

Table 4.3 Parameters and properties used (Wagner and Kretzschmar 1998)

	Superheated Water	**Heavy Fuel Oil**	**Carbon-Steel**
Phase	Liquid	Liquid	Solid
P (kg m^{-3})	917.02	695.23	7850
μ (kg m^{-1}sec^{-1})	1.80E-04	1.02E-03	-
C_p (J kg^{-1} K^{-1})	2.41E+03	1.67E+03 (at T_{in}) 1.80E+03 (at T_{fin}) NASA polynomials (McBride at al. 1993)	470
K (W m^{-1} K^{-1})	6.82E-01	1.44E-01	48

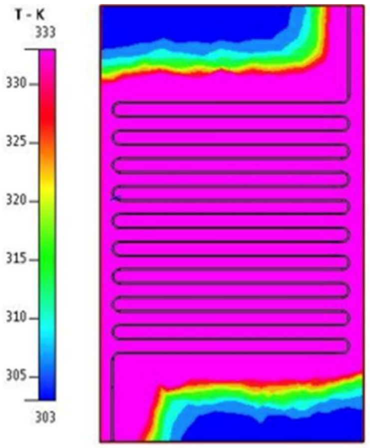

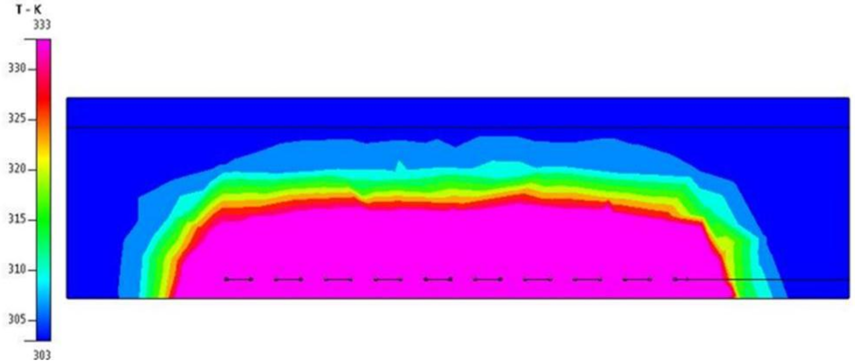

Figure 4.10 Typical microscopic results: (a) perpendicular cut and (b) footprint

Areas of lower temperature (blue and green) are attributed to isothermal conditions (T=303K) and presented at less than 1m length from the walls of the tank and less than 0.30m from the surface of the HFO. These areas correspond to 20% of the total volume of the HFO for 140m length tube and obviously can be minimized up to 14% by considering a longer layout coil (~160m) as it will be discussed later. Also, by duplicating the established overall coil length (~300m) i.e. 2 horizontal rows of 150m length this percentage can be reached 2% to 3% in a 5hours time interval. During real life heating process HFO presents better homogeneity than this as presented above due to its physical stirring within its entry in the banker tank. In order to quantify the HFO's heating process, oil temperature has been spatially averaged and next presented in Figure 6 for various coils lengths.

These microscopic results indicate that the tank approaches the desirable temperature of 333K in the time period of 14.5hours time limit, for the shortest coil (~120m). Considering longer coils, the time period can be calculated to approx. between 12.5h and 10h, a result that is in an acceptable agreement with thermodynamic analysis.

This approach allows for a more detailed calculation of the temperature profile; thus some areas of significantly lower temperature can be recognized in the tank's volume. Furthermore, these results are consistent with those of Figures 24 &25: the longer the coil, the shorter the time needed for the oil to reach the desirable temperature of 333K.

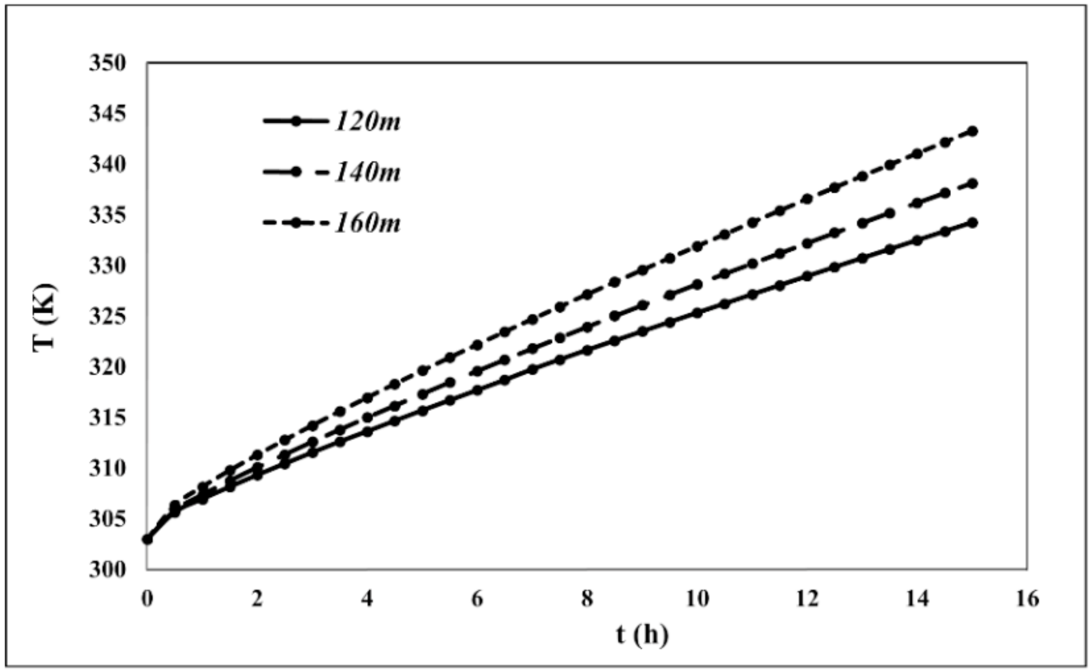

Figure 4.11 Average temperature as a function of time for various coil's lengths

Also by keeping as constant the overall length of the carbon-steel tube (~160m), the longer of the above scenarios as depicted in Figure 4.12, two more different layout scenarios were considered on the establishment of the coil (one established at the half height of the tank and one installed in two different vertical rows, 80 meters each, in the middle) in order to be investigated the effect of the different placements over the time intervals during the heating process. More precisely, Figure 4.12 reveals that the change of the coil's placement does not significantly influence the results on the time interval of 10h which is essential for the fuel oil to reach the desirable temperature of 333K.

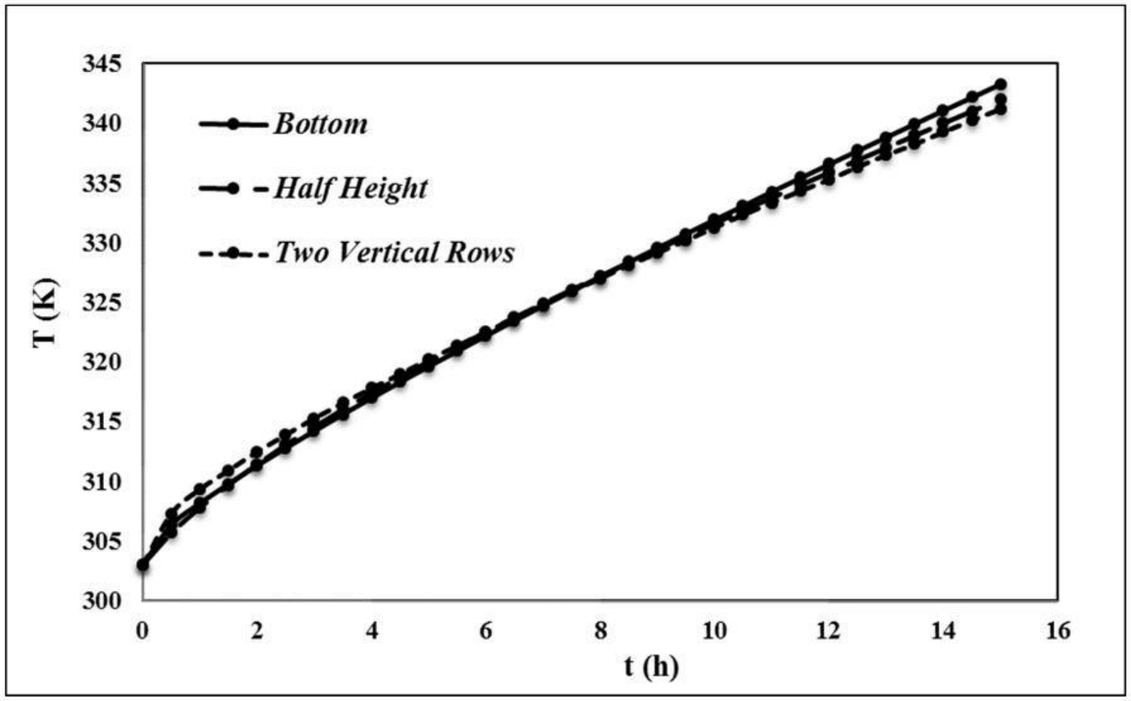

Figure 4.12 Effect of different placements on average T.

It has to be underlined that by considering two vertical rows with total length of 160m the HFO slightly increases its temperature in a shorter period of time compared to other layouts at the beginning of the process but at the end drops and the estimated time increases at about 1.5h which constitutes an important result for the process's optimization. Moreover, the main disadvantages for the "half height" and the "two vertical rows" layouts are the stability as well as the complexity of the establishment construction due to the high pressure (~5bar) flowing superheated water through the coil.

4.2.5. MODELING RESULTS AND DISCUSSION

The heat transfer problem when a tank of specific dimensions is filled at about 85% with HFO is heated from 303K to 333K by exploiting the flow of superheated water through a coil of serpentine design and of various lengths, diameters and thicknesses. To obtain length values, both a thermodynamical analysis as well as detailed 3D simulations has been carried out, while the effect of the most crucial parameters on the results was investigated. It is found that the optimal length is approx. 160m for the shortest time period that the process takes place. More specifically, the maximum length which can be established due to the limitations on geometrical characteristics of the banker tank cannot exceed 160m for one layer of carbon-steel coil of 50mm diameter and 4mm thickness and this can increase the HFO temperature to 333K in about 9.5h according to the thermodynamic analysis and 10h through the detailed 3D, CFD-ACE+, simulations which constitutes the most favorable result for the feeding process to the engines.

The most efficient scenario can be presented through the installation of a double layer of carbon-steel coil which increase the overall length at about 300m and the needed time can be limited at an interval of 5 hours. The main disadvantages for such an established scenario can be observed on the homogeneity of the temperature of the total HFO and on the increased initial establishment costs for this construction. Finally, it must be mentioned that the temperature of the HFO inside the banker tank found hardly uniform, for lower time interval processes, due to stirring physically occurs during the oil's entering in the tank and due to the variation of its viscosity among the several time steps.

4.3. CASE STUDY 3: MODELLING OF FOOD - PACKAGING - ENVIRONMENT SYSTEMS

Among, the most important physical-chemical interactions within a food-packaging-environment system, migration, sorption and permeation of substances through the various material phases are of high concern for the food quality (Figure 4.13). Sorption of environmental (S_E) or food (S_F) origin substances may be defined as sorption of substances by mater, either from foodstuffs to the packaging or vice versa. Migration is presented in Figure 4.13 as M_F and M_E for substances originating either from the packaging material to its containing food volume or the other way around. The above phenomena can potentially impact the product quality. The evolution of these processes is depended on the physical and chemical characteristics of the polymer, the nature of the substances and the type, composition and physical characteristics of the foodstuff. Regarding the public health safety, migration is by far the most significant process, since chemical substances that migrate into foodstuffs could potentially introduce a risk to human health (Sanches-Silva et al, 2008).

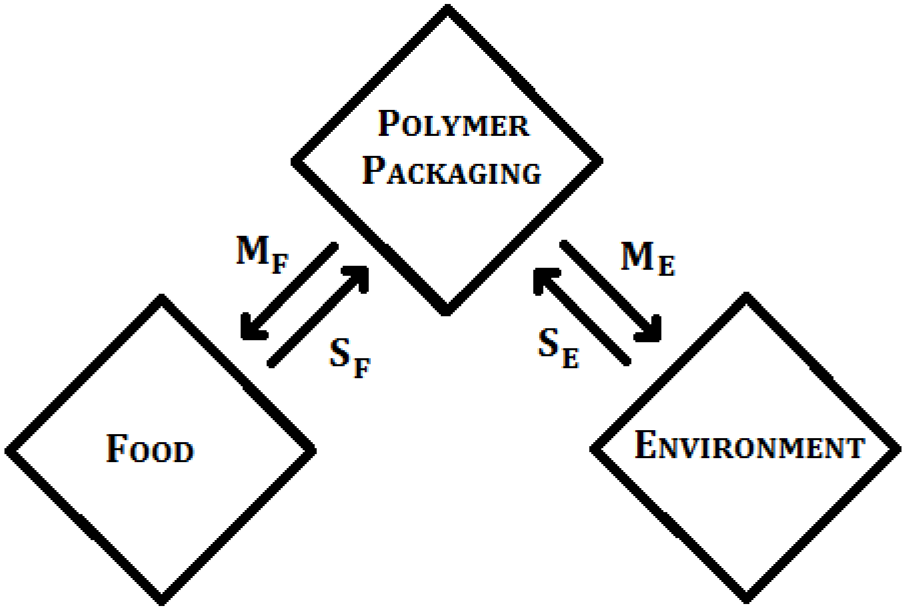

Figure 4.13 Food – Packaging – Environment possible mass transfer processes.

In general, migration can be considered via all of the following four major steps. As the first step we may consider the process of diffusion of chemical compounds through the packaging matrix. As the second step we may consider the process of desorption, of the diffused molecules, from the polymer surface. As a third step we may consider the sorption of the compounds at the polymer-food interface and last but not least as the final and fourth step we can consider the desorption of the migrated compounds in the food volume.

The main mechanism of the mass transfer during migration of chemical compounds from packaging material to food has been broadly attributed to the fundamental process of diffusion. Food contamination occurs due to the dissolution of the migrant in the food, when in contact with the migrated substances on the polymer surface. By definition, the term “migration” refers to the diffusion of chemical substances from a zone of higher concentration (the food-contact layer) to one of a lower concentration (usually the food surface) due to the concentration gradient. This process is often influenced by food-packaging interactions as well as by the temperature of the system (Arvanitoyannis and Bosnea, 2004).

Consequently, food-packaging interaction has become a rather important filed to be studied, as it affects the processing, preservation, distribution, marketing and even the cooking preparation of foods. However, although the existing packaging materials’ components serving as process aids, colorants, active compounds or functioning means, must be safe for the consumers. For that, it is the containing food that may or may not interact with the adjoining packaging materials. In result, this might change the initial mechanical and barrier properties of the materials, as well as the safety of the product at consumption. Understanding and controlling the migration process of a toxic substance from a packaging material retains a major role in the selection and use of the materials for food packaging for the possible effect upon human health. Analytical laboratory testing should provide knowledge and allow for expertise in defining the compliance of the food-contact plastics to the relevant EU regulations (Traiastaru et al, 2013).

During the last three decades, a rather enormous scientific knowledge has been accumulated concerning the migration process and its behavior on food-packaging materials (Piringer et al, 2000). The usage of extensive migration data sets using food simulants was established in Europe and in USA. Most of the research and developments have been carried out in support of the international and European food-contact materials legislations and guidelines. In relation to that, upcoming scientific studies have been performed using officially authorized food simulants, avoiding the migration analytical studies with real foodstuffs, for the reason of confirming the materials’ compliance under systematic hurdles. Furthermore, all of the various investigations performed, demonstrated that migration from food-contact materials could be a predictable physical and mathematically describable, process. In that sense, the mass transfer from a plastic material into food simulants has been considered a foreseeable process that in most cases obeys the Fick’s laws of diffusion (Franz, 2007). The below Figure 2, summarily depicts the diffusion steps on a polymer-food interface.

Usually, the mass transport due to sorption or desorption phenomena was estimated via studies allowing the distinction among the prevailing internal, interfacial and thermodynamical systemic phenomena.

Vitrac and Hayert (2006) analyzed the detectability and identification of different diffusion properties that control migration from a single desorption/sorption kinetic, which can be subject to physical constraints. They focused their study in achieving the estimation of standard diffusion coefficients of additives and monomers in plastic materials when in contact to food simulants used to examine the compliance with the European Directive 2002/72/EC. A new solution of the general dimensionless mass transport problem controlling desorption/sorption kinetic was presented resulting to the evolution of the migrant concentration in the food or the packaging phase shown in a new approximation space called “Kinetic phase diagram”, where the concentration at equilibrium could be easily extrapolated and where internal and external mass transfer resistances could be clearly distinguished. However, the authors pointed out that when the thermodynamic and external mass transfer coefficients were falsely neglected, the results had a significant overestimation of the internal mass transport resistance in the solid phase and hence a significant underestimation of the real migration value in the solid phase. Finally, they proposed an estimation strategy in order to simultaneously identify the three properties (namely, diffusion; partition coefficient; interfacial mass transfer coefficient) controlling the sorption kinetics.

A broad number of literature citations regarding the levels of migrants, their reaction products and the role of additives can be found (see, for instance, (Gilbert et al, 1980), (Downes, 1987), (Tehrany and Desobry, 2004). In addition, the loss of compounds from the food phase migrating into a polymeric packaging material has been considered as a sorption mechanism receiving a significant consideration as well (Risch, 1988) (Tehrany and Desobry, 2004), (Vitrac, 2005), (Vitrac, 2006). Since food-packaging mass transport phenomena may also have a major impact in many particular technological areas, thus, it has also been investigated from experimental and theoretical point of view (Vitrac, 2006).

Recently, several migration studies of different experimental techniques were reviewed by Kadam et al (2015), aiming in estimating the sorption/migration events and their respective advancements and limitations for plastic packaging materials a major type of materials for the global markets (Robertson, 2012). In that review, it was suggested that it was both the quality of a product and its shelf life that were affected by either natural and/or superficial factors such as: mechanical stress, temperature, permeability of gases and vapors. In addition, the natural factors affecting the quality of a packaged food were: properties of the packaging material such as design and compatibility to the food itself, as food - packaging interact occur till the end of the products’ use. Interactions such as sorption and migration appeared to be rate dependent by the food-packaging exposure environmental conditions. Concluding, in their work they categorized and compared the different ways to experimentally study sorption and migration.

According to the EU regulation (EU, 2011), migration testing is requested only for plastic packaging materials. Even though the EU legislation establishes that specific migration limits for 17 different types of materials, at present, specific measures exist only for a few of them (i.e. plastics, regenerated cellulose and active materials). The concentrations of migrated contaminants should be below the legally accepted specific migration limits (SML). The verification of the compliance of food packaging materials with the existing regulations can be done by comparing the SML with the values predicted by ‘‘generally recognized migration models” (Cruz, Studies of mass transport of model chemicals from packaging into and within cheeses., 2008). The main principals behind EU and USA regulations for food contact materials has been the protection of consumers against toxic migrating substances. Therefore, agencies producing and designing paced-foods and packaging materials used for food, must apply and confirm the compliance via appropriate experimental techniques. This opened an opportunity for modeling the migration and the use of subsequent models for predicting it (Begley et al, 2005). The theoretical predictions of migration from packaging to food with the use of models are often made using equations, which are usually not designed especially for the problem attended. Therefore, FDA has been using mathematical models to estimate migration from food contact in order to enhance their test protocols (F.D.A., 2007).

The overall migration limit (OML) has been applied by EU to control the total amount of additive migration from the packaging material into food, irrespectively of the toxicological significance of the migrants. The aim of this OML is to reduce the number of specific migration determinations carried out to ensure that the packaging material is legit and safe to use when in contact with food. Even if the migration of an additive is below the OML, it is not sure if it's safe to be used as a food contact material. That is due to the unknown chemical substance and its toxicity. Only materials and substances appearing in the "positive" lists in the EEC Directives can be used as food-contact materials for commercial applications (Arvanitoyannis and Bosnea, 2004). The use of the mathematical modeling on the food-packaging system has been applied, for many years and is called ‘packaging use’ factors (Franz and Welle, 2008), (US_FDA., 1995a), (US_FDA, 1995b). An important note concerns the use of migration modeling for plausibility considerations in support of regulatory decisions. Analysis limitations within certain regulations have been set by specific and detailed migration testing rules. Although migration testing in food prevails, migration estimation is usually calculated by using 'food simulants', representative for a specific food category.

A large volume of studies can be found on the development, improvement and testing of migration mathematical models. In particular, in order to determine the migration levels using migration data, Limm and Hollifield (1996) and Baner et al (1996) developed some semi-empirical models relying on the estimation of diffusion coefficients based on the nature of the migrant and the properties of the polymer. It should be noted that other aspects of migration, such as partitioning, mass transfer, polymer morphology, shape/polarity of the migrant, as well as plasticization of the polymer were not considered in full for these models. These factors should be considered carefully when deriving migration levels to food using modeling techniques since they might cause erroneous values (Franz, 2007). Uses of plastic materials in food contact applications have been primarily focused in adhesives applications, urethane polymers, and repeat-use applications.

Modeling of potential migration has already been used in the United States as an additional tool to help make regulatory decisions, while the European Union uses this tool as a quality assurance instrument (Brandsch et al, 2002). To set up a worst-case scenario of the migration, in a first approximation, the following two assumptions can be made (Baner and Piringer, 2008), (Pennarun et al, 2004):

i. the solubility of the migrant in food is high,
ii. the diffusion coefficient of the migrant has an “upper bound” value, D*

where, D* is a value which, with a given statistical certainty, is larger than any possible real D_P for the specific migrant. Whereas the first assumption leads to a simple relation, $K_{P,F} \leq 1$, (where $K_{P,F}$ is the polymer – food partition coefficient) the second one is much more difficult to quantify. This is because a real D_P may range from about 10^{-7} cm^2s^{-1} down to about 10^{-18} cm^2s^{-1}. Therefore the primary task is to find a way for predicting D_p values which in combination with the diffusion equations and $K_{P,F} = 1$ can provide a calculated migration value, equal or above the real migration value under the same conditions.

In order to be on the safe side and protect the health of the consumer the equations describing migration should overestimate it (Helmroth et al, 2002). The use of modeling for the estimation of potential migration of a food packaging system as well as for making regulatory decisions should always be referenced to typical migration found to food simulating liquids and food (Ferrara et al, 2001).

The main objective of this study is the presentation of a critical summary of mathematical models regarding the substances migration from packaging material to foodstuffs or food simulants under several storage conditions. The focus is actually on the critical discussion of the relative wide accepted models, judging their compensations and drawbacks, in order to actually identify the lack of existing knowledge and, hopefully, indicate a direction for the forthcoming research on that topic.

4.3.1. BACKGROUND THEORY

The scope of mathematical migration model for packaging materials is to predict the concentration of the migrant in the food after contact with the package during a certain time period defined as “shelf-life” of the product. In addition to the mathematical approach a number of relevant transport phenomena controlling the migration process can be identified. Knowing these phenomena is very important in order to allow realistic simulations of the migration process. A reliable and accurate model should take under consideration all mass transport phenomena along with any external factors affecting the process taken into account. Such phenomena are the diffusion, convection, and chemical reactions. It's important to note that these phenomena can occur in both food and packaging phases. It’s important to know that practically, the phenomena controlling the migration process are the diffusion of the migrant and the chemical reaction in both phases. Convection of the migrant is very much restricted in normal conditions of use, so it will not have a significant influence on the migration process (see, for example, (Del Nobile et al, 2003).

The main studies in the migration modeling area employed a deterministic approach, have been considering the migration process to be controlled by the diffusion of the migrant, through the volume of the packaging material, as described by Fick's 2nd law (Reynier et al, 1999), (Pocas et al, 2008), (Limm and Hollifield, 1996), (Crank, 1975). That approach was based on specific assumptions (constant packaging thickness, homogenous media, no boundary effects, no chemical processes, etc.). Such approaches assisted the model development and application, yet not necessarily valid, in each and every case of substances’ migration between various phases. According to the aforementioned approach, the diffusion coefficient of a compound in a particular matrix follows Fick's 1st law, stating that the mass flux of a compound during a time "t" through a control volume is proportional to the gradient of the concentration of the compound. Mathematically it can be written as the following equation:

$$\frac{\partial C}{\partial t} = D\nabla^2 C \tag{4.18}$$

Further to diffusion, some chemical reactions were sometimes taken into account, modifying the above expression as follows:

$$\frac{\partial C}{\partial t} = -D\nabla^2 C \pm kC^n \tag{4.19}$$

The above equation (4.19) describes the Fickian diffusion in combination with the chemical reaction where *k* is the reaction rate constant and *n* is the order of the chemical reaction.

Various models aiming towards the prediction of diffusion coefficient for a given migrant have been developed through the year (Piringer 1994), (Limm and Hollifield, 1996), (Mercea, 2000a), (Mercea, 2000b), (Begley et al 2005), (Pennarun et al, 2004), (Han, 2003). Basically, the two main models namely Piringer‘s model (Piringer 1994) and Limm & Hollifield model (Limm and Hollifield, 1996), used widely by the scientific community, are presented below.

A number of assumptions should be made to analytically solve the second order partial differential equation (4.20). First of all, the diffusion coefficient is assumed to be constant in both the food and the packaging material (see, for instance, (Brandsch et al 2006a), (Brandsch et al 2006b). By solving the general diffusion equation (4.21), it can be concluded that the diffusion and the partition coefficient of the migrant should be known in order to practically apply the equation. As it has been explained above, from a regulatory point of view, the worst-case scenario, over-predicting migration is of primary interest. Therefore, it is often assumed that the solubility of the migrant in the polymer is very high, which consequently results to the assumption of $K_{P/F}=1$, where $K_{P/F}$ is the partition coefficient avoiding difficulties for the estimation of the partition coefficient for a given migrant - packaging material - food (Brandsch 2002).

The following discussion summarizes the current state of knowledge regarding the way of solving the migration problem by using mathematical modeling.

4.3.2. THE MAIN MIGRATION MODELS

The Piringer model, called also as “Piringer’s Interaction Model” is by far the most widely used model in this scientific area. The deterministic model was proposed initially by Baner et al, (1996) and it is recommended for use by the EU commission for regulatory purposes by regulation (10/2011/EC) regarding the estimation of specific migration in food contact materials (Piringer 1994), (Brandsch et al, 2002).

The proponents argue that its theoretical background might lead to false results, whereas the United States Food and Drug Administration (FDA) quotes it as —an empirical correlation based on the molecular weight of the migrant (F.D.A., 2006) (F.D.A., 2007). The general models’ equation was said to be multipurpose as it describes a uniform model predicting the diffusion coefficients in gases and condensed phases, including the plastic materials (Baner and Piringer, 2008). The general form of Piringer’s equation is presented below (Helmroth et al, 2002), (Brandsch et al, 2002), (Piringer 1994):

$$D_P \leq D_P^* = 10000e^{(Z_P - a_{mw}\, MW_i - \frac{Z_T}{T})} \qquad (4.20)$$

where, D_p is the real additive diffusion coefficient, D_p^* is the overestimated additive diffusion coefficient, Z is a polymer specific constant, α_{mw} is an additive molecular weight specific constant, Z_T is a temperature specific constant, MW is the molecular weight of the additive i and finally T is the temperature.

In their approach, the diffusion coefficients were determined by empirical correlation of the coefficients obtained from literature against the molecular mass of the migrants, with a specific parameter, A_p and with the absolute temperature, T (Limm and Hollifield, 1996), (Brandsch et al, 2002). The model can be adapted to different types of polymer, simply by changing the specific polymer parameters, which can be derived for a large amount of polymer types. The aim of Piringer's model is the prediction of the migration value for a worst-case scenario solving Fick's 2nd law. Reynier et al (1999) have proposed an empirical correlation between an upperbound value of the diffusion coefficient and the molar mass of the migrant enabling the calculation of an upperbound value of migration. The model has been validated by the work of O'Brien and Cooper (1999) as well as in (Reynier et al, 1999), (O' Brien and Cooper 2001)**.** The two teams mentioned above have modeled the migration of four different additives in olive oil food simulant migrating from HDPE and PP. Their results showed that most of the migration values predicted by "Piringer model" were indeed overestimated for the 83% of the migration values. For all measurements of the predicted migration, the values were found to be greater than the 50% of the experimentally observed values (O' Brien and Cooper, 1999), (O' Brien and Cooper, 2001), (Helmroth et al, 2002).

More recent validation work has been made by Brandsch et al, (2002) where it was found that the model results overestimated more than 95% of the experimental values, while the smallest differences between the "worst case" estimations and the experimental values appeared at high temperatures**.** Also, it's important to underline, that according to Reynier et al (2002), Piringer 's model tends to underestimate the temperature influence on diffusion of high molecular mass components. Experimental tests with high molecular weight components, at high temperatures, generally showed diffusion coefficient values, 2-3 orders of magnitude lower than the values predicted by Piringer 's model. This could be explained by considering the effect of the molecules size and shape on the diffusion. As it was presented in the work of Chan et al, (2015) that the bigger the size of the molecules, the lower the real diffusion coefficient (Pennarun et al, 2004). As the molecules got larger, they noticed that the diffusion rates of planar solutes were reduced or even reversed, as compared to those of the spherical ones of the same size (Chan et al, 2015). Their real initial diffusion coefficients are very low compared to the coefficients calculated by the model, which overestimated the fastest molecules. It has been supposed that this overestimation covers the inadequacy of using the accurate activation energies. However, the temperature effect on diffusion has been described by Reynier et al, (2002) where they observed that the increase of mobility lead to lower diffusivity sensitivity to the molecular weight.

Brandsch et al, (2002) used a new equation where it estimated the diffusion coefficients, which do not rely on experimental data:

$$D_P = D_0 \exp(A_P - 0.1351 MW_i^{2/3} + 0.003\ MW_i - \frac{10454}{T} \tag{4.21}$$

The equation combined the molecular masses with the parameter, A_P, having the role of a "conductance" of the polymer matrix to the diffusion of the migrant (Brandsch et al, 2002). To calculate migration rates within a safety margin from the regulations limit it is possible to match the "conductance in equation (4.21) to yield a "worst case" migration estimation. In order to achieve that the polymer specific parameter can be modified by using an upper limit polymer specific diffusion parameter (A'_p), the temperature (T), the polymer specific parameter (τ_P) which is actually a contribution of the polymer matrix to the diffusion activation energy:

$$A_P = A'_P - \left(\frac{\tau_p}{T}\right) \tag{4.22}$$

Under these assumptions, the migration value of a migrant from the polymer to the food in contact, can be calculated by the following well known, equation of Fick's 2nd law,

$$\frac{M_{F,t}}{s} = C_{p,0}\,\rho_P\,d_P\left(\frac{a}{1+a}\right)\left[1 - \sum_{n=1}^{\infty}\frac{2a(1+a)}{1+a+a^2q_n^2}\,exp\left(-D_P t\,\frac{q_n^2}{d_P^2}\right)\right] \tag{4.23}$$

where $M_{F,t}$ represents the migration value at time t, S is the contact surface area, $C_{P,0}$ is the initial concentration of the migrant in the polymer, ρ_F and ρ_P are the densities of food and polymer respectively, d_P is the thickness of the polymer, $\alpha = (V_F/V_P)/K_{P,F}$ where V_F and V_P are the volumes of food and polymer respectively and finally $K_{P,F}$ is the polymer-food partition coefficient. The parameters q_n are the positive roots of the equation: $\tan(q_n)=\alpha q_n$.

A comprehensive list of available diffusion coefficients data for LDPE, HDPE and PP was published by (Mercea, 2000a) (Mercea, 2000b). The data occurred by an extensive literature review of hundreds of published scientific papers. These data have been used by Brandsch et al (2002), to derive the specific diffusion parameter Ap to be used in equation (4.21). Using these values in equation (4.21) the authors validated the relation $D_P^* \geq D_P$ with 95% certainity resulting to a succesfull calculation of a “worst case scenario”.

More migration experiments were carried out in order to validate their work using several migrants from HDPE towards a fatty food simulant, the well-known olive oil. Begley et al, (2005) re-evaluated the parameters of Piringer's model in order to estimate the diffusion coefficient. There results were found to overestimate the migration value at a rate of 95% of 366 experimental values. The underestimations found between the experimental and modeling values were underestimating the modeling values of migration at 26% of the real value.

Reynier et al, (1999) focused their work on the determination of the diffusion coefficients process by proposing other constants for the calculation of the upper bound value using experimental data instead of literature data. This is the main difference between Reynier's and Piringer's approach. This, in fact, is the weakness of Piringer's model (Reynier et al, 1999). Piringer's model, uses many data found in literature, data that were most likely the results of very different type of experiments and were obtained from different mathematical treatments. The results of Reynier's method showed that their method had a general trend to slightly overestimate the migration values of migrants in PP materials to a food simulant. However, it's crucial to sum up to the conclusion that often this model overestimates too strongly the migration amount in the actual polymer-migrant system resulting to false conclusions (Brandsch et al, 2002), therefore authors proposed the need of improving the constants of the model for LDPE and LLDPE at 40°C and to involve variations of diffusion coefficients taking into account food and polymer interactions (Reynier et al, 1999).

Limm and Hollifield (2006), proposed a semi empirical model of additive diffusion prediction in polyolefins (POs). In accordance to Piringer's model, they proposed a direct relationship between the diffusion coefficient and the molar mass of the migrant. In contrary of Piringer's model, their model required a minimal amount of data (Reynier et al, 1999), (Pocas et al, 2008). Their deterministic approach was based upon existing physical diffusion theories, such as diffusion theories developed for rubbery polymers to model PO packaging materials. Based on those theories the model relied on some empirical constants determined from migration experiments. This is the main reason why this model gives good correlation with experimental values, especially for migration of additives with high molecular masses into oils interacting with POs at high temperatures (Brandsch et al, 2002), (Limm and Hollifield, 1996).

This model was the first step in systematically predicting additive migration. It utilized the relationships between molecular diameters and activation energies, which have been established for relatively small molecules with molecular weight of 100 Daltons. The diffusion of an additive molecule through a polymer matrix is considered to be adequately expressed by an Arrhenius-type equation:

$$D = D' e^{\left(\frac{-E_a}{RT}\right)} \qquad (4.24)$$

Limm & Hollifield's model, used this Arrhenius described behavior as the basis for quantifying the temperature dependence of additive diffusion for various additives given a specific polymer. Their model has been tested on a large number of diffusion coefficients found in the literature and was found to have from 2 times lower and up to 8 times higher migration level prediction (Limm and Hollifield, 1996), (Helmroth et al, 2002). A very important part of their study is the fact that if the thermal expansion is neglected, it leads to a slight overestimation of the activation energy at high temperatures, resulting to a conservative estimation of diffusion coefficients. However, the main disadvantage of their work is its applicability. Their model can be applied only for polyolefins, limiting the use of it as a global solution. This model has been evaluated with the use of diffusion coefficients derived from weight grain experiments owing to absorption of penetrants. The diffusion data used for the evaluation of the model, were data for aldehydes in

HDPE in 298°K (Johansson, 1994). By using the diffusion coefficients from Johansson and Leufven, the authors found a prediction accuracy of one order of magnitude compared to experimental data (Johansson and Leufven, 1994). Similarly, diffusion coefficients for limonene in LDPE given by Sadler and Braddock (1990), where used for simulating the migration process. A direct comparison of these results demonstrated that this model might be useful in estimating additive migration at elevated temperatures by using only the molecular weight of the migrant and a small amount of migration data.

Finally, Limm & Hollifield's model has been recommended by the United States Food and Drug Administration (FDA) office where it serves as a framework to evaluate experimental data which may not have been collected under optimal conditions (Limm and Hollifield, 1996).

As it has been mentioned in the discussion above the two modes used by the EU and US FDA are Piringer's and Limm & Hollifield's models, respectively. However, both models are prone to a number of limitations, which are important to consider before using them. Because of the necessity of an accurate estimation of the diffusion coefficient it is important to note that both of these models can only be applied accurately on polyolefins. It should be noted that polyolefins are currently the most frequently used materials in the food packaging industry. On the other hand, it must also be noted that when fatty foods are in contact with packaging made of polyolefins, negative migration of triacylglycerols will occur, resulting to a time depended change of the diffusion coefficients of the migrating substance in the polymeric system. This fact can be considered as a big disadvantage of these models (Meulenaer, 2009).

Several similar models based on Fick's law can be found in the literature. Since currently, the only models accepted by the EU and USA regulations are the models developed by Piringer and Limm & Hollifield the following models won't get the same depth of analysis (Piringer 1994), (Limm and Hollifield, 1996).

Pennarun et al, (2004), predicted the migration of PET materials in contact with aqueous food simulants at 313^{o}K, using some empirical equations, overestimating the diffusion coefficients. Their method has been applied successfully to POs and their empirical equation was based on D values from the literature and can be expressed as:

$$logD^* = AMW_m + \frac{B}{T} + C \tag{4.25}$$

where *A,B,C* are constants, D* is the worst case diffusion coefficient determined empirically from a graphical correlation logD = f(MW_m), MW_m is the molecular weight of the migrant and T is the temperature. It's important to note that the experimental conditions, as well as the experimental background theories, found in literature are strongly different between each other giving different D values. However the very large number of data used gave confidence and accuracy to equation (4.26). These parameters found in the literature are obtained with many overestimating assumptions (due to reasons explained above) and are heavily on the side of the protection of public health. Only the maximum of the experimental uncertainty range of the diffusion coefficient values was taken into account and then the largest of these values were taken as the reference diffusion coefficients (Pennarun et al, 2004).

Han et al, (2003) developed and applied a model based on a numerical treatment method known as Finite Element Method (FEM) for quantifying the migration through multilayer structures. In their approach several assumptions were made such as no swelling of the polymer, time dependent partition coefficient, 1-D mass transfer, diffusion coefficients depend only on temperature, finite packaging, etc. Based on the assumptions of constant diffusion coefficient and negligible resistance for the mass transfer between the plastic and the food simulant, the mathematical equation of their model can be expressed as:

$$\frac{M_{F,t}}{S} = 2C_{p,0}\left(\frac{Dt}{\pi}\right)^{0,5} \qquad (4.26)$$

Where, S is the surface area of the polymer in contact with the food, $C_{P,0}$ is the initial concentration of the migrant in the polymer volume at time t=0, D is the diffusivity of the migrant within the polymer and finally $M_{F,t}$ is the amount of mass that has migrated from the polymer into the food after time "t". The diffusion coefficient of the migrant in the outer layer was estimated algebraically using the empirical equation (see equation 4.22) proposed by Piringer (1994), (Brandsch et al, 2002). They successfully validated their model using HDPE and LDPE materials for two bulk concentrations (100% and 50%) of food simulant (ethanol) and three different temperatures (296^{o}K, 304^{o}K and 313^{o}K) comparing their simulated results to experimental data (Han, 2003). Their model results were found to be accurate as the deviation from the experimental values was negligible.

Lickly et al, (1997) proposed a simple, analytical model, based on the general theory of mass transfer. They assumed a semi-infinite flat sheet of polymer in which the additive migrated towards the surface and then into the bulk solution. This analytical model similarly to the others was based on the diffusion theory as described by Fick's 2nd law. The main equation describing the migration phenomenon in this study is:

$$M_{F,t} = C_{po}aK_{P,F}(1 - e^{z^2}erfc(Z_{err})) \qquad (4.27)$$

where,

$$Z_{err} = \frac{(D_p t)^{1/2}}{aK} \qquad (4.28)$$

Where, $M_{F,t}$ is the migrated quantity of the component migrated for time t, a is the volume of simulant, $K_{P,F}$ is the food-polymer partition coefficient, C_{po} is the initial concentration of the component in the polymer phase and erfc(Z_{err}) is the error function term of Z_{err}. The use of this expression assumes infinite thickness of the polymer phase, homogeneously distributed migrant in the polymer, a temperature-only- dependent diffusion coefficient and no interactions occurring between polymer and external phase. The model was validated by experimentally estimating the migration for specific additives and materials from different sample configurations (Lickly, 1997).

A quite different model was proposed by Fauconnier et al, (2001) where the migrated quantity was described as a polynomial function of temperature and time. The influence of time and temperature on the additives was modeled with the response surfaces method. The polynomial equation used by the response surface method is;

$$z = A_m + B_mT + C_mt + D_mT^2 + E_mt^2 + F_mTt \tag{4.29}$$

where, T and t are temperature and time respectively, the response z is the migrated quantity (mg/g) and A to F are coefficients calculated for all migrants in each migration liquid. The modeling of desorption data used in their model was based on a correlation procedure using a polynomial equation. Such a procedure that is neglecting physical principles such as diffusion, lies in the extrapolation of the diffusion coefficient into regions where the results are not acceptable, resulting to false values. Therefore, for avoiding the error it is important to eliminate some critical regions. In order to validate the method proposed the authors executed a series of experiments using HDPE and three different aqueous food simulants. They used ethanol, lemon terpenes and an emulsion of terpenes. The results showed accuracy over 90% for all phenolic migrants as well as for polymers' oligomers.

By calculating the diffusion coefficients with the use of any of the two main models (or even with any of the rest of them) the migrated concentration of the additive can be calculated. The diffusion in the polymer is assumed to obey Fick's 2nd law (equation 4.18). During the migration modeling several phenomena should be taken into account. Some of them are the swelling of the polymer, the kinetics limitations at the surface, the partition coefficient*, etc*. As there are many phenomena taken into account there is no analytical solution of equation (4.18) leading to the use of numerical analysis for the calculation of the migration amount.

For a better understanding of the insufficient and inaccurate use of the current migration models due to the oversimplicity of the transport phenomena by the two main models, a series of recently published studies are briefly presented below.

O'Brien and Cooper (2001), studied the polymer additive migration from polypropylene (PP) to a food simulant (olive oil). For their study, they used the 'Migratest Lite' program which uses the model proposed by Piringer (1994), designed to overestimate the overall migration value. Their results showed, as expected an overestimation, for the 97% of the values calculated, for an amount greater than 70% of the observed value. It can be said with considerable confidence that this model provided inadequate results for estimating a realistic migration value.

Gillet et al, (2009) studied the migration of a model migrant from plastic materials (HDPE) in a food simulant, using the model proposed by Piringer (1994) and under the assumptions described by Vitrac and Hayert (2005) and (2006). Their results highlighted the assumption that the model fails to demonstrate a consistency in the calculations of the exact overall migration value. Welle and Franz (2012), studied the migration of model migrants from PET bottles to water. For their study, they used the model proposed by Piringer (1994). Comparing their results with literature data they noticed a positive difference up to one order of magnitude resulting to the overestimation of the overall migration value. Reinas et al (2012), studied the migration of two antioxidants from packaging into a solid food and into a food simulant. For their study, they used the equations proposed by Piringer's model (1994). Their results showed the expected overestimation of the overall migration value, up to several orders of magnitude. Haldimann et al (2013), studied the migration of the heavy metal – antimony in a food simulant and in a foodstuff from PET trays. For their study, they used the model proposed by Limm & Hollifield (1996). Their results showed a 95% agreement between the experimental and overestimated theoretical migration measurements. Zhang and Zhao (2014), studied the migration of flavonoids from LDPE to aqueous food simulants. For their study, they used the model proposed by Limm & Hollifield (1996). As they concluded, when comparing their theoretical results with the experimental values did not fit very well due to the complexity of the migration tests. Maia et al, (2016), studied the migration value of a model migrant (BZP) from plastic (LDPE) into different foodstuffs. For their study, they used the model proposed by Piringer (1994). After analyzing their results, they observed that the values predicted by the model had a large margin of uncertainty making them improper to find the exact overall migration value. Han et al, (2003), studied the migration of photoinitiators from paper to fatty food simulants by using the model used by Zulch and Piringer (2010). Their results showed a linear irrelativity up to approximately 20% making them improper to use for the estimation of the real overall migration value.

Nevertheless, the main problem of a realistic estimation of the diffusion coefficients describing the migration process still remains. When a quite realistic estimation of migration is considered as necessary, the use of underestimated diffusion coefficients will lead to overestimated migration values, making the practical use of migration models rather impractical and inaccurate (Brandsch et al., 2000, Meulenaer, 2009).

4.3.3. PROBLEM MODELING

Based on the above discussion, it is clear that a more accurate theoretical model must include the environment as part of the system. It must consider a strongly coupled system in the form "environment - packaging - food" rather than "food - packaging". This model must add to the mass transfer equations the appropriate conditions for the phenomena occurring beyond just the diffusion. Today this scope of view is unusual, mainly because these simulations are used for the determination of safety limits in food consumption. As it has been discussed above in detail, overstatement of immigration will lead to stricter limits, which is very useful for food safety. This case study focuses on the control of the products qualitative characteristics, without, of course, questioning the approach of the diffusion process as a tool to determine the safety limits for the consumption of packaged food.

As a case study, our approach, expands the migration of a substance from the material into food, beyond the simple diffusion, considering the multiple-studied oxidation of packaged olive oil. The phenomenon of migration concerns the transfer of oxygen from the environment to the material and then to the oil.

It is known that oxidation is generally described by the reaction:

$$RH + O_2 \overset{k}{\rightarrow} ROOH \tag{4.30}$$

where, RH is a fatty acid and ROOH is the corresponding peroxide, which results in conversion to characteristic aromas. Among them, the increase in the amount of hexanal is considered to be the main indicator of the oxidative lesion of packaged olive oil. It is evident that the above reaction requires the presence of oxygen in the oil phase, either inherently (as a component of the oil phase, but in a small proportion) or because of its penetration through the porous permeable material of the package.

Given the known environmental temperature and oxygen's atmospheric pressure and the absence of light, it is obviously necessary to have a minimum value of the oxygen concentration in the oil phase, below which the reaction (4.30) is not proceeding. In order to test the reliability of the proposed approach, we considered the mass transfer of oxygen, as oxygen migration to olive oil, and we took into account two cases: (a) packaging is impermeable, so the reaction occurs only because of the oxygen present soluble in olive oil, and (b) the package is permeable, thereby entering the olive oil and oxygen from the environment through the package. In any case, the presence and effects of mass transfer of oxygen are described by the following equations (Coutelieris and Kanavouras, 2006):

$$\frac{\partial C_{O_2}}{\partial t} = D_{O_2} \nabla^2 C_{O_2} - k C_{O_2} C_{RH} \tag{4.31}$$

$$\frac{\partial C_{RH}}{\partial t} = -kC_{O_2}C_{RH} \tag{4.32}$$

$$\frac{\partial C_{ROOH}}{\partial t} = D_{ROOH}\nabla^2 C_{ROOH} + kC_{O_2}C_{RH} \tag{4.33}$$

Where, D_i is the diffusion coefficient of component i and k is the kinetic reaction constant. Considering three control volumes (one for the environment, one for the packaging and one for the olive oil) to which the above equations apply, and framing them with appropriate initial and boundary conditions, we can numerically solve the system and export prices for three unknown concentrations.

Analogous typical microscopic scale results are shown in the following figure (4.14), where a two-dimensional section including all three volumes of interest has been considered. In each picture of the figure, left is the area containing the olive oil and right the environment, and the two areas are separated from the packaging. Concentrations have been calculated when the system has reached a steady state, and have been normalized for the purpose of directly comparing them. Typical ambient temperature ($T = 296^oK$) and pressure ($P = 1$ atm) and indicative values for the porosity of the packaging material ($\varepsilon = 0.012$) (Coutelieris and Kanavouras, 2006), have been considered. The diffusion coefficients are D_{O2}, oil = $2.3X10^6$ cm^2 / sec, D_{O2}, packaging = $4.9X10^9$ cm^2 / sec and D_{ROOH}, packaging = $3.6X10^{11}$ cm^2 / sec (Coutelieris and Kanavouras, 2006). Finally, for the production of the three images to the right of Figure 1, the reaction (4.30) with k = $2.5x10^{125}$ sec^{-1} is considered, while the corresponding three on the left of Figure 4.14 are without reaction (k = 0 sec^{-1}) (Coutelieris and Kanavouras, 2006).

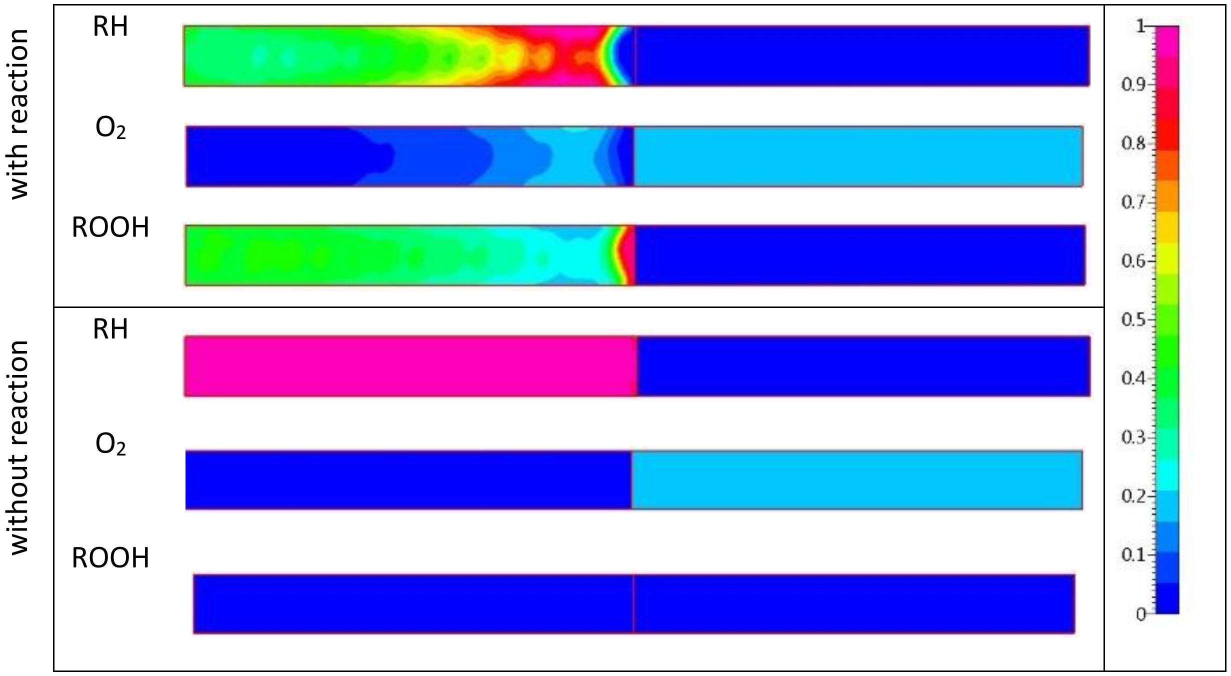

Figure 4.14 Typical results for system concentrations of equations. (4.32) - (4.34) in a permanent state.

By the results depicted in Figure 4.14, we note that in any case the area of interest is close to the olive oil-packaging interface, where the consumption of oxygen and the resulting ROOH production is relatively high. It is worth noting that in the case where there is no longer oxygen in the packaging, this concentration is negligible, demonstrating the limited ability of diffusion to describe the phenomenon and the consequent necessity of a vision and reaction (4.30) in the mechanism of describing migration .

The above is also shown in Figure 4.15, which shows the time course of the corresponding normalized concentrations when taken (left graph) and when the reaction is not taken (right graph).

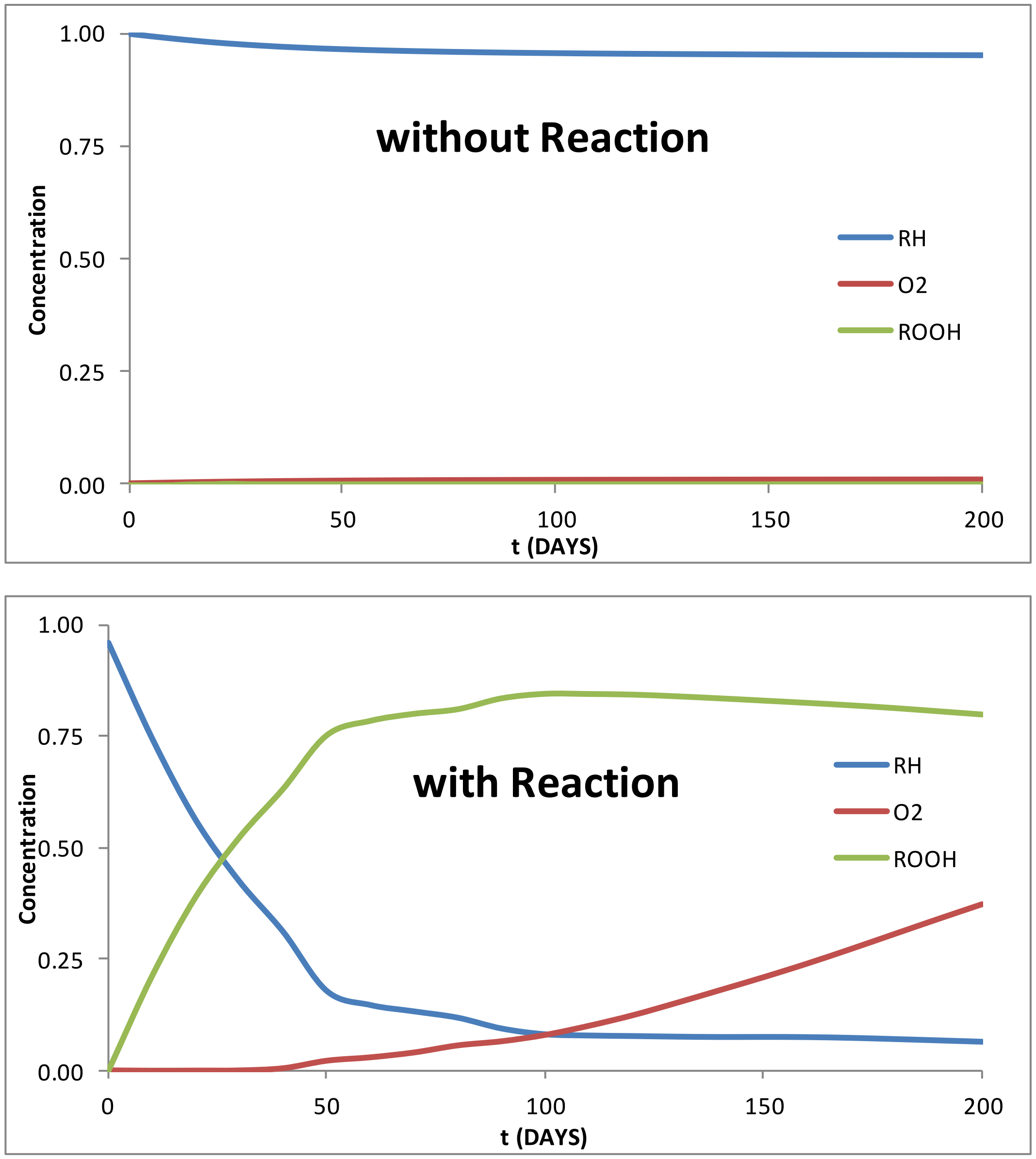

Figure 4.15 Time evolution of system concentrations for equations (4.31) - (4.33).

When the reaction (4.30) is not taken into account, the concentration of the fat components is practically stable, whereas when the reaction is taken into account, we see the systematic reduction of RH with the constant oxygen supply and the corresponding increase of the peroxides (ROOH). The concentration of the latter reaches stable production (given the sufficiency of reactive fatty acids) after a critical time (here about 100 days), because the area is overcharged in oxygen, so there can be no greater extent of the reaction (4.30). It is obvious that this critical moment depends on the conditions of pressure and temperature that apply each time, as well as on the packaging material. The difference in RH concentrations at the end of the time considered is about 93%, which now proves the necessity of a visa for migration, mechanisms more sophisticated in diffusion.

This case study critically examined the prevailing perception of modeling of food migration on the basis of the laws of Fick, given the divergences between the theoretical approach and the various experimental measurements for different foods, packaging materials and conditions as identified in the literature until today. Since all theoretical approaches to date regard diffusion as the dominant or even single mechanism for migration, these deviations have been attributed to the way the parameters are determined, and research efforts have focused on improving this determination.

4.3.4. MODELING RESULTS

In this case study, divergences are attributed both to the simplified view of the mechanisms and to the lack of understanding of the role of the environment in the system to be studied. In order to ascertain in principle, the credibility of such an assertion, we applied this proposed broader approach to packaged olive oil, where it was predominant to conclude that the diffusion-only view leads to concentration values that deviate too much from those that occur when it is considered a reaction. On this basis, we can safely infer that immigration is not fully and adequately described by Fick's laws. Therefore, a more complex modeling is needed, which should ideally include all the phenomena that occur in the case study system under study. Consequently, it will now be possible to transfer the study of the migration of substances to food from the legal field of safety in the field of food quality control and consumer preferences.

4.3.5. DISCUSSION

The only practical way to use migration modeling for quality assurance is to start with the simplest migration estimation procedure. The two simpler models are the two main models, suggested by the EU and US FDA, the Piringer's model (Piringer, 1994) and Limm & Hollifield's model (Limm and Hollifield, 1996). Piringer's model correlates the diffusion coefficients with the relative molecular mass of the migrant with a specific parameter along with the absolute temperature. This approach seems to be the simpler and most widely used for the purpose of migration modeling. Limm & Holifield proposed a similar approach for migration modeling with the limitation of use only for POs, fact leading us to the conclusion of eliminating the specific model from our list of choices. However, on the other hand O'Brien and Cooper, compared the two main models for the migration of a number of additives from HDPE in olive oil and found that Limm & Holifield’s model is more accurate in most of the situations, but underestimates the results more frequently.

Additionally, certain theoretical issues need to be addressed. Among the most significant comments to be made at this point is that all the approaches converge to the fundamental consideration that the migrant mass transfer is diffusion driven, therefore the process may be adequately described by Fick's laws. For that reason, the differences among the most widely used migration predictive models have been actually categorized in such a way that the diffusion coefficient is basically estimated, while models being otherwise essentially similar in their insight. As stated earlier in this present review, the fundamental considerations for the Fick's law valid use, are actually dependent on the following specific assumptions:

- → The migrant was distributed homogeneously in either the packaging material or the food phase.
- → There was no boundary resistance in the transfer of the migrant between packaging and food phases.
- → There were no interactions between packaging and food.
- → No swelling phenomena occurred within the food-packaging system.
- → A specific partition coefficient between food and polymer might be assumed.
- → There was no external supply of migrant during migration process, i.e. the sum of the total migrant amount in the food-packaging system is constant.

Although the aforementioned points may be valid for the vast majority of the migration applications in nature, it seems apparently rather less likely for this consideration to be incorporated in more complicated phenomena, such as sorption of specific food contaminants by the packaging material, partitioning on the food-packaging interface, chemical reactions of packaging material or of some of its byproducts with the food content, etc., all of which possess a high potential within real food-packaging systems. We may safely assume then, that the above assumptions cannot be valid, in a universal way. In general, it is rather easy to identify a case where at least one of the above assumptions breaks down. For example, within a more precise context of pragmatic hesitations we may report on the assumption #1 which could not be valid for packaging materials other than plastic polymers, on assumption #2 that might not be valid for sticking migrants, and so on.

Concluding on a rather obvious non-Fickian behavior of migrants, such a mass transport process has to be modeled via more complicated mathematical expressions, potentially containing non-linear terms to express the above-mentioned phenomena. Summing up, equation (4.19) is sufficient either for defining norms, rules and laws, or for rough estimation of mass transport for industrial purposes, but it seems quite weak when a deeper, a more thorough and highly descriptive, in a scientific way, insight is in demand. Needless to say, equation (4.20) is a significant improvement, although it has found quite a limited apparent applicability, most possibly mainly due to its inevitable complexity.

On top of the above-mentioned shortcomings, another significant drawback has been encountered in the widely accepted published literature regarding the system consideration: the environment is usually considered as the entity that just imposes the conditions (boundary/initial conditions as well as values of the parameters involved in the equations) without being part of the system. Consequently, environmental influence is not engaged directly in the transport problem but only through the conditions and parameters, being therefore somehow arbitrary. Therefore, it seems absolutely necessary to rework and potentially restructure the traditionally accepted “packaging-food” system with the suggested novel one being “environment-packaging-food”, which allows for a more detailed and rather solid consideration of the totality of the transport phenomena occurring within a complete system.

A further discussion point quite relevant to the previous specific criticism has to do with the main difficulty of migration modeling. Meaning that we should no longer work for the purpose of elaborating a model (Han et al, 2003), but it seems much more important to be able to obtain the parameters requested for the most appropriate, descriptive and accurate calculations:

→ the diffusion coefficients D of the migrant in each layer; if they are not available.

→ the partition coefficient between layers as only little data are available. If the different layers are made from the same or from similar polymers, the partition coefficient can be assumed to be $K_{p/fb} = 1$

→ the partition coefficient between functional barrier and food $K_{fb/f}$. Again, in absence of data, a worst-case value must be selected, such as $K_{fb/f} > 10^{-2}$.

→ swelling of the plastic layers by food constituents leads to a continuous increase of D during contact with food: use of D* values often takes into account swelling.

→ the mass transfer coefficient at the interface. In absence of data the interface may assumed to be infinite, as a worst-case scenario.

The models described above are only to predict the migration of known and already characterized migrants from polyolefins. Hence, these models are not capable to predict the total accurate migration of a substance migrating from a contact material to the food volume, as the material might contain a number of completely unknown compounds. As these models tend to overestimate the migration value, they cannot be used in the process of food manufacturing where the migration of an additive might be essential and necessary for the optimum quality of the product. In such cases an accurate value of the migration process must be calculated in order to have the optimum quality.

5. CONCLUSIONS

The main aim of the work of this PhD was to present the capabilities and the features of mathematical modeling when transport phenomena are under investigation. After the introduction and the background review conducted in Chapter 1, the content of Chapter 2 investigates the fundamental transport processes, affected by advection and diffusion, for all the used scales, microscopic, mesoscopic and macroscopic. Chapter 2 includes a brief but detailed discussion regarding the most widely used CFD models and the modules utilized by the selected CFD-ACE

To establish an easy-to-use and efficient method for scale transition, the transport phenomena presented in chapter 2, were studied in chapter 3, aiming to enhance our understanding of and obtain quantitative relation between the parameters and quantities under investigation, using three-dimensional porous media models of different characteristic scales. The result of this work is the development of a fast and easy method of matching the macroscopic quantities (such as adsorption efficiency) during a scale transition process from mesoscopic to macroscopic (scale-up), or to microscopic (scale-down) and vice versa geometries. In order to be able to move from one scale to another, the fundamental transport processes (laminar flow, convection, diffusion and heterogeneous reaction) were detailed described for all three scales, following the same flow conditions given by the use of a dimensionless number, known as Peclet Number. In order to achieve this, the effect of the surface catalytic reaction on species mass fractions was analyzed. The reactants ($C_{10}H_{22}$ and O_2) were consumed on the catalytic surface and their mass fraction as expected decreased as the exit of the porous media was reached. On the other hand, the steam and carbon dioxide were produced due to the oxidization reaction and their mass fraction increased towards the exit. It should be noted that for the microscopic case (sphere-in-cell) and the mesoscopic scale (assemblage of spheres), which represent a more analytical view of the porous media, formed a gradient from the catalytic surface towards the pores due to the combinatory effect of the prevailing transport phenomena. After simulating the three scales it was concluded that as Peclet number increases, the adsorption efficiency value becomes lower for all scales, meaning that as the convection increases the lower amount of the reactant reaches the catalytic surface in order to react. However, in the case of the unit cell model, this behavior was found to be accurate only for relatively low to medium Peclet numbers ($Pe<50$). For high Peclet numbers, the velocity reached high values at the point where the inlet surface meets the outlet surface leading to discontinuities. Although omitting the problematic areas from λ calculations resulted in reducing the error incorporated in λ values, it was proved that the sphere-in-cell geometry is insufficient to simulate the mass transport phenomena for high Peclet numbers. Furthermore, the same effect of porosity on adsorption efficiency, was found for all scales, as it is observed that the λ value increases, as porosity decreases. This phenomenon can be explained because as porosity decrease the catalytic surface, where the oxidization reaction takes place also increases. Hence, if the surface increases then the available surface for a reaction increases too. It should also be mentioned that the sphere-in-cell model presented an opposite behavior for high Peclet numbers (*Pe*>100) as reduced porosity yielded in lower λ values. Finally a method of matching the geometrical parameters when scale transition occurs is proposed, underlying the necessary steps that should be followed. As the first step the calculation of the geometrical characteristics of the detailed geometry is a necessity as it will be the base where the transition will be relied on. Next, the inlet mixture flow needs to be adjusted in order to preserve the Peclet number for all of the scales. Since the diffusion coefficients are practically constant, this adjustment can be made only by adapting the velocity to the necessary value. Finally, the last two most important adjustments are required to be made in order to have an identical characterization of the geometry without any discrepancies. The characteristic ratio, S/V of the porous material, is a measurement value of the available surface where the reaction may occur. By correctly adjusting this value, the geometry will have the same amount of reaction if it is simulated in any of the needed scales. Last, but not least the average pore size needs to be adjusted proportionally to the transition ratio. If the average pore size isn't adjusted correctly it could lead to a discrepancy of the geometry as the hypothetical pores would have been squeezed or extended in order to preserve that lower or higher void space, respectively. It's also very important to notice that all the behaviors presented in Chapter 3, are validated by the work of Couteliers et al. (2003) The three models were also validated with typical results found in the relative literature. Specifically, the comparison of simulation results for the microscale model were validated with these work of Kløv et al (2003), while the validation for the sphere assemblage scale (mesoscale) validated, against the results presented by Delgado, (2006). Finally, the results for the macroscopic scale were compared with the results of Abriola et al (2004). In each case, it can be observed that the qualitative behavior of the adsorption efficiency is in good accordance with the existing literature data. The fairly high discrepancy in terms of quantitative comparison observed in all scales, are attributed to the arbitrary values of the parameters ϕ and ω used here, as well as the different surface reactions and/or sorption mechanisms considered in these works. Unfortunately, in order to validate the results of this work, a direct comparison of experimental or theoretical results of the reaction of decane oxidation in porous materials would be necessary. However, neither experimental nor theoretical results have been found as a reaction like this is not frequently used when studying mass transfer in a porous medium. To further ensure the validity of the model, the effect of porosity on the dimensionless number known as overall Sherwood number, was validated against the results of Gunn (1978). As expected, the results comparison shows that Sh_o number decreases as the porosity value increases. A general trend is observed here, i.e. that adsorption efficiency is found to decrease with Peclet number and porosity. This trend is found to be fully compatible with numerous published results by (Kløv et al, 2003), (Delgado, 2006), (Abriola et al, 2004) and (Gunn, 1978) regarding all the scales considered in this work.

After studying the transport phenomena, in Chapter 2 and 3 and reassuring their analysis with the necessary validations, three case studies implementing the transport phenomena in different scales were analyzed. The three studies considered the applicability of the mathematical simulation of transport phenomena in the cases of water remediation, heat transfer in industrial scale and last the food packaging transport phenomena occurring in a microscopic scale.

The study solving the case of the water remediation, investigated the adsorption process from both experimental and theoretical (modeling) point of view. The adsorption process of phosphate onto Phoslock^{TM}, is an increasingly used worldwide restoration tool aiming the control a minimization of phosphorus in natural water ecosystems. Bench-scale batch experiments were performed examining Phoslock's^{TM} efficiency as an adsorbent and detailed simulations were carried out, allowing a better understanding of the phosphate removal process. The adsorption efficiency estimated by the simulations was found to be approximately 87.41%, being in excellent agreement with the one measured experimentally (approx. 87%). However, it is important to notice the discrepancy between experimental measures and simulation estimations. Although the agreement is perfect for T = 25°C, it was found to be more and more poor as temperature decreases, approaching approximately 10% difference for the low temperature of 10°C. This inconsistency between the experimental and theoretical efficiency can be attributed to the internal inefficiencies of unit cell approach, which in particular is found to overestimate the adsorption efficiency.

The study solving the heat transfer case utilized in an industrial scale problem investigated a rather common practice for marine industry. In marine industry the use of superheated water in heating coils for heating up heavy fuel oil is essential. Fundamentally, the efficiency of heat transfer process is strongly coupled with the dimensions of the coil (length, thickness, and diameter) as well as on the operational parameters (oil temperature, steam temperature, steam pressure). In this case study, the heat transfer from superheated water, considered at high temperature (~424K) and fixed pressure (5bar) to fuel oil tanks of specific dimensions and of various lengths, diameters and thicknesses was theoretically investigated, by both macroscopic thermo-dynamical approach and microscopic simulations. The goal of this study was to estimate the necessary size and length under the assumption of insulated tank. A parametric analysis was also performed in order to identify the relative influence of each parameter on the process performance. To obtain length values, both a thermodynamic analysis and as well as a detailed 3-D simulation were carried out. The effect of the most crucial parameters on the results was investigated resulting to the optimal length of approximately 160m for the shortest time period that the process takes place. More specifically, the maximum length which can be established due to the limitations on geometrical characteristics of the banker tank cannot exceed 160m for one layer of carbon-steel coil of 50mm diameter and 4mm thickness and that can increase the HFO temperature to by 30K in about 9.5h according to the thermodynamic analysis and 10h through the detailed 3-D, CFD-ACE+, simulations which constituted the most favorable result for the feeding process to the engines. The most efficient scenario was found to be presented through the installation of a double layer of carbon-steel coil which increased the overall length at about 300m and limited time at an interval of 5 hours. The main disadvantages for such an established scenario can be observed on the homogeneity of the temperature of the total HFO and on the increased initial establishment costs for this construction. Finally, it must be mentioned that the temperature of the HFO inside the banker tank was found hardly uniform, for lower time interval processes, due to the physically occurred stirring, during the oil's entrance to the tank and also due to the variation of its viscosity among the several time steps.

The concept of migration from polymeric packaging materials to food and food simulants, under the environmental conditions expected during the food products' complete life cycle, was investigated for the third case study. The most widely approved models that deal with migration as a diffusion-driven process are found to be neglecting more complicated mass transport mechanisms, and environmental involvement that occur either in parallel or simultaneously in the whole system. The aim of this case study was to consider these models and weight them against their extensive use. After having identified the areas of their inadequacies in validating the migration during food process applications were found to potentially affect food quality rather than safety. This study outlined and proposed specific and eventually more complete directions, for future modeling approaches regarding the food–packaging interactions, comprehensively involving the storage environment in terms of both conditions and constituents. The outcome of this work is the proposal to go beyond the consideration of the diffusion process as being the single mechanism to describe the migration from packaging to foodstuffs, but rather to incorporate more complicated phenomena (sorption, surface reactions, etc.) to overcome the above-mentioned discrepancies.

Overall, in the present thesis, the transport phenomena were studied and it was proved that the use of simulation with a computerized mathematical model imitates the behavior of a real-world process or system over time. Simulation is used to describe and analyze the behavior of a system when asking "what-if" questions about the real system and aid in the design of real systems, may be in order for the porous media to be simulated easier and quicker, is feasible.

Simulation modelling is a versatile technique well suited for the study of complex problems. Mathematical simulation using a computerized model like CFD is the obvious tool to be used superseding the old techniques. Mathematical simulation (aka modelling) is specifically useful for policy makers and strategic management, gaining insight into general future developments. However even if the mathematical simulation is proved to be accurate it stands or falls on the availability, applicability, and reliability of the data.

6. FUTURE WORK

As it has been mentioned above, the concept of migration from food packaging materials to food and food simulants is found to be attributed to the process of diffusion, which occurs due to the dissolution of the migrant in the food (see, for example, Brandsch et al., 2002, Arvanitoyannis and Bosnea, 2004). Migration modeling engages a deterministic approach, usually considering the migration process to be controlled by migrant’s diffusion through the packaging material, as described by Fick's second law (Pocas et al., 2008), relying on specific assumptions needed for assisting the model development and application, yet, not being necessarily extensively valid, in each and every case of substances’ migration between various phases.

The mathematical models utilized by the main legislation forces of both USA and EU are based on that single process using the Fick’s approach to describe mass transfer. They solve the elliptical differential equation for diffusion and spent most of their effort in determining the parameters applied (e.g. the diffusion coefficient), on which they base the differences among their existing models (see, for instance, Baner et al., 1996).

The models of Limm and Hollifield as well as Piringer’s model fundamentally overestimate the migration so it will always be on the safe side. However overestimating migration is not a solution. The inadequacy of the models lead to an inadequacy of the regulatory body to apply fines and sanctions to industries causing health effects to the public health. By applying accurate prediction using accurate models it will create a win-win situation where all parts, such as consumers and industries will be protected by different ways of means.

The models are only used to predict the migration of known and already characterized migrants mainly from polyolefins. Hence, these models are not capable to predict the total accurate migration of a substance migrating from a contact material to the food volume, as the material might contain a number of completely unknown compounds. As these models tend to overestimate the migration value, they cannot be used in the process of food manufacturing where the migration of an additive might be essential and necessary for the optimum quality of the product. In such cases an accurate value of the migration process must be calculated in order to have the optimum quality. Therefore, such models in their philosophy tend to inaccurately estimate migration, of a migrating additive potentially adversely impacting on the optimum product quality. In such cases a highly accurate prediction of the migration process must be in hand in order to reassure the optimum quality of a food within the complete supply chain environment.

As it has been presented above these widely approved models deal with migration as a diffusion-driven process are found to be neglecting more complicated mass transport mechanisms, and environmental involvement that occur either in parallel or simultaneously in the whole system. Aspects of migration, such as partitioning, heterogeneous reactions, packaging-material morphology, shape/polarity of the migrant, etc., have are not taken under consideration within these models, although discrepancies in their predictions and experimental observations have been revealed (Franz, 2007).

In this context, a critical discussion on the widely-accepted Fickian approach and its applicability and drawbacks, for identifying and predict inadequacies was presented in chapter 4. After having identified the areas of their inadequacies in validating the migration during food process applications were found to potentially affect food quality rather than safety. This will outline and propose specific and eventually more complete directions, for the prediction of migration regarding the food–packaging interactions, comprehensively involving the storage environment in terms of both conditions and constituents.

Certain theoretical concerns are raised by the work of Gavriil et al, (2018), regarding the approaches convergence to the widely accepted theory of concerning that the migrant mass transfer is driven by diffusion, and adequately described by Fick’s laws. Up to today, the main effort is placed on identifying the diffusion coefficients and other parameters within the models in order to identify the application area for each and every model. At the same time the Fickian approach is considered without much hesitation since models provide an over estimation of the migrants present in foods at the upper acceptance limits for food safety in terms of legal purposes.

We may safely propose then, that the above assumptions cannot be valid, in a universal way. In support of that, we have identified cases where at least one of the above assumptions cannot be valid as, for example, the case that the assumption of homogeneous migrant distribution in either the packaging material or the food phase cannot be valid for packaging materials other than plastic polymers. Also, in the same work the assumption it is mentioned that the assumption that there is no boundary resistance in the transfer of the migrant between packaging and food phases results in not be valid estimation of the migration of sticking migrants, and so on. (Gavriil et al, 2018)

As it has been concluded by this PhD there is a need for science and legislation forces to go beyond the consideration of the diffusion process as a single mechanism describing the migration from packaging to foodstuffs. This new approach must incorporate more complicated phenomena (sorption, surface reactions, etc.) which should be strongly coupled with the environmental conditions, to overcome the pre-mentioned discrepancies.

The main goal of this proposal concerns the mathematical modeling off substances migration from the packaging material to foodstuff under various environmental expected during the food products' complete life cycle. The main migration models discussed before may well enough predict the migration of known and already characterized migrants from commonly used plastic containers, while when the contact material contains a number of completely unknown compounds, these models may not be capable for accurately predicting the overall migration of each substance.

Therefore, we be apt to conclude on the need to study the actual non-Fickian behavior of migrants on a universal scale by taking under consideration the mass transport process via more complicated mathematical expressions, potentially containing non-linear terms, for a more complete expression of the migration phenomena.

7. REFERENCES

Abriola L.M., Bradford S.A., Lang J., Gaither C.L., (2004) Volatilization of Binary Non-aqueous Phase Liquid Mixtures in Unsaturated Porous Media. Vadose Zone Journal, Vol.3, pp: 645–655.

Akanni K.A., Evans J.W., Abramson I.S., (1987). Effective transport coefficients in heterogeneous media. Vol. 42, pp. 1945-1954.

Akhurst D.J., Jones G.B., McConchie D.M., (2004). The application of sediment capping agents on phosphorus speciation and mobility in a sub-tropical dunal lake. Journal Marine & Freshwater Research, Vol. 55, pp 715-725.

Anderson D.A., Tannehill J.C., Pletcher R.H., (1984), Computational fluid mechanics and heat transfer. McGraw-Hill New York: Hemisphere.

Anderson J.D., Wendt J., (1995). Computational fluid dynamics, Springer, Berlin, Heidelberg

Arvanitoyannis I., Bosnea L., (2004). Migration of substances from food packaging materials to foods. Critical Reviews in Food Science and Nutrition, Vol. 44(2), pp. 63-73.

Atkins P., De Paula J., (2010). Physical Chemistry (9th ed.). New York: W. H. Freeman.

Bachmat Y., Bear. J., (1991). Introducing to modeling of transport phenomena in porous media. London: Kluwer Academic Publishers.

Baner A., Brandsch J., Franz R., Piringer O., (1996). The application of a predictive migration model for evaluating the compliance of plastic materials with European food regulations. Food Additives & Contaminants, Vol.13(5), pp. 587-601.

Baner A., Piringer O., (2008). Plastic Packaging: Interactions with Food and Pharmaceuticals. Weinheim: 2008 WILEY-VCH Verlag GmbH & Co. KGaA,.

Bear, J. (1972). Dynamics of fluids in porous media. Elsevier.

Beekman, J. (1990). Mathematical description of heterogeneous materials. Vol.45, pp. 2603-2610.

Begley T., Castle L., Feigenbaum A., Franz R., Hinrichs K., Lickly T., Mercea P., Milana M., O'Brien A., Rebre S., Rijk R., Piringer O., (2005). Evaluation of migration models that might be used in support of regulations for food-contact plastics. Food Additives & Contaminants, Vol. 22(1), pp 73-90.

Bejan, A. (1993). Heat Transfer. New York: Wiley.

Berkowitz B., Cortis A., Dentz M., Scher H., (2003). Modelling non-Fickian transport in geological formations as a continuous time random walk. Vol. 44 (2)

Berkowitz B.,.Scher H., (1998). Theory of anomalous chemical transport in random fracture networks. Vol 57(5), pp. 58–69.

Bhattacharya R., Gupta U.K., (1990). Application of central limit theorems to solute dispersion in saturated porous media: From kinetic to Darcy scale. In J. Cushman (Ed.), Dynamic of fluid in hierarchical Porous media (pp. 61-96). New York: Academic Press.

Bird R. B., Stewart W. E., Lightfoot E. N., (1960). Transport Phenomena. New York: John Wiley & Sons Inc.

Blazek, J. (2001). Computational Fluid Dynamics: Principles and Applications. Switzerland, Baden-Daettwil: ELSEVIER.

Bode, J. (1994). Applications of computational fluid dynamics in the chemical industry. 17, pp. 145-148.

Bourgeat A., Quintard M., Whitaker S., (1988). Comparison between homogenization theory and volume averaging method with closure problem, pp. 463-466.

Bouteville, A. (2005). Numerical simulation applied to chemical vapour deposition process. Rapid thermal CVD and spray. Journal of Optoelectronics and Advanced Materials, Vol. 7(2), 599-606.

Brandsch J. Mercea P., Piringer, O., (2000). Possibilities and limitations of migration modeling. In O. B. Piringer, Plastic packaging materials for food, barrier function, mass transport, quality assurance and legislation (pp. 446-468). Weinheim: Wiley - VCH.

Brandsch J., Mercea P., Rüter M., Tosa V., Piringer O., (2002). Migration modelling as a tool for quality assurance of food packaging. Food Additives & Contaminants. Vol. 19, pp 29-41.

Brandsch R., Mercea P., Zulch A., Piringer O.G., Tosa V., (2006a). Determination of physica-chemical parameters of food. Proceedings of Closing Conference of FoodMigrosure Project. Baveno, Italy.

Brandsch R., Mercea P., Zulch A., Piringer O.G., Tosa V., (2006b). Migration model for foods. Proceedings of Closing Conference for FoodMigrosure Project. Baveno, Italy.

Brenner, G. (2009). CFD in Process Engineering. In E. K. Egon H.H, 100 Volumes of Notes on numerical Fluid Mechanics. Vol. 100, pp: 341. Berlin: Springer.

Bruggemann, D. (1935). Berechnung verschiedener physikalischer konstante von heterogen substanzen. Vol. 24, pp. 636-664.

Butler R. M., Mcnab G. S., Lo H. Y., (1981). Theoretical studies on the gravity drainage of heavy oil during in-situ steam heating. The Canadian Journal of Chemical Engineering, Vol. 59, pp 455-460.

CFX. (2004). CFX manual. CFX.

Chapman, S.; Cowling, T. G., (1990), The Mathematical Theory of Non-Uniform Gases. 3rd edition. Cambridge etc., Cambridge University Press

Chapra S. C., Canale R. P., (2015) Numerical Methods for Engineers, 7th Edition, McGraw-Hill Education. New York, USA.

Chan T. C., Li H. T., Li K. Y., (2015). Effects of shapes of solute molecules on diffusion: A study of Dependences on solute size, solvent and temperature. Journal of Physical Chemistry B, Vol. 119(51), pp. 15718-15728.

Coutelieris, F.A., Kainourgiakis M.E, Stubos A., (2003), Low Peclet mass transport in assemblages of spherical particles for two different adsorption, Journal of Colloid and Interface Science. Vol. 264, pp. 20-29.

Coutelieris F.A., Kainourgiakis M., Stubos A., (2005). Low to moderate Peclet mass transport in assemblages of spherical particles for a realistic adsorption–reaction–desorption mechanism. Powder Technology, Vol. 159, pp. 173-179.

Coutelieris F.A., Kanavouras A., (2006) Experimental and theoretical investigation of packaged olive oil: Development of a quality indicator based on mathematical predictions, Journal of Food Engineering., 73, pp: 85-92

Coutelieris, F. (2011). Modeling of adsorption–reaction–desorption in granular media. Separation and Purification Technology, Vol.81, pp. 279-285.

Coutelieris F. A., Delgado J. M., (2012), Transport Processes in Porous Media, Springer, ISBN 978-3-642-27910-2, Berlin

Coutelieris F.A., Kainourgiakis M., Stubos A., (2002), The effect of Peclet on the Sherwood number in high porosity granular media. Vol. 144, pp. 753-760.

Crank, J. (1975). The Mathematics of Diffusion. Bristol: Oxford University Press.

Cushman J.H., Bennethum L. Y., Huc B. X., (2002), A primer on upscaling tools for porous media. Advances in Water Resources, Vol.25, pp: 1043-1067.

Dagan, G. (1989). Flow and transport in Porous Formations. New York: Springer.

Dai Z., Ritzi R.W., Huang C., Rubin Y.N., Dominic D. F., (2004), Transport in heterogeneous sediments with multimodal conductivity and hierarchical organization across scales. Vol. 294(1-3), pp. 66-86.

Das M.K., Mukherjee P. P., Muralidhar K., (2018), Modeling Transport Phenomena in porous media with applications, Springer International Publishing

Del Nobile M. A., Bove S., La Notte E., Sacchi R., (2003). Influence of packaging geometry and material properties on the oxidation kinetics of bottled virgin olive oil. Journal of Food Engineering, Vol. 57, pp: 189-197.

Delgado, J.M.P.Q. (2006) Mass transfer and dispersion around an active cylinder in cross flow and buried in a packed bed. Heat and Mass Transfer, Vol. 42, pp: 1119–1128.

Downes, T. (1987). Practical and theoretical considerations in migration. In J. E. Gray.

DyKaar, B. B., Kitanidis P.K., (1992). Determination of the effective hydravlic conductivity for heterogeneous porous media using a numerical spectral approach: 2.Results. Water Resources Research, Vol. 28(4), pp. 1167-1178.

Dzida M., Mucharski J., (2009). On the possible increasing of efficiency of ship power plant with the system combined of marine diesel engine, gas turbine and steam turbine in case of main engine cooperation with the gas turbine fed in parallel and the steam turbine. Polish Maritime Research, Vol. 16, pp: 47-52.

Ene, H. I. (1990). Application of the homogenization method to transport in porous media. (J. H. Cushman, Ed.) London: Academic Press.

ESI-Group. (2004). CFD-ACE+ Manual. ESI-Group.

EU. (2011). On plastic materials and articles intended to come into contact with food.

F.D.A. (2006). Guidance for Industry: Use of Recycled Plastics in Food Packaging: Chemistry Considerations. Washington, DC: USA.

F.D.A. (2007). Preparation of Premarket Notifications for Food Contact Substances: Chemistry Recommendation. Guidance for Industry, Washington DC.

Fauconnier M. L., Panhaleux V, Vanzeveren E, Marlier M, Wathelet J.P., (2001). Modelling migration from high-density polyethylene containers into concentrated solutions used as food flavourings. Food additives & Contaminants, Vol. 18, pp: 1040-1045.

Ferrara G., Bertoldo M., Francesco M., Ciardellid F., (2001). Diffusion coefficient and activation energy of Irganox 1010 in poly (propylene-co-ethylene) copolymers. Polymer Degradation and Stability, Vol. 73(3), pp. 411-416.

Fluent, I. (2005). Fluent Manual. Fluent inc.

Fokker, P. (2001). General anisotropic effective medium theory for the effective permeability of heterogeneous reservoirs. Vol. 44(2), pp. 205-218.

Franz, R. (2007). Migration modelling from food-contact plastics into foodstuffs as a new tool for consumer exposure estimation. Food Additives & Contaminants, Vol. 22(10), pp. 920-937.

Franz R., Welle F., (2008). Migration measurement and modeling from poly(ethylene tetraphthalate) (PET) into soft drinks and fruit juices in comparison with food simulants. Food Additives & Contaminants: Part A., Vol. 25(8), pp: 1033-1046.

Gavriil G., Kanavouras A., Coutelieris F.A., (2018), Can Fick law-based models accurately describe migration within a complete food product life cycle? Food Processing and Preservation, Vol 42(2),

Geist G. A., Kohl J. A., Papadopoulos P.M., (1996). PVM and MPI: a comparison of features. Calcul Paralleles, Vol. 8(2), pp: 137-50.53.

Gelhar L., Axness C. L., (1983). Three-dimensional stochastic analysis of microdispersion in aquifers. Vol.19(1), pp: 161-180.

Gilbert S. G., Miltz J., Giacin J.R., (1980). Transport considerations of potential migrants from food packaging materials. Journal of Food Processing and Preservation., Vol. 4(1-2), pp: 27-49.

Gillet G., Vitrac O., Tissier D., Saillard P., Desobry S., (2009) Development of decision tools to assess the migration from plastic materials in contact with food. Food Additives and Contaminants, Vol. 26 (12), pp:1556-1573.

Glatzel T., Litterst C., Cupelli C., Lindemann T., Moosmann C., Niekrawietz R., Streule W., Zengerle R., Koltay P., (2008). Computational fluid dynamics (CFD) software tools for microfluidic applications – A case study. Computers & Fluids, Vol.37, pp: 218-235.

Gunn, D. (1978). Transfer of heat or mass to particles in fixed and fluidized beds. International Journal of Heat and Mass Transfer, Vol. 21(4), pp: 467-476.

Haghseresht. F., Wang S., Do D.D., (2009). A novel lanthanum-modified bentonite, Phoslock, for phosphate removal from wastewaters. Applied Clay Science., Vol. 46(4), pp: 369-375.

Haldimann M., Alt A., Blanc A., Brunner K., Sager F., & Dudler V., (2013). Migration of antimony from PET trays into food simulant and food: determination of Arrhenius parameters and comparison of predicted and measured migration data. Food Additives & Contaminants. Part A, Chemistry, Analysis, Control, Exposure & Risk Assessment, Vol. 30(3), pp: 587–598.

Han J., Selke S. E., Downes T. W., Harte B. R., (2003). Application of a computer model to evaluate the ability of plastics to act as functional barriers. Packaging Technology and Science, Vol. 16, pp. 107-118.

Harris C. K., Roekaerts D., Rosendal F.J.J., Buitendijk F.G.J., Daskopoulos Ph., Vreenegoor A.J.N., Wang H., (1996). Computational fluid dynamics for chemical reactor engineering. Chemical Engineering Science, Vol. 51(10), pp: 1569-1594.

Harvard L., Thomas H. Pulliam (1999). Fundamentals of Computational Fluid Dynamics. Toronto: University of Toronto.

Helmroth I. E., Rijk, R., Dekker, M., Jongen, W.M.F., (2002). Predictive modelling of migration from packaging materials into food products for regulatory purposes. Trends in Food Science & Technology, Vol.13, pp. 102-109.

Himmelblau D. M., Riggs J.B., (2012), Basic principles and calculations in chemical engineering.—8th ed., Pearson Education, Inc., Prendince Hall, Michingan USA.

Holman, J. (1990). Heat Transfer. New York: McGrawl-Hill.

Horung, U. (1997). Homogenization and Porous media. New York: Springer.

Huang, H. Hu B. X., (2001). Nonlocal nonreactive transport in heterogeneous porous media with rate-limited sorption and interregional diffusion. Water Resources Research, Vol. 37(3), pp. 639-747.

Johansson F., Leufven A. (1994). Food packaging polymer films as aroma vapor barriers at different relative humidities. Journal of Food Science, Vol. 59(6), pp. 1328-1331.

Kadam A., Karbowiak T., Voilley A., Debeaufort F., (2015). Techniques to measure sorption and migration between small molecules and packaging. A critical review. Journal of the Science of Food and Agriculture, Vol.95, pp: 1395-1407.

Kauzmann, W. (1966). Kinetic Theory of Gasses, W.A. Benjamin, New York.

Kaviany M., (1991), Principles of Heat Transfer in Porous Media, Springer-Verlag, New York.

King, P. (1989). The use of renormalization for calculationg effective permeability. Transport in Porous Media, Vol.4(1), pp. 37-58.

Kløv T., Øren P.E., Stensen J. A., Lerdahl T.R., Berge L.I., Bakke S., Boassen T., Virnovsky G., (2003). Pore-to-Field Scale Modeling of WAG. Society of Petroleum Engineers, SPE Annual Technical Conference and Exhibition, 5-8 October, Denver, Colorado

Kuwabara, S. (1959). The forces experienced by randomly distributed parallel circular cylinders or spheres in a viscous flow at small Reynolds numbers. Journal of the Physical Society of Japan., Vol.14(4), pp: 527–532.

Kuzmin D., (2010), A Guide to Numerical Methods for Transport Equations, Friedrich – Alexander Universitat Erlanger Nurnberg.

LeVeque R.L., (1990), Numerical Methods for Conservation Laws, Springer, Birkhäuser Basel

Lickly T.D., Rainey M.L., Burgert L.C., Breder C.V., Borodinsky L., (1997). Using a simple diffusion model to predict residual monomer migration - consideration and limitations. Food Additives & Contaminants, Vol.14(1), pp. 65-74.

Limm W., Hollifield H.C., (1996). Modelling of additive diffusion in poleolefins. Food Additives & Contaminants, Vol.13(8), pp. 949-967.

Lőhner, R., (1988b) “Three-Dimensional Grid Generation by the Advancing Front Method,” Int. J. Num. Meth. Fluids 8, 1135-1149,

Lürling M., Tolman Y., (2010). Effects of lanthanum and lanthanum-modified clay on growth, survival and reproduction of Daphnia magna, Water Resources., Vol. 44, pp: 309–319.

Maia J., De Quirós A. R-B., Sendón R., Cruz J. M., Seiler A., Franz R., Simoneau C., Castle L., Driffield M., Mercea P., Oldring P., Tosa V., Paseiro P. (2016) Determination of key diffusion and partition parameters and their use in migration modelling of benzophenone from low-density polyethylene (LDPE) into different foodstuffs, Food Additives & Contaminants: Part A, Vol. 33(4), pp: 715-724.

Malekjani N., Jafari S. M., (2018) Simulation of food drying processes by Computational Fluid Dynamics (CFD); recent advances and approaches, Trends in Food Science & Technology Vol. 78, pp: 206–223

McBride B., Gordon S., Reno M.A., (1993). Coefficient for calculating Thermodynamic and Transport Properties of Individual Species. NASA - TM-4513, USA.

McCabe W., Smith J., Harriott P.E., (2004), “Unit Operations of Chemical Engineering” 7th edition, McGraw Hill Chemical Engineering Series

Mercea, P. (2000a). Plastic packaging materials for food - barrier function, Mass transport. Quality assurance and legislation. In O. G. Piringer, Diffusion data for LDPE, HDPE and PP. (pp. 470-530). Weinheim: Wiley-VCH.

Mercea, P. (2000b). Models for diffusion in polymers. In O. G. Piringer, Plastic packaging materials for food - barrier function, Mass transport. Quality assurance and legislation (pp. 125-157). Weinheim: Wiley-VCH.

Meulenaer, B. D. (2009). Migration from packaging materials. In R. Costa, Predictive modeling and risk assessment, pp: 139-151. Springer.

Miller M.T., Bederson B., (1978) Atomic and Molecular Polarizabilities-A Review of Recent Advances, Advances in Atomic and Molecular Physics, Academic Press, Volume 13, pp: 1-55,

Molz F., Rajaram H., Lu S., (2004). Stochastic fractal-based models of heterogeneity in subsurface hydrology: origins, applications, limitations and future research questions. Rev. Geoph Vol. 42(1) pp:1-42.

Montroll E. W., Scher H., (1973). Random walks on lattices. IV. Continuous time random walks and influence of adsorbing boundaries. Vol. 9(2), pp. 101-135.

Neuman, S. (1990). Universal scaling of hydraulic conductivities and dispersivities in geological media. Water Resources Research, Vol. 26(8), pp. 1749-1758.

Noetinger, B. (1994). The effective permeability of a heterogeneous porous media. Transport Porous Media, Vol. 15(1), pp: 99-127.

Noetinger B., (2000). Upscaling of double porosity fractured media using continuous time random walk methods. Vol. 39(3), pp: 315-337.

Noetinger.B., Estebenet.T. (2001). Up-scaling of double porosity fractured media using continuous-time random walks methods. Vol. 39(3), pp. 315-337.

O' Brien A., Cooper I. (2001). Polymer additive migration to food - a direct comparison of experimental data and values calculated from migration models for polypropylene. Food Additives and Contaminants, Vol. 18(4), pp. 343-355.

O' Brien A., Cooper I. (1999). Polymer additive migration to food - a direct comparison of experimental data and values calculated from migration models for high-density polyethylene (HDPE). Food Additives and Contaminants, Vol. 16(9), pp. 367-380.

Patankar, S. V. (1980). Numerical Heat Transfer and Fluid Flow. Taylor & Francis.

Pennarun P., Dole P., Feigenbaum A., (2004). Overestimated diffusion coefficients for the prediction of worst case migration from PET: application to recycled PET and to functional barriers assessment. Packaging Technology and Science, Vol.17(6), pp. 307-320.

Peric, M. Kessleer R., Scheuerer G., (1988). Comparison of Finite-Volume Numerical Methods with Staggered and Colocated Grids . Vol.16(4), pp. 389-403.

Perry, R. H. (1999). Perry's Chemical Engineers handbook. New York: McGraw-Hill.

Peube, J.-L. (2010). Fundamentals of Fluid Mechanics and Transport Phenomena. London, UK: Wiley & Sons NJ USA.

Piringer O., Bransch J., Mercea P., (2000). Plastic packaging materials for food – barrier function, mass transport, quality assurance and legislation In book: Plastic Packaging Materials for Food: Barrier Function, Mass Transport, Quality Assurance, and Legislation, pp.445 - 468. Weinheim: Wiley-VCH.

Piringer, O. G. (1994). Evaluation of plastics for food packaging. Food Additives & Contaminants, Vol. 11, pp. 221-230.

Pocas M., Oliveira J.C., Oliveira F.A., Hogg T., (2008). A critical survey of predictive mathematical models for migration from packaging. Critical Reviews in Food Science and Nutrition, Vol. 48, pp. 913–928.

Quintard M., Whitaker S., (1994). Transport in Ordered and Disordered Porous Media V: Geometrical Results for Two-Dimensional Systems. Transport in Porous Media. Vol.15(2), pp. 183-196.

Quintard M., Whitaker S., (1988). Two-phase flow in heterogeneous porous media: The method of large scale averaging. Vol.3(4), pp. 357-413.

Rajaram, H. (1997). Time and scale dependent effective retardation factors in heterogeneous aquifers. Advances in Water Resources. Vol. 20(4), pp. 317-330.

Ramachandran R. P., Akbarzadeh M., Paliwal J., Cenkowski, S. (2017). Three-dimensional CFD modelling of superheated steam drying of a single distillers' spent grain pellet. Journal of Food Engineering, Vol. 212, pp. 121–135.

Ranade, V. V. (2002). Process Systems Engineering - Computational Flow Modeling for Chemical Reactor Engineering (Vol. 5). London, UK: Academic Press.

Reinas I., Oliveira J., Pereira J., Machado F., Pocas M.F. (2012). Migration of two antioxidants from packaging into a solid food and into Tenax ®. Journal of Food Control. Vol.28, pp: 333-337.

Reynier A., Dole P., Feigenbaum A., (1999). Prediction of worst case migration: presentation of a rigorous methodology. Food Additives & Contaminants, Vol. 16(4), pp. 137-152.

Reynier A., Dole P., Feigenbaum A., (2002). Intergrated approach of migration prediction using numerical modelling associated to experimental determination of key parameters. Food Additives & Contaminants, Vol. 19, pp. 42-55.

Rhie C., Chow W. L., (1983). Numerical study of the turbulent flow past an airfoil with trailing edge separation. AIAA Journal, Vol.21(11), pp. 1525–1532.

Risch, S. (1988). Scientific status summary. Migration of toxicants, flavours and odour-active substances from flexible packaging materials to food. Food Technologist, Vol.7, pp: 95–102.

Rizzi A., Nørstrud H., Siikonen T., (2009). CFD Developments in the Northern European Countries. In E. K. H.H, 100 Volumes of ‘Notes on Numerical Fluid Mechanics. Vol. 100, pp. 133. Berlin: Springer.

Roache, P.J. (1972) Computational Fluid Dynamics. Hermosa

Robb A. M., Greenop B., GossGrant Z., Douglas G., Adeney J., (2003). Application of Phoslock TM, an innovative phosphorus binding clay, to two Western Australian waterways: preliminary findings. Hydrobiologia, Vol 494(1-3), pp: 237-243.

Ross, G. C. (2006). Phoslock® Field Trial at K’shani Lake Lodge, Hartbeespoort Dam. J Summary of Results,, pp: 1–15.

Rubin, Y. (2003). Applied Stochastic Hydrogeology. New York: Oxford University Press.

Sadler G.D., Braddock R.J., (1990). Oxygen permeability of LDPE as a function of limonene absorption: an approach to modeling flavor 'scalping'. Journal of Food Science, Vol.55(2), pp. 587-588.

Salamon P., Fernàndez-Garcia D., Gómez-Hernández J. J., (2006). Modeling mass transfer processes using random walk particle tracking. Water Resources Research, Vol. 42(11).

Sanches-Silva A., Cruz Freire J. M., Franz R., Losada P., (2008). Mass transport studies of model migrants within dry foodstuffs. Journal of Cereal Science, Vol.48(3), pp: 662-669.

Sato, N. (2004). Chemical Energy and Exergy - An introduction to chemical thermodynamics for engineers. Elsevier.

Se H. Oh, Cavendish J.C., (1981). Transients of monolithic catalytic converters. Response to step changes in feedstream temperature as related to controlling automobile emissions. Industrial Engineering Chemistry Product Research and Development., Vol. 21 (1) pp. 29-37.

Silbert, L. E., Ertaş D., Grest G.S., Halsey T.C., Levine D., Plimpton S.J., (2001). Granular flow down an inclined plane: Bagnold scaling and rheology. Physical Review E., Vol.64, pp: 64-78.

Slattery, J. (1967). Flow of viscoelastic fluids through porous media. AI.Ch.E.J, Vol.13(6), pp. 1066-1071.

Søndergaard M., Jensen J.P., Jeppesen E., (2003). Role of sediment and internal loading of phosphorus in shallow lakes. Hydrobiologia, Vol. 506(135-145) pp: 135-145.

Songyan Li, Li Z., Li B., Li R., (2010). Modeling of lifting heavy oil assisted by enclosed thermal fluid circulation in hollow rod. Journal of Petroleum Science and Engineering, Vol.75(1-2), pp: 135-142.

Tehrany E., Desobry S., (2004). Partition coefficients in food/packaging systems: a review. Food Additive & Contaminants., Vol.21(12), pp: 1186-1202.

Traiastaru E., Rivis A., Moldovan R.C., Menelaoy A., Georgescu C., (2013). Modelling migration from plastic packaging materials used in food industry. Journal of Agroalimentary Processes and Technologies, Vol. 19(2), pp: 180-184.

Uchida, S. (1949). Slow Viscous Flow through a Mass of Particles. Rep. Inst. Sci. Technol, 97–106.

Uchida, S. (1954). Viscous flow in multiparticle systems: slow viscous flow through a mass of particles. Vol. 46, pp. 1194-1195.

US_FDA. (1995b). Estimating exposure to direct food additives and chemical contaminants in the diet. Washington, DC: US Food and Drug Administration,

US_FDA. (1995a). Recommendations for chemistry data for indirect food additive petitions. Washington, DC: US Food and Drug Administration.

Verger, R., Ladd, A. J., (1999), Simulation of Low-Reynolds-Number Flow via a Time- Independent Lattice-Blotzmann Method, Physical Review E., Vol.60(3).

Versteeg, H.K.; Malalasekera, W. (1995) An introduction to Computational Fluid Dynamics- The finite volume method Longman Group Ltd. pp. 149–151.

Vitrac O., Hayert M., (2005). Risk assessment of migration from packaging materials into foodstuffs. American Institute of Chemical Engineers Journal, Vol.51(4), 1080-1095.

Vitrac O., Hayert M., (2006). Identification of Diffusion Transport Properties from Desorption/Sorption Kinetics: An analysis Based on a New Approximation of Fick Equation during Solid – Liquid Contact. Industrial & Engineering Chemistry Research, Vol.45, 7941-7956 .

Voltz S.E., Morgan C.R., Liederman D., Jacob S. M., (1973). Kinetic study of carbon monoxide and propylene oxidation on platinum catalysts. Industrial Engineering Chemistry Product Research and Development. Vol.12(4) pp. 294-301.

Wagner, W., Kretzschmar, H-J., (1998). International Steam Tables, Properties of Water and Steam Based on the Industrial Formulation. IAPWS-IF97. Springer, Berlin.

Wang, C.Y. and Cheng, P., (1997), Multiphase Flow and Heat Transfer in Porous Media, Advances in Heat Transfer, Vol.30, pp: 93-196,.

Welle F., Franz R. (2012). Diffusion coefficients and activation energies of diffusion of low molecular weight migrants in Poly(ethylene terephthalate) bottles. Journal of Polymer Testing. Vol.31, pp: 93-101.

Whilson, K. (1971). Renormalization group and critical phenomena. Physical Review .B. Vol.4(9) pp: 3174-3183

Whitaker, S. (1967). Diffusion and dispersion in porous media. Al.Che.J, Vol.13(3), pp. 420-427.

Whitaker, S. (1986). Flow in Porous Media: A theoretical derivation of Darcy's law. (3), pp. 3-25.

Whitaker, S. (1993). The closure problem for two phase flow in homogeneous porous media. Chemical engineering science, 49, pp. 765-780.

Whitaker, S. (1999). The method of volume averaging. Kuwel Academic Publisers.

Yadav, P. (2011). On the Slow Viscous Flow through a Swarm of Solid Spherical Particles Covered by Porous Shells. Applied Mathematics., Vol. 2, pp: 112-121.

Zamparas M., Gavriil G., Coutelieris F.A., Zacharias I., (2015). A theoretical and experimental study on the P-adsorption capacity of Phoslock^{TM}. Applied Surface Science, Vol.335, pp: 147-152.

Zamparas M., Drosos M., Georgiou Y., Deligiannakis Y., Zacharias I., (2013). A novel bentonite–humic acid composite material Bephos^{TM} for removal of phosphate and ammonium from eutrophic waters, . Chemical Engineering Journal, Vol. 225, pp: 43-51.

Zamparas, M. Deligiannakis Y., Zacharias I, (2013). Phosphate adsorption from natural waters and evaluation of sediment capping using modified clays. Desalin. Water Treat. , Vol. 51, pp: 2895–2902.

Zamparas M., Drosos M., Deligiannakis Y., Zacharias I., (2014). Eutrophication control using a novel bentonite humic-acid composite material BephosTM, . Journal Environmental Chemical Engineering. Vol.10 pp: 1016

Zamparas, M., Gianni A., Stathi P., Deligiannakis Y., Zacharias I., (2012). Removal of phosphate from natural waters using innovative modified bentonites. Appl. Clay Sci., Vol. 62-63, 101-106.

Zamparas M., Zacharias I., (2014). Restoration of eutrophic freshwater by managing internal nutrient loads. A review. Sci. Total Environ., Vol. 496, p: 551-562.

Zhang S., Zhao H. (2014). Study on flavonoid migration from active low-density polyethylene film into aqueous food simulants. Journal of Food Chemistry. Vol.157. pp: 45-50.

Zhou, Q. M. (2007). Field-scale effective matrix diffusion coefficient for fractured rock: results from literature survey. J.Contam.Hydrom. Vol.93, pp: 161-187.

Zulch A., Piringer O. (2010). Measurement and modeling of migration from paper and board into foodstuffs and dry food simulants. Food Additive & Contaminants, Vol.27. pp: 1306-1324.

8. CURRICULUM VITAE

Personal information	

First name and Surname	**GAVRIIL M. GAVRIIL**
Address	Larnaca, Cyprus
Nationality	Cypriot
Education and training	
Dates	01/10/2007 - 22/07/2012
Title of qualification awarded	Bachelor Degree
Principal subjects / occupational skills covered	Transport Phenomena, Mass and Energy Balances, Fluid Mechanics, Environmental Impact Assessment, Feasibility Study, Fortran 90/95 programming, Partial differential Equations, Remote Sensing, Statistics (SPSS), Process Safety and Work Hygiene, Solid waste management, Soil resources management, Meteorology, Methods of Spatial Analysis, Microbiology, Instrumental Methods in Environmental Analysis, Material Engineering, Materials Science and Environmental Applications, Environmental Organic Chemistry, Geochemistry, Applied Numerical Analysis, Applied Geo-Informatics, Applied Hydraulics.
Name and type of organisation providing education and training	University of Western Greece, Department of Environmental and Natural Resources Management.
Level in national or international classification	Higher education/University
Dates	03/09/2012 - 25/06/2014
Title of qualification awarded	Master of Science M.Sc.
Principal subjects / occupational skills covered	Liquid Transport Phenomena in Porous Media, Groundwater Hydrology, Advanced Topics in Environmental Engineering, Physicochemical and Biological Processes for the Treatment of the Wastewaters, Sustainable Built Environment, Air Pollution Monitoring and Control.
Name and type of organisation providing education and training	University of Cyprus, Department of Civil and Environmental Engineering.
Level in national or international classification	Higher education/University
Dates	09/2013 – Present
Title of qualification awarded	Doctorate of Philosophy candidate – Ph.D. Candidate

Principal subjects / occupational skills covered	Mathematical simulation of transport phenomena: scale transition and engineering applications / Liquid Transport Phenomena in Porous Media, Transport phenomena, Advanced Topics in Environmental Engineering, Physicochemical and Biological Processes, Sustainable Environment
Name and type of organisation providing education and training	University of Patras, Department of Department of Environmental and Natural Resources Management.
Level in national or international classification	Higher education/University
Work experience	
Dates	07/2015 – Present
Occupation or position held	Consultant – Environmental Engineer
Name of employer	Qualitylink Ltd
Dates	07/2015 – 05/2017
Occupation or position held	Sorting and Classification Center Manager
Name of employer	Weee Electrocyclosis Cyprus Ltd- GreenDot Cyprus
Dates	05/2015 – 07/2015 - Short-time contract
Occupation or position held	Environmental Inspector
Name of employer	Department of Environment - Ministry of Agriculture, Rural Development and Environment - Republic of Cyprus
Dates	12/2014 – 05/2015
Occupation or position held	Environmental Engineer - Human Resource Development Authority of Cyprus
Name of employer	Larnaca Municipality – Public Health Department – Environmental Management Sector
Technical skills and competences	Excellent knowledge on Fortran 90/95. Excellent knowledge on Microsoft Office 2003 & 2007. Knowledge on ESI Group Computational Fluid Dynamics Simulator (CFD-ACE+, CFD-GEOM, CFD-VIEW).

	Basic knowledge on Comsol Multiphysics Simulator. Knowledge on UTCHEM Chemical Compositional Simulator. Knowledge on ArcMap and ArcGIS remote sensing software. Basic knowledge on basic use of AutoCad. Basic knowledge on basic use of IBM SPSS Statistics. Knowledge on Adobe Photoshop Lightroom 4. Knowledge on Adobe Illustrator CS6.
Computer skills and competences	Excellent Knowledge on Windows Operating System. Excellent Knowledge on Macintosh Operating System. Beginner on Linux Operating System.
Other skills and competences	Excellent Mathematical Knowledge. Excellent analytical ability. Ability to work as part of a team. Semi-professional photographer.
Driving licence(s)	Holder of a Driving licence [Type: A1, B]
Army Obligatory Service	Completed as a BMP3 - Tank Operator